JHU/APL
TG 1331
(TSC-W36-37)
AUGUST 1982
Copy No. 17

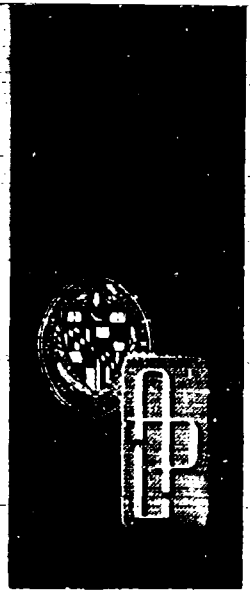

Technical Memorandum

MISSILE GUIDANCE: INTERFEROMETER HOMING USING BODY-FIXED ANTENNAS

J. F. GULICK and J. S. MILLER

THE JOHNS HOPKINS UNIVERSITY ■ APPLIED PHYSICS LABORATORY

PLEASE FOLD BACK IF NOT NEEDED FOR BIBLIOGRAPHIC PURPOSES

REPORT DOCUMENTATION PAGE

1 REPORT NUMBER TG 1331	2 GOVT ACCESSION NO AD-A119957
3 RECIPIENT'S CATALOG NUMBER	
4 TITLE (and Subtitle) **Missile Guidance: Interferometer Homing Using Body-Fixed Antennas**	5 TYPE OF REPORT & PERIOD COVERED Technical Memorandum
6 PERFORMING ORG. REPORT NUMBER TG 1331	
7 AUTHOR(s) **Joseph F. Gulick and James S. Miller**	8 CONTRACT OR GRANT NUMBER(s) N00024-81-C-5301
9 PERFORMING ORGANIZATION NAME & ADDRESS The Johns Hopkins University Applied Physics Laboratory Johns Hopkins Road Laurel, MD 20707	10 PROGRAM ELEMENT, PROJECT, TASK AREA & WORK UNIT NUMBERS B3
11 CONTROLLING OFFICE NAME & ADDRESS Naval Sea Systems Command A. W. Doherty, PMS 400P Washington, DC 20362	12 REPORT DATE August 1982 13 NUMBER OF PAGES 125
14 MONITORING AGENCY NAME & ADDRESS Naval Plant Representative Office Johns Hopkins Road Laurel, MD 20707	15 SECURITY CLASS (of this report) Unclassified 15a DECLASSIFICATION/DOWNGRADING SCHEDULE
16 DISTRIBUTION STATEMENT (of this Report) Approved for public release; distribution unlimited	
17 DISTRIBUTION STATEMENT (of the abstract entered in Block 20, if different from Report)	
18 SUPPLEMENTARY NOTES	

19 KEY WORDS (Continue on reverse side if necessary and identify by block number)

Interferometer, radar interferometer, interferometer antenna, guidance, missile guidance, radar guidance, radar homing guidance, terminal guidance, air defense systems, homing guidance.

20 ABSTRACT (Continue on reverse side if necessary and identify by block number)

Six chapters comprise this document, which is a discussion of the history and technical development of homing guidance via signals from body-fixed interferometer antennas as it is used in a tactical surface-to-air missile. Chapter 1 provides an introduction and background; Chapter 2 reviews homing guidance, giving brief consideration to the guidance technique and the concept of body-motion decoupling from the interferometer signal, as well as to the attractive features and critical factors that are characteristic of interferometers; Chapter 3 deals with early developments in interferometer guidance; Chapter 4 presents angle-measurement techniques along with their characteristic ambiguities and the methods for resolving them, describes instrumentation techniques for phase measurement by both scanning and nonscanning systems, and discusses the effects of glint noise and multiple targets; Chapter 5 describes the methods used to decouple body motion from the interferometer signal, the effects of a nonrigid airframe, and the types of measuring instruments and their tolerances; and Chapter 6 considers the use of homing guidance for current and future missiles, its compatibility

DD FORM 1 JAN 73 1473

Line 20

with other guidance modes for a multimode missile, and its low-frequency capability and suitability for guided projectiles. This last chapter is also directed toward the modern implementation of interferometer homing using strapdown inertial instruments and digital processing.

The comprehensive bibliography on body-fixed interferometer homing was assembled from memoranda from The Johns Hopkins University Applied Physics Laboratory, the Defense Research Laboratory of the University of Texas, the Massachusetts Institute of Technology Defense Technical Information Center, U.S. patents, and miscellaneous sources.

JHU/APL
TG 1331
(TSC-W36-37)
AUGUST 1982

MISSILE GUIDANCE: INTERFEROMETER HOMING USING BODY-FIXED ANTENNAS

J. F. GULICK and J. S. MILLER

Prepared by

Technology Service Corporation
Silver Spring, Maryland 20910
Contract No. 601249-S

THE JOHNS HOPKINS UNIVERSITY ■ APPLIED PHYSICS LABORATORY
Johns Hopkins Road, Laurel, Maryland 20707
Operating under Contract N00024-81-C-5301 with the Department of the Navy

ABSTRACT

Six chapters comprise this document, which is a discussion of the history and technical development of homing guidance via signals from body-fixed interferometer antennas as it is used in a tactical surface-to-air missile. Chapter 1 provides an introduction and background; Chapter 2 reviews homing guidance, giving brief consideration to the guidance technique and the concept of body-motion decoupling from the interferometer signal, as well as to the attractive features and critical factors that are characteristic of interferometers; Chapter 3 deals with early developments in interferometer guidance; Chapter 4 presents angle-measurement techniques along with their characteristic ambiguities and the methods for resolving them, describes instrumentation techniques for phase measurement by both scanning and nonscanning systems, and discusses the effects of glint noise and multiple targets; Chapter 5 describes the methods used to decouple body motion from the interferometer signal, the effects of a nonrigid airframe, and the types of measuring instruments and their tolerances; and Chapter 6 considers the use of homing guidance for current and future missiles, its compatibility with other guidance modes for a multimode missile, and its low-frequency capability and suitability for guided projectiles. This last chapter is also directed toward the modern implementation of interferometer homing using strapdown inertial instruments and digital processing.

The comprehensive bibliography on body-fixed interferometer homing was assembled from memoranda from The Johns Hopkins University Applied Physics Laboratory, the Defense Research Laboratory of the University of Texas, the Massachusetts Institute of Technology Defense Technical Information Center, U.S. patents, and miscellaneous sources.

CONTENTS

ILLUSTRATIONS

TABLE

1.0 INTRODUCTION

1.1 BACKGROUND

Use of interferometers for missile guidance spans most of the history of missile technology from some of the earliest homing missiles up to current use of interferometers in operational and developmental missiles. RF interferometers measure the angle of arrival of an RF wavefront by processing the phase difference between signals received at two displaced RF antennas. When this device is used as a sensor for missile guidance, it has a number of useful characteristics that are different from the characteristics of guidance systems that use other antennas.

Since shortly after World War II, The Johns Hopkins University Applied Physics Laboratory (JHU/APL) has been active in the development of RF interferometers for a variety of weapon system applications. On occasion, lack of complete familiarity with interferometer guidance technology by segments of the defense community has resulted in selection of alternative approaches without due consideration being given to interferometer systems.

Successful application of RF interferometers to missile guidance demands careful attention to fundamental principles of RF interferometer technology. Unfortunately, the literature on this subject is not as comprehensive or as widely available as that for other missile guidance techniques. Recent searches of two of the principal U.S. respositories for guidance and control references — the Defense Technical Information Center (DTIC) and the Guidance and Control Information and Analysis Center (GACIAC) — did not reveal a single document that thoroughly covers the subject of interferometer guidance. Even more distressing was the fact that some of the documents that were found reported analysis that concluded that all body-fixed guidance systems, including interferometers, are fundamentally unsuited for use against air targets — a conclusion that ignores the operational performance record of the Talos missile.

JHU/APL recognized the limitations of the available literature on interferometer guidance, and so issued a contract to the Washington Division of Technology Service Corporation (TSC) to prepare this survey of RF interferometer guidance. The survey does not report new analysis or development results, but instead draws heavily on information from patents, in-house reports, and published reports originated by JHU/APL, Bendix Mishawaka, the Defense Research Laboratory at the University of Texas (DRL), and MIT Lincoln Laboratories. This task was proposed by J. F. Gulick and J. S. Miller, whose many years of experience on the JHU/APL professional staff in all aspects of RF interferometer homing developments provide outstanding qualification to be the authors of this document.

1.2 PURPOSES OF THE DOCUMENT

This survey of RF interferometer guidance technology has several goals:

1. Describe attractive features and critical factors of RF interferometer guidance;

2. Review successful interferometer guidance techniques so that they can be imitated and refined;

3. Review interferometer guidance techniques that have known pitfalls so they can be avoided;

4. Recognize the contributions of organizations that participated in the early development of interferometer guidance; and

5. Document the successful operational use of RF interferometric guidance against air targets.

1.3 ORGANIZATION OF THE DOCUMENT

This document is divided into six chapters. Chapter 1 is the introduction. Chapter 2 is an overview of interferometer guidance, describing how body-fixed interferometers can be used to obtain the data required for proportional navigation homing, introducing the concept of body-motion decoupling, and providing a concise summary of attractive features and critical considerations for interferometer guidance.

Chapter 3 reviews early development of RF interferometer guidance with the METEOR program at MIT and the beginning of the Talos program at DRL and JHU/APL.

Chapter 4 examines interferometer processing for angle measurement, developing the equations that relate the interferometer angle to the electrical phase difference between the signals measured by two interferometer antennas, explaining angular ambiguity and scale factor variations, and describing specific hardware implementations that have been used for angle measurement processing.

Chapter 5 addresses the extremely important topic of body-motion decoupling, critical not only for interferometer systems, but for any guidance system that uses a body-fixed sensor and proportional navigation. The chapter also describes specific implementations that have been used for body-motion decoupling.

Chapter 6 looks to the future by examining the suitability of interferomter guidance for current and future missiles and suggesting ways that contemporary technology can be used to improve the performance and reduce the cost of interferometer guidance.

2.0 OVERVIEW OF INTERFEROMETER GUIDANCE

2.1 THE GUIDANCE FUNCTION OF BODY-FIXED INTERFEROMETERS

A homing missile makes onboard measurements of some aspects of the relative geometry between itself and its intended target, and based on these measurements, steers itself to intercept the target. The guidance law is the steering policy that the missile uses to determine its turning as a function of measured geometric parameters. Most homing missiles use guidance laws that are a form of pursuit guidance or proportional navigation. Proportional navigation generally provides better performance in the face of target maneuvers, external disturbances such as cross winds, and various measurement errors. For exact proportional navigation, the missile steers to maintain the turning rate of its velocity vector proportional to the angular rate of the line-of-sight (LOS) between the missile and the target.

Figure 1 is a block diagram of a typical proportional navigation guidance loop. The trajectories of the target and the missile determine the LOS between the missile and the tar-

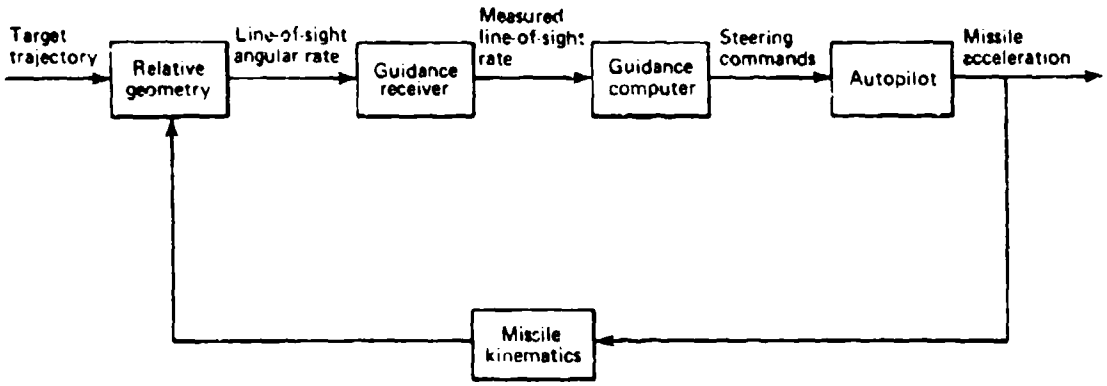

Fig. 1 Block diagram of proportional navigation.

get, as well as the angular rate of the LOS relative to inertial space. The functions of the missile hardware blocks in Fig. 1 are:

1. The guidance receiver measures the LOS rate and supplies that measurement to the guidance computer.

2. The guidance computer uses the measured LOS rate to generate steering commands for the autopilot in accordance with the proportional navigation guidance law, and

3. The autopilot drives aerodynamic control surfaces to generate missile acceleration in response to the steering commands from the guidance computer.

The focus of this document is the use of body-fixed interferometers for the guidance receiver function.

The angular rate of the LOS is a vector quantity that will have a component along the centerline of the missile unless the LOS itself is along the centerline. However, a typical missile autopilot does not control the component of acceleration along the missile centerline — it only controls the components of missile acceleration along two axes, $\hat{m}$ and $\hat{n}$ in Fig. 2,

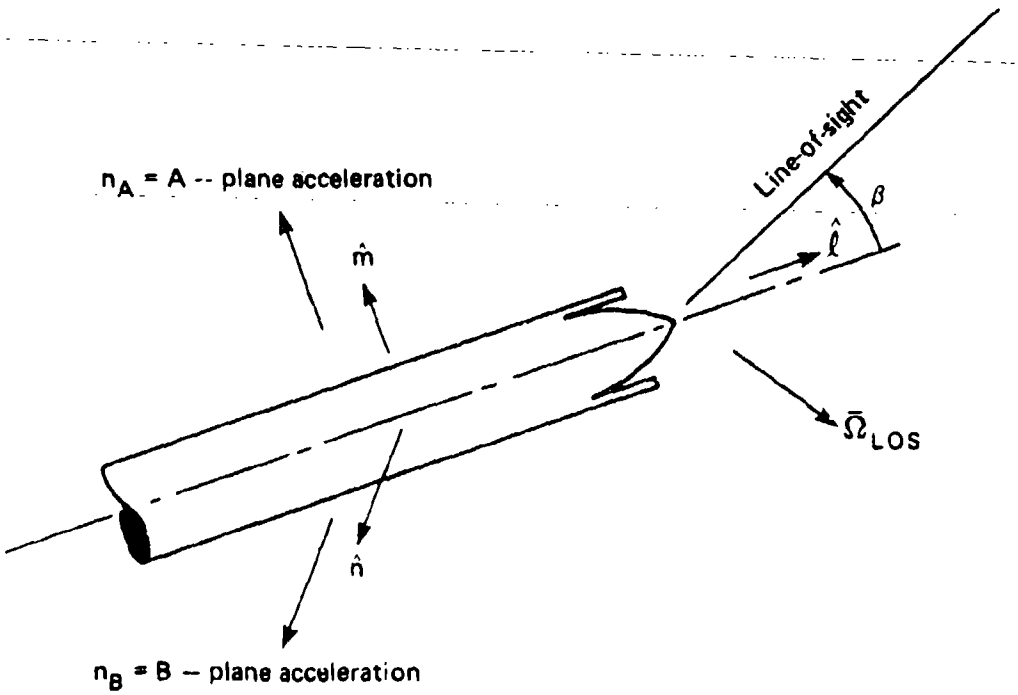

Fig. 2 Missile axes.

normal to the centerline. A common approximation for three-dimensional implementation of proportional navigation is therefore based on ignoring the component of LOS rate along the centerline and setting the steering commands (η_{A_C} and η_{B_C}) proportional to the components of the LOS rate along $\hat{m}$ and $\hat{n}$. This is done as follows:

$$\eta_{A_C} = \lambda \hat{\Omega}_{LOS} \cdot \hat{n} \tag{1}$$

$$\eta_{B_C} = \lambda \hat{\Omega}_{LOS} \cdot \hat{m} \tag{2}$$

For a homing missile using this approximate implementation of proportional navigation, a more specific statement of the guidance receiver function that is performed by body-fixed interferometers is: "The guidance receiver measures the m and n components of the inertially referenced angular rate of the LOS between the missile and the target."

2.2 CONCEPT OF BODY-MOTION DECOUPLING

Proportional navigation in a single plane requires a measurement of the angular rate of the LOS from the missile to the target, relative to inertial space. If this measurement is to be obtained from interferometer measurements, the guidance system must include a method for subtracting from the interferometer signal the apparent LOS rate caused by airframe rotation. There are two methods of accomplishing this body-motion subtraction or decoupling: (a) signals representing relative LOS rate from the interferometer can be combined with body rate measurements after angle demodulation of the interferometer signal or (b) prior to angle demodulation. Figures 3a and 3b are block diagrams illustrating methods (a) and (b), respectively.

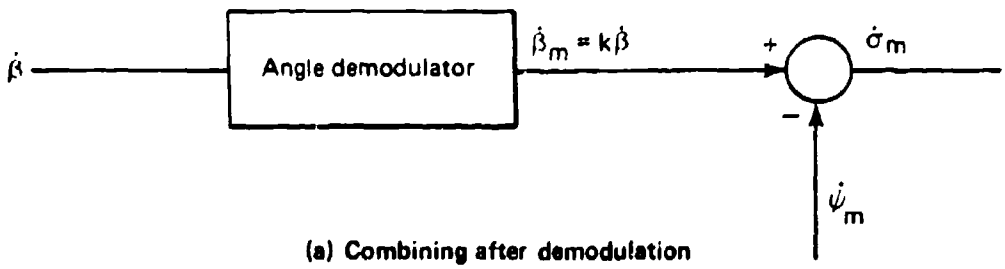

(a) Combining after demodulation

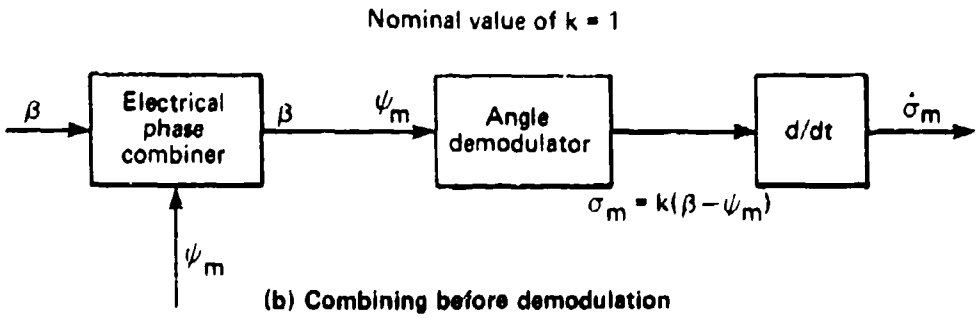

(b) Combining before demodulation

Fig. 3 Methods of body-motion decoupling.

Figure 3a shows combining after demodulation. A signal, $\dot{\beta}_m$, representing the measured value of the time derivative of β is combined with a signal that is a measure of the airframe angular rate, $\dot{\psi}_m$. This method produces a signal, $\dot{\sigma}_m$, that is a measured value of the angular rate of the LOS relative to inertial space. This form of decoupling seems attractively straightforward and simple to implement, but unfortunately it has a serious problem. Depending on the power of the received RF signal and the effects of countermeasures, the scale factor on the demodulation signal representing β may vary widely from its nominal value. Therefore, regardless of the geometric value of $\dot{\beta}$, $\dot{\beta}_m$ could be zero during a target

fade or whenever the signal-to-noise (S/N) ratio is very low. Figure 3a shows that if $\dot{\beta}_m$ goes to zero in such a situation, then $\dot{\sigma}_m$ will equal the measured airframe angular rate, $\dot{\psi}_m$, with the sign reversed. The resulting airframe motion feedback is destabilizing.

The second body-motion subtraction technique, combining before demodulation (see Fig. 3b) combines electrical phase angles proportional to β and ψ to produce an electrical phase angle proportional to σ. This process is not sensitive to the power level of the RF signal, but the angle demodulator processes a signal proportional to the geometric angle σ and provides an output proportional to $\dot{\sigma}$, the angular rate of the LOS. Changes in the scale factor angle demodulator caused by signal fades or by signal processing errors do affect the $\dot{\sigma}_m$ signal, but they do not introduce any airframe motion coupling or destabilization. Figure 4 shows conceptual signal processing diagrams for implementation of the two body-motion compensation techniques that have been described.

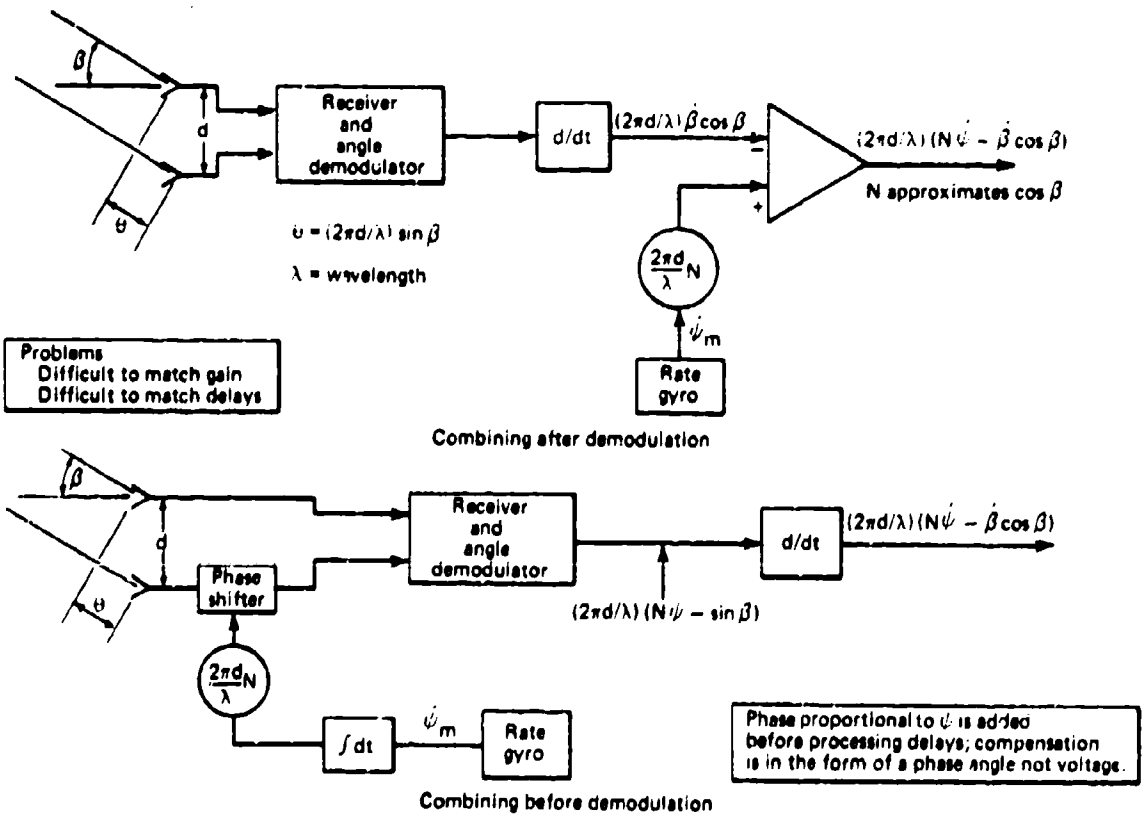

Fig. 4 Conceptual interferometer seekers.

A number of different body-motion decoupling techniques were used for the Talos missile during the two decades in which that missile was being developed and was deployed. However, all of the body-motion decoupling techniques used for Talos can be shown to be combining before demodulation.

2.3 ATTRACTIVE FEATURES OF INTERFEROMETERS

This section describes the attractive features of the interferometers, whereas the critical factors and limitations are discussed in Section 2.4.

A radar interferometer uses two widely spaced receiving antennas in each guidance plane to derive angle information. Since the receiving elements are rigidly mounted to the airframe, the antenna patterns of the individual elements must be sufficiently broad to cover the entire look angle between the missile axis and the LOS to the target. Target detection field of view is determined by the field of view of a single antenna, while angle measurement is based on processing the phase difference between signals received by the two antennas. Therefore, angular resolution is a function of antenna spacing in wavelengths of the radar signal, and look angle coverage is a function of the pattern of a single element. These characteristics are the basis for several of the attractive features of interferometer guidance.

2.3.1 Unobstructed Innerbody

One of the attractive features of an interferometer guidance system is that the antennas can be located in such a way that they do not influence the design of the innerbody for a nose inlet ramjet missile. In the development of Talos (the first operational missile to use RF interferometers) one of the requirements was to provide a homing system compatible with this type of inlet design. Ramjet engine inlets have critical requirements associated with their shape and, at least at that time, a homing seeker was needed that would not influence or depend on the shape of the ramjet innerbody. Use of radar interferometers met this requirement because the individual interferometer receiving elements were located outside and a little forward of the ramjet compressor duct. This configuration proved to be very successful because the guidance system design was not significantly affected by the innerbody design changes that were made through the years of the Talos program.

2.3.2 Wide Field-of-View

Another attractive feature of interferometer guidance was used to satisfy a second requirement for Talos. Talos demanded a homing system that would be able to perform inflight acquisition without accurate designation of the target direction. This derived from an operational requirement for intercept of air targets at ranges of 50 to 400 mi. Such intercepts required inflight acquisition a long time after launch at long ranges from the launching ship. Under these circumstances, precise target designation was impossible. To achieve target acquisition without accurate target designation, a guidance system must either search for the target or have a wide field-of-view. The interferometer guidance system can easily perform this function because of its wide field-of-view, which is equal to the antenna pattern of an individual element.

2.3.3 Freedom from Radome Errors

Gimballed seekers normally require a radome, which is an RF-transparent cover in front of the seeker. The shape of the radome is determined by a compromise between the design of the missile aerodynamics and that of the missile guidance system, since the best radome shape for one is the worst shape for the other. The aerodynamics designer prefers a

long, tapered nose for minimum drag, while the seeker designer prefers a hemispherically-shaped nose for minimal signal distortion. The compromise design is not optimal either for aerodynamic or guidance performance. The compromise in guidance system performance is manifested as angular errors caused by radome refraction.

Careful control of the radome wall thickness is one critical factor for minimizing the radome distortions. Two choices have been used extensively. One is to use a thin wall radome, the thickness of which is less than one-fifteenth of the wavelength in the dielectric material. The other usual approach is to use a radome with a wall thickness that is slightly greater than one-half wavelength. Although the thin wall radome is able to operate over a wide range of wavelengths that meet the thin wall criterion, often this is not mechanically practical. The more desirable half wavelength, tuned radome is widely used with a resulting bandwidth limitation of approximately 10% depending on the missile performance requirements.

Radome errors and the corresponding bandwidth limitations do not apply for radar interferometers because each receiving element is a low gain radiator, often a simple dielectric loaded horn or polyrod. These individual elements do not require an additional radome.

2.3.4 Broadband Coverage with Simple Antennas

Another advantage of interferometers is that the individual antenna elements do not need to have difference patterns. They can be simple, single-mode antennas. Depending on the required bandwidth, polarization, and gain, many different forms of individual antenna elements are suitable. This flexibility favors achievement of wide-band frequency coverage.

A linearly polarized element is usually used for semiactive seekers because the polarization of the illuminating signal is usually linear. The linear element used for a semiactive seeker typically is also suitable for operating in an HOJ (home on jammer) mode since airborne jammers are usually circularly polarized. Linearly polarized polyrod elements are practical up to approximately 20% bandwidth, while various forms of log periodic antennas can be used over a greater bandwidth, as much as several octaves.

In situations where circular polarization is necessary, such as some ARM (antiradiation missile) applications, interferometer antennas are readily available. Constant diameter helix antennas with bandwidths on the order of 20% have been used for this application. Greater bandwidths can be achieved with some sacrifice in gain by using flat spiral elements having bandwidths of two to three octaves. Such flat spiral elements are both feasible and practical.

2.3.5 Low-Frequency Coverage, Angular Accuracy, and Resolution

Missile guidance interferometers used for angle measurement are usually separated by the missile body diameter; this has several major benefits.

The accuracy of the interferometer angular measurement is strongly dependent on the aperture dimension (in wavelengths) of the received RF signal. Using the maximum aperture allows the interferometer to achieve greater angular accuracy or lower frequency

coverage than a typical monopulse antenna for the same missile airframe. The relationship is discussed in Ref. 1. For example, at a particular frequency, the interferometer system will achieve greater angular accuracy than a typical monopulse antenna in the same airframe. Or, for a particular level of angular accuracy, the interferometer system will be able to operate at a lower frequency than a typical monopulse antenna in the same airframe. This comparison of angular accuracy is significant because angular accuracy is strongly related to terminal miss distance.

When a missile is confronted with multiple targets within the field-of-view of its seeker, the success in intercepting one individual target depends on more than the angular accuracy of the seeker measurements. The missile will have no hope of intercepting an individual target unless the seeker is at some point able to develop guidance signals that will steer the missile toward an individual target, rather than toward a centroid of the multiple targets. Even this, however, will not assure a small miss distance. If and when the missile seeker generates steering commands toward an individual target, the missile's intercept capability will still depend on whether the remaining time-to-go until intercept is sufficient for the required steering corrections, given the missile maneuverability and responsiveness. Missile performance against multiple targets, therefore, depends strongly on the range at which the missile seeker can first generate commands to steer the missile toward an individual target. This critical range is approximately twice as great for a seeker using interferometers separated by the airframe diameter as it is for a typical monopulse seeker in a missile of the same diameter.

The performance at greater wavelengths can be further improved by mounting interferometer sensors considerably outside the missile body diameter. Reference 2 describes work performed in this area by MIT. Other tests, performed at JHU/APL, used a model similar to the one shown in Fig. 5. The data from the JHU/APL tests, although no longer available, indicated that acceptable performance could be expected against a moderate performance air target, and good performance could be expected against fixed or slowly moving targets.

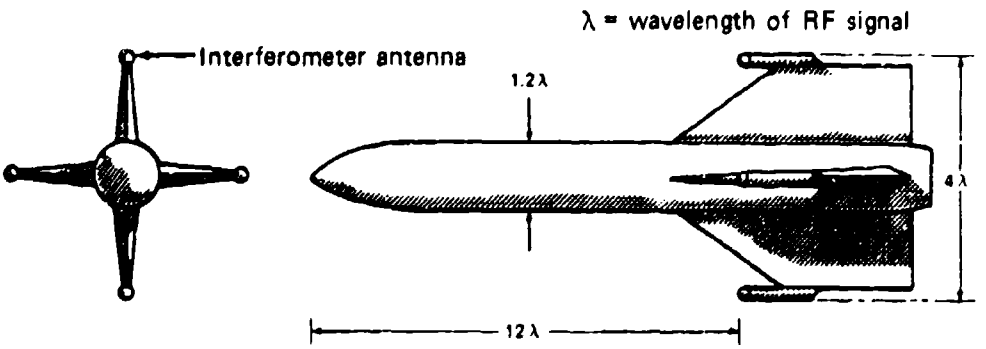

Fig. 5 Anechoic-chamber test model.

1. J. F. Gulick, E. C. Jarrell, and R. C. Mallalieu, "Fundamental Limitations of ARM Seekers at Low Radar Frequencies," JHU/APL FS-77-006 (Jan 1977).
2. I. Stiglitz, *Journal of Defense Research* (Summer 1979) MIT Lincoln Laboratories, Lexington, MA.

2.3.6 Compatibility for Multimode Guidance Systems

The ever-changing picture of EW (electronic warfare) and missiles has shown that seekers operating in more than one mode and in widely separated portions of the electromagnetic spectrum provide greatly improved performance in a countermeasures environment. An interferometer guidance mode is particularly suitable for multimode guidance systems because the interferometer antenna elements do not use the central portion of the missile nose, leaving an unobstruced aperture for a second guidance mode.

A number of dual-mode or multimode missile systems have been proposed using the interferometer as one of the modes. These include:

1. RF (semiactive and HOJ) plus RF millimeter wave active,
2. RF (semiactive and HOJ) plus IR passive, and
3. RF (semiactive and ARM) plus IR passive.

An RF ARM and IR passive dual-mode missile has been in development for some time and is now in Engineering Development for the U.S. Navy (Ref. 3).

2.4 CRITICAL FACTORS IN INTERFEROMETER SYSTEM DESIGN

2.4.1 Angular Ambiguity

Interferometer processing measures electrical phase difference between the RF signals received by two interferometer antennas; however, the range of the phase measurement is only from $-\pi$ to $+\pi$ radians. Angle measurements based on the electrical phase measurements are, therefore, ambiguous since there is no unique space angle corresponding to the measured electrical phase difference. However, since proportional navigation is not based on target direction but on the angular rate of the target direction, the angular ambiguity of the interferometer does not affect the implementation of proportional navigation.

One effect of the ambiguity problem is the inability to measure β as discussed in Subsection 2.4.2. A second obvious difficulty occurs if a true measurement of β is needed to point a second system. Methods to eliminate the cos β term entirely or to resolve the ambiguities are discussed in detail in Sections 4.2 and 4.3.

3. "Technical Report RAM Missile Round Advanced Development," DTIC/AC-CO20879 (Feb 1980).

2.4.2 Cosine β Gain Factor

It can be shown that the measured value of $\dot{\sigma}_m$ is given by the following equation:

$$\dot{\sigma}_m = \frac{\lambda_o}{\lambda} \frac{\cos\beta}{\cos\beta_o} \dot{\sigma} + \left(\frac{\lambda_o}{\lambda} \frac{\cos\beta}{\cos\beta_o} - 1 \right) \dot{\psi} , \qquad (3)$$

where:

λ_o is the nominal operating wavelength for which the signal processing is calibrated,

λ is the actual operating wavelength, which may or may not match λ_o,

β_o is the design value of the look angle β for which the signal processing is calibrated, and

β is the actual value of the look angle.

This equation shows that the scale factor for the measurement of $\dot{\sigma}$ will deviate from unity if the actual value of the look angle β differs from the calibration value, β_o. The equation also shows that, in addition to affecting the measurement of $\dot{\sigma}$, deviation of β from its calibration value can also cause the measurement of $\dot{\sigma}$ to be corrupted by a component proportional to the missile airframe angular rate, $\dot{\psi}$. This second effect is the controlling factor that determines how well β and λ must be known.

A variety of schemes have been devised, and some of them put to use, to adjust the signal processing calibration for variations in β. Some missiles were designed with two different calibration settings for β. Prior to missile launch, one of the settings was selected as best suited for that particular engagement, based on the expected intercept geometry and the ratio of missile speed to target speed. For many applications, this approximation is too coarse. As a result, a number of methods (discussed in Section 4.2) have been developed to estimate the cosine of β more accurately so that measurement calibration and body-motion can be maintained.

2.4.3 Frequency Dependence

The above equation for the measured value of $\dot{\sigma}_m$ shows that the measurement has, in addition to its sensitivity to β, a dependency on the actual wavelength of frequency of the signal. Like variations in β, deviations in the operating frequency from the calibration value affect the scale factor for measurement of $\dot{\sigma}$, and can also cause body-motion coupling into the measured value of $\dot{\sigma}$. Section 5.6 describes some possible implementations for eliminating body-motion coupling caused by variations in the operating frequency.

2.4.4 Mechanical Alignment

An interferometer guidance system must have interferometer sensors and missile motion sensors in each of two lateral missile planes in order to allow two-plane steering. Alignment of the interferometer sensors with the missile motion sensors is critical to prevent undesirable cross-plane coupling. Alignment tolerances usually can be readily met if mechanical references are used, but it is extremely difficult to adjust the actual physical alignment by electrical signal nulling schemes.

2.4.5 Airframe Stiffness

The interferometer measures target motion with respect to the antennas, and the body-motion sensors measure motion at the sensor location. As previously mentioned, the steering signal is obtained by subtraction of these two quantities. It is, therefore, important that consideration be given to body bending effects if the body-motion sensor is physically displaced some longitudinal distance from the interferometer antennas.

2.4.6 Tolerance Requirements

For an interferometer guidance system, body-motion decoupling is performed by taking the small difference between two large signals, $\dot{\beta}_m$ and $\dot{\psi}_m$. If this body-motion decoupling is imperfect, missile body motion will be coupled into the guidance loop, which in some circumstances can destabilize the overall guidance loop. There are, therefore, stringent tolerances established for the quality of body-motion decoupling.

The tolerances on body-motion decoupling are influenced by many factors so that simulation is usually required to establish these tolerances. Some of the factors that have a strong influence are:

1. The amount of pitch and yaw motion associated with missile maneuvers;
2. Type of control, e.g., wings, canards, or tail control;
3. Allowable missile time constant;
4. Total available homing time;
5. Target maneuver characteristics; and
6. Guidance loop gain.

The body-motion decoupling tolerances are essentially tolerances on the matching of the body-motion measurements obtained from inertial sensors by the interferometer measurements. Since body-motion decoupling is a dynamic process, the body-motion measurements must match the interferometer measurements in phase as well as in gain response.

The cumulative effect of the error sources described in Subsections 2.4.2 through 2.4.4 must not exceed the body-motion decoupling tolerances. Chapter 5 covers body-motion decoupling in detail.

2.4.7 Wide-Beam, Low-Gain Antennas

Any body-fixed antenna used for missile guidance must have angular coverage sufficient for the entire range of possible off-axis look angles between the missile centerline and the LOS to the target. This look angle is the algebraic sum of two angles: the aerodynamic angle of attack and the angle between the missile heading direction and the LOS to the target. In practice, the size of the look angle is restricted by virtue of aerodynamic limita-

tions on the angle of attack and kinematic limitations on the angle between the missile heading direction and the LOS. The total look angle might, however, be as large as 55° corresponding to a requirement that a body-fixed antenna have a total field-of-view of 110°. This is several times the required field-of-view for a missile guidance antenna that is gimballed relative to the missile body and allowed to track the LOS to the target.

The large field-of-view required for body-fixed missile guidance antennas limits antenna gain. A pair of interferometer antennas will readily provide the necessary field-of-view, but their gain would be only approximately 5 dB above the gain of an isotropic antenna, assuming 50% efficiency for the individual interferometer antenna elements.

The interferometer antenna configuration has two characteristics that must be understood. First, the body fixed nonsteerable configuration requires a total field-of-view consistent with the maximum required look angle. Second, the gain associated with such an antenna is considerably below the gain available with a steerable antenna. A complete comparison of these body-fixed antenna characteristics with steerable antenna characteristics is quite complex, and the results depend heavily on the geometry assumed for the encounter.

2.4.7.1 Gain Considerations. For many conditions the low gain of the interferometer antennas is not a problem. Detection of a target is determined by the S/N at the detector. The noise is the sum of thermal noise within the receiver and external noise from standoff jammers or other interfering sources. The external noise is likely to be much greater than the thermal noise. Therefore, for those geometries in which a standoff jammer would be in the main beam of a dish antenna, the increased gain of the dish antenna would not improve the S/N as compared with an interferometer. If the reflected signal from a target is sufficiently large to permit acquisition in these environments, the low gain of the interferometer antennas is not a limiting factor. The case where the target is not in the dish main beam is discussed in sub-subsection 2.4.7.2.

2.4.7.2 Wide Field-of-View Considerations. The penalty of the wide field-of-view in a multiple target geometry involving a standoff jammer is offset by the fact that no pointing of the seeker toward the desired target is required for successful homing.

Consider a case where a target is screened by a standoff jammer, and during the first part of the homing flight both the steerable seeker and the body-fixed seeker have acquired in an HOJ mode on the standoff jammer. The missiles are guiding toward the jammer. Since the jammer has a range much greater than that of the desired target, the signal from the target increases at a higher rate than the jammer signal. At some point, sufficient signal to noise may be available to allow burn-through on the desired target for the interferometer case.

For the high-gain steerable seeker case, the desired target could easily be expected to be in the antenna side lobes at the range where burn-through should occur. In this case the missile would never see the target.

The wide field-of-view of the interferometer has been shown to have essentially no deleterious effects on target tracking, and in the case of multiple passive targets, the dichotomous tracking characteristic of the interferometer signal processing caused the interferometer to give preference to the strongest target, even when the power difference was only on the order of 1 lb. Results of some testing in this area are given in sub-subsection 4.3.7.7.

2.4.8 Antenna Shadowing

The location of the interferometer antenna must allow a clear unshadowed look over the required field of view to eliminate errors resulting from secondary reflections as discussed in Ref. 1. When the ratio of the body diameter to wavelength is small, diffraction around the body may provide adequate steering when the target is in the geometric shadow of the body.

2.5 APPLICATIONS OF INTERFEROMETER TECHNOLOGY

Development of the radar interferometer as a missile seeker has been a continuing process for more than 30 years. It has been deployed operationally for more than 20 years. Figure 6 shows a number of weapon systems employing interferometer technology.

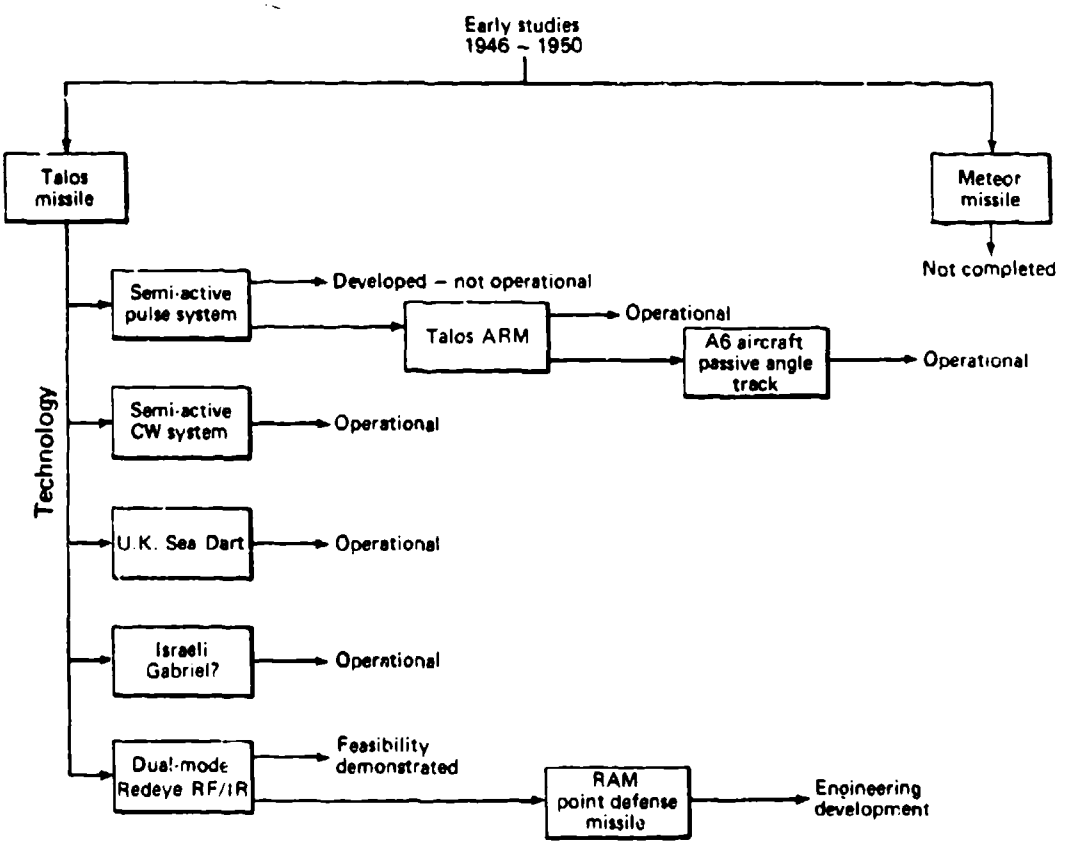

Fig. 6 Applications of interferometer technology to weapons systems.

3.0 EARLY DEVELOPMENT OF INTERFEROMETER GUIDANCE

Modern electronic technology entered antiaircraft warfare during World War II with the development and deployment of the VT (variable time) proximity fuze. The proximity fuze substantially increased the effectiveness of antiaircraft gunfire, but faster and more maneuverable aircraft and the devastating accuracy of kamikaze glide bombers against ships led to further refinements — the addition of radar directors and computers to shipboard gun systems. In spite of these advancements, antiaircraft shells were still fired toward targets with all the intercept computations based on the premise that the target would not change its course or speed during the shell's flight time. This kind of defense was all but useless against highly maneuverable targets. The concept of a guided missile would allow the projectile to alter its course as necessary after launch to provide an intercept even if the target maneuvered.

The U.S. Navy sponsored a program to exploit the guided missile concept by developing a supersonic ramjet-powered missile with guidance derived from target detection and tracking by the shipboard radars. Initial studies showed that the missile could be designed to fly up the radar's transmitted beam and thus intercept a target being tracked by the radar. This type of guidance was called beam riding and was considered accurate enough for short intercept ranges. Since long intercept ranges were planned, it was concluded that a homing system on the missile would be required in order to achieve lethal terminal accuracy. The Defense Research Laboratory of the University of Texas (DRL/UT), working under JHU/APL technical direction, proposed a homing system compatible with the ramjet engine that had been selected for the long range missile. Independently, the Massachusetts Institute of Technology (MIT) was working on the problem of homing guidance of a missile. Almost simultaneously, the two organizations separately conceived the idea of body-fixed, widely spaced antennas as a radar interferometer to provide steering signals for a missile.

The originators of the interferometer guidance concept at DRL/UT and MIT were, respectively, O. J. Baltzer and the late L. J. Chu. Baltzer has stated* that Dr. Chu's concept probably pre-dated his own by a short time. The MIT and the DRL/UT concepts use similar antenna configurations, but there the similarity ends. It is shown in Sections 3.1 and 3.2 that the MIT and DRL/UT signal processing concepts were quite different.

Table 1 is a chronological listing of technical reports generated in conjunction with these early development activities. A number of other reports by DRL/UT pertaining to instrumentation techniques followed shortly after the reports listed in Table 1. Reports of particular interest are included in the bibliography.

3.1 METEOR PROGRAM AT MIT

The following paragraphs describe interferometer guidance work in the METEOR Program at MIT.

*Telephone communication between L. J. Chu and J. F. Gulick, Oct 1980.

Table 1

EARLY REPORTS ON INTERFEROMETER GUIDANCE

O. J. Baltzer (DRL/UT), "A Radar Interferometer for Homing Purposes," JHU/APL CM-260, May 15, 1946.

C. W. Horton, "The Scheme for Missile Navigation Suggested by Dr. L. J. Chu," DRL/UT Internal Memo 38, May 15, 1946.

"METEOR Introductory Report," MIT Guided Missile Program, METEOR Report M1, July 15, 1946.

C. G. Matland and C. C. Loomis (MIT), "A Preliminary Study of the Radar Homing Head for an AA Missile Program," METEOR Report M2, August 15, 1946.

L. J. Chu (MIT), "The Seeker Problem of Guided Missiles," METEOR Report M3, September 15, 1946.

3.1.1 L. J. Chu's Interferometer Guidance Concept

The MIT work on interferometer guidance was based on a concept originated there by Dr. L. J. Chu. Although no MIT document describing Chu's guidance concept has been located, it is described and attributed to Chu in a 1946 DRL/UT internal memo written by C. W. Horton (Ref. 4).

The following paragraph from Horton's report shows that Chu's concept included a constant bearing trajectory for the homing missile:

> It appears that the most desirable course for the missile is as follows: When a target is detected the missile should immediately turn with maximum turning rate until the predicted collision course lies on the axis of the missile and then proceed in a straight line until the collision is accomplished.

Chu proposed that the steering commands be obtained by taking the difference between two measured quantities:

1. The angular rate of the missile-to-target LOS relative to the missile centerline measured by interferometer antennas, and

2. The pitch and yaw motions of the missile about its center of gravity measured by rate-sensing gyroscope.

4. C. W. Horton, "The Scheme for Missile Navigation Suggested by Dr. L. J. Chu," DRL/UT Internal Memo No. 38 (15 May 1946).

Figures 7 and 8 are diagrams of two different methods proposed by MIT for obtaining the difference between these quantites. The notation in both figures is:

β = angle between missile longitudinal axis and missile-to-target line of sight.

ω = angular rate of pitch or yaw about missile center of gravity.

The two methods of Fig. 7 and 8 are described more completely by Ref. 5.

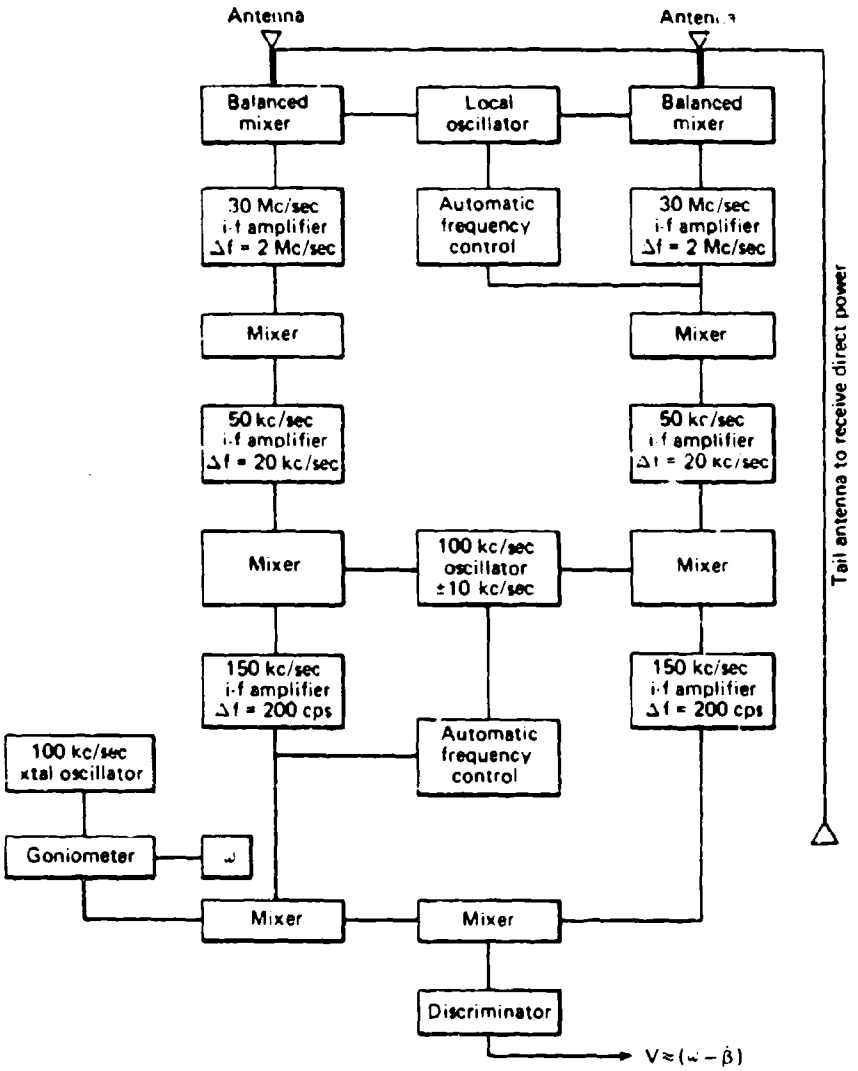

Fig. 7 C-W system with transmitter on the ground (from Ref. 5).

5. C. G. Matland and C. C. Loomis (MIT), "A Preliminary Study of the Radar Homing Head for an AA Guided Missile," METEOR Report M2 (15 Aug 1946).

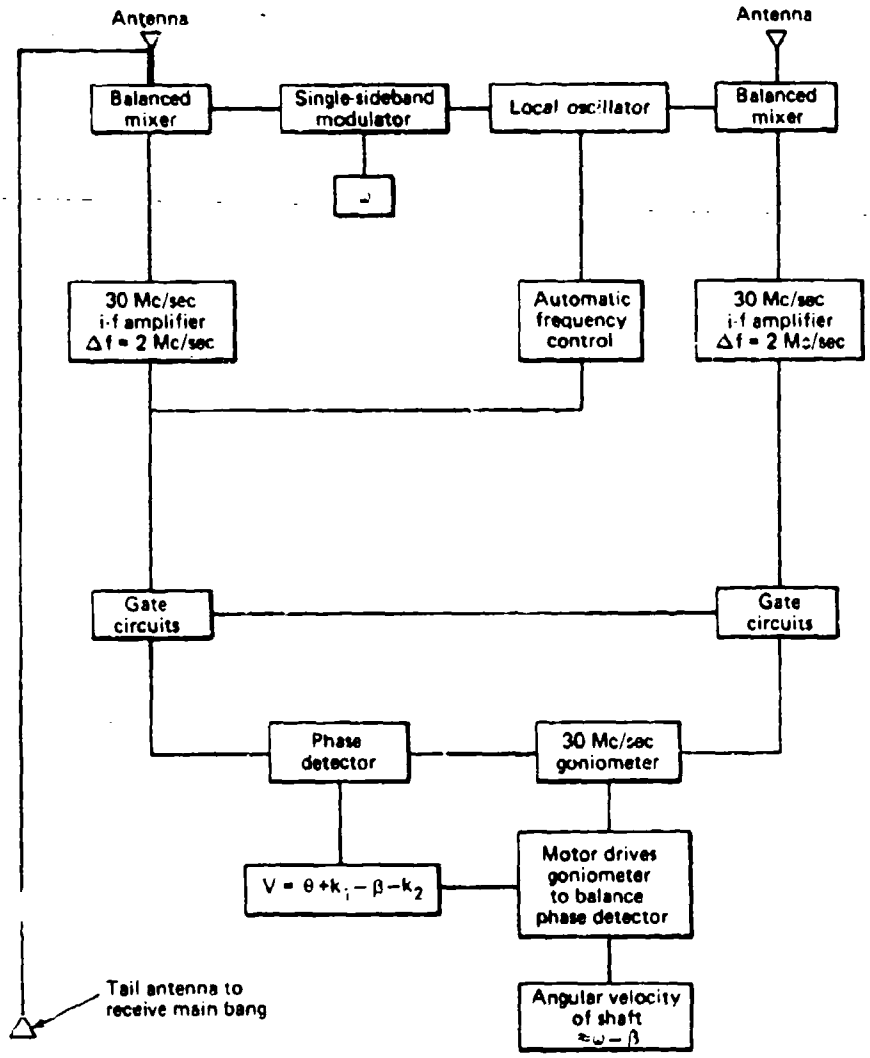

Fig. 8 Pulsed system with transmitter on the ground (from Ref. 5).

Several of the figures in this chapter are reproduced from old documents. In some cases the terminology is obsolete, but for the sake of preserving their originality they have been left intact.

Both Fig. 7 and Fig. 8 include a goniometer, a device normally associated with radio direction finders. However, this instrument can also be used to shift continuously the phase of a radio frequency signal by rotating a coil in a field formed by two loops. The goniometer therefore contains a servomechanism where the shaft rotation changes the electrical phase of a signal.

3.1.2 METEOR Seekers

During the late 1940's and the early 1950's, MIT built several versions of the METEOR seeker and evaluated them in a variety of test conditions including tests of captive aircraft. These were pulse seekers, and are described in Ref. 6.

Reference 6 describes two of the later METEOR seekers, the P5 and the P6. Both of these used vacuum tubes since solid state devices were not yet available. The P5 had four separate channels of IF amplification and, consequently, required 98 vacuum tubes, resulting in a very large device that used a lot of power. The P6 Seeker, a simplified design, allowed processing of both pitch and yaw channels in a single IF amplifier, thus reducing the number of vacuum tubes. Details of the P5 and P6 Seekers are given in Ref. 4. Figure 9 is a simplified diagram of the P6.

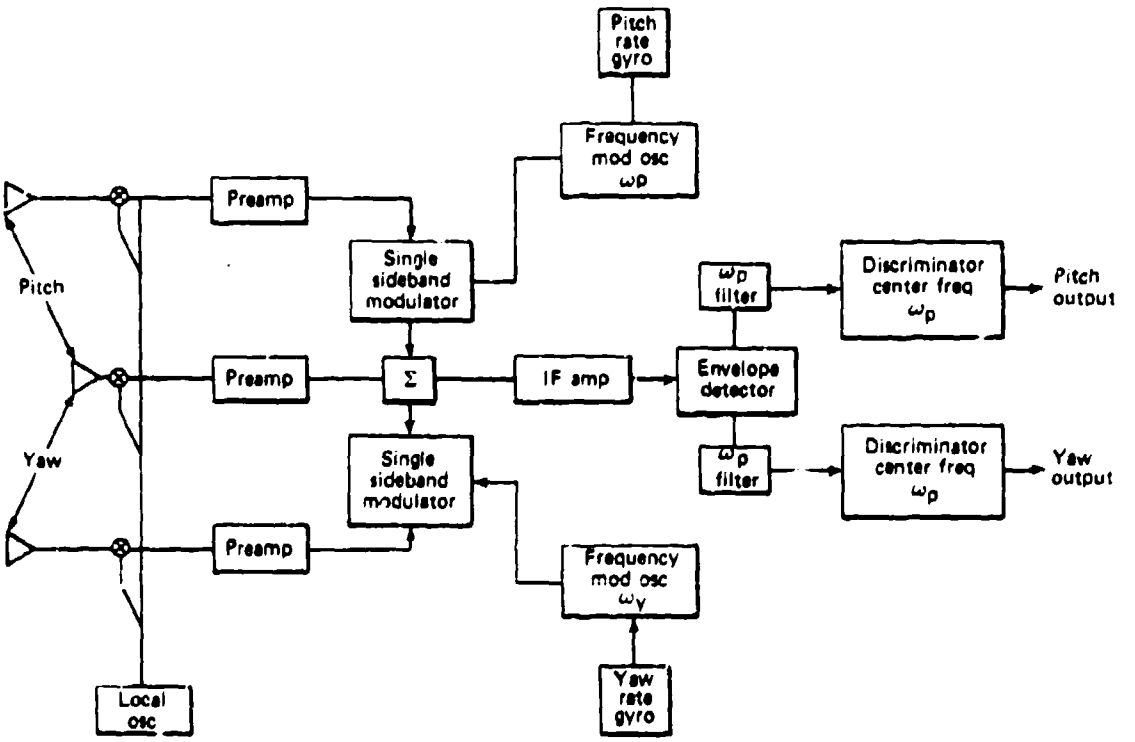

Fig. 9 Simplified diagram of METEOR P6 seeker.

The principle of operation of the P5 Seeker (shown in Fig. 10) is as follows: The two antenna signals are phase compared by in-phase and quadrature-phase detectors, providing the sine and cosine of the phase angle differences. These detector outputs are used to

6. B. Loesch, R. Long, M. Moore, and J. C. Nowell, "Design and Test of Simplified Pulse Interferometer Seeker," DTIC/DLA AD No. 107338 (30 Sep 1955).

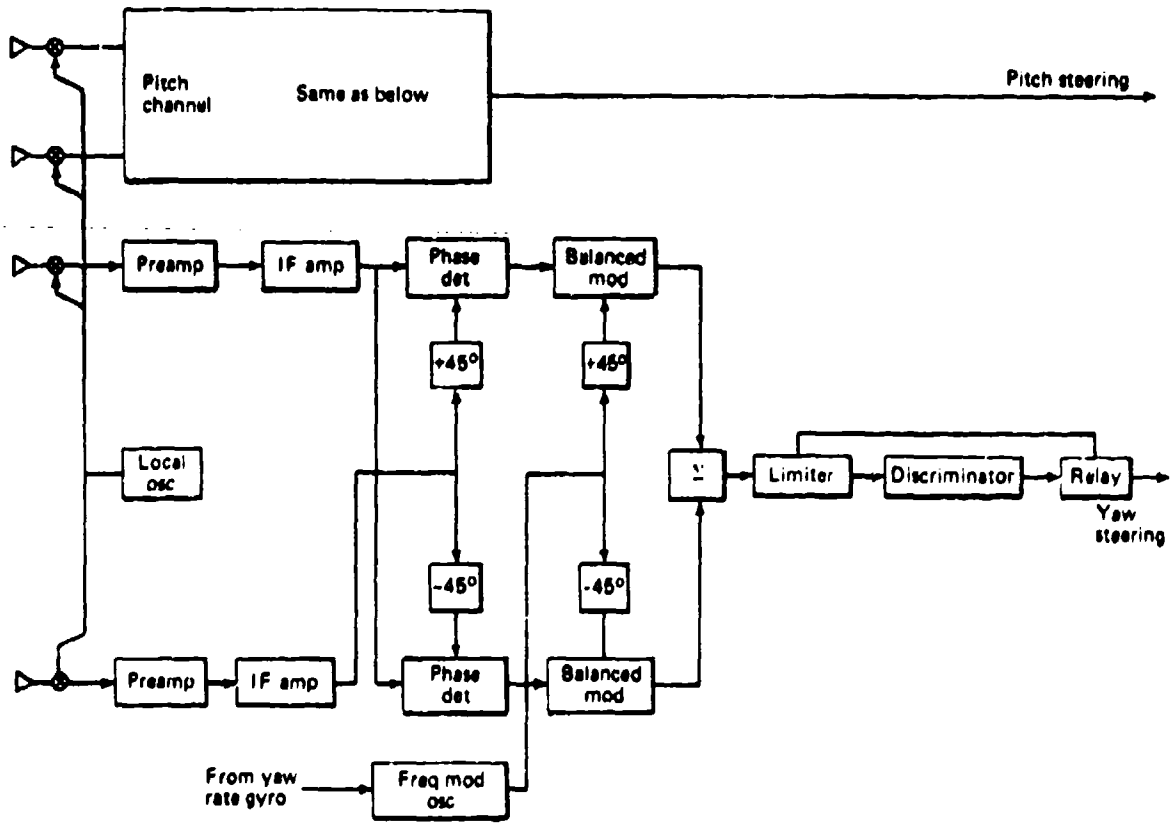

Fig. 10 Simplified diagram of METEOR P5 seeker.

modulate two quadrature components of a frequency modulated oscillator. This process is a single sideband modulation of the oscillator in which the output frequency is modified by the phase rate of the interferometer. Since the oscillator is modulated in frequency by a rate-measuring gyro, the frequency of the resulting signal, which is the limiter input, represents the difference between the interferometer phase rate and the missile body rate. A discriminator following the limiter measures the frequency deviation of this signal from its nominal value and provides a measure of the target LOS in inertial space. When the P5 Seeker did not receive an RF signal from the target, imperfections of the balanced modulators allowed a gyro signal to appear at the seeker output. The sense of this seeker output is destabilizing to the overall guidance loop. Therefore, the P5 included a relay switch at the seeker output to disconnect missile steering commands whenever the target return was lost.

The distinctive feature of the P6 Seeker was its method for multiplexing both pitch and yaw channels into a single amplifier and then extracting them at the output by appropriate filters. Nominal oscillator frequencies were selected that were compatible with a 2-kHz pulse rate. The difference between the pitch and yaw frequencies was set wide enough to

allow good separation. The selection of frequencies, of course, required considerable study to ensure that harmonics of each frequency and harmonics of difference frequencies did not cause problems in the signal processing.

Both the P5 and P6 would have had a severe problem if they had been subjected to input signals at the frequency of the IF image (Ref. 7). Input signals at the image frequency would have reversed the sense of the interferometer phase comparison resulting in a positive feedback path around the guidance loop.

3.2 TALOS MISSILE PROGRAM AT JHU/APL AND DRL/UT

The early concepts of the Talos Missile Program at JHU/APL were based on the assumption that the missile would use beam-rider guidance. It was evident early in the program, however, that if the range potential of the Talos ramjet engine were to be fully exploited, some form of homing guidance would be required for the terminal portion of the flight to achieve acceptable accuracy. A particular problem was to devise a homing concept that would be compatible with the ramjet diffuser on the front of the Talos missile that would not allow a conventional gimballed radar antenna for homing guidance.

DRL/UT proposed a homing technique that is compatible with the ramjet diffuser. The following abstract is from O. J. Baltzer's memorandum "A Radar Interferometer for Homing Purposes," (Ref. 8) that describes the DRL/UT proposal:

> It is proposed that a group of two or more microwave antennas, with the separation between each antenna limited only by the physical dimensions of the missile body, be used as a homing radar interferometer to initially steer and to maintain a guided missile on a constant bearing collision course. With such a collision course, it is not necessary to determine the location of the target with respect to the homing missile, either at the point of the initial detection or at any subsequent time along the trajectory; instead it is sufficient to determine only the polarity (positive, negative, or zero) of the apparent change in true bearing of the target relative to an observer in the missile. Several methods of measuring the shift in true bearing are suggested, and it is believed that one of these methods may be suitable for use with a homing missile.

A block diagram of the system proposed by Baltzer is shown in Fig. 11.

Following Baltzer's formulation of his homing concept, a number of experiments and derivative concepts resulted. One of the most significant was that of C. R. Rutherford (Ref. 9, "Double Modulation Radar Interferometer"). The following is the abstract of that report:

> In previous proposals for a radar interferometer which used a motor driven phase shifter, it was necessary to have a very constant speed motor. With the present proposed interferometer system, frequency changes of ½ cycle per second in the envelope frequency are detected for guidance information. This means that the motor speed must be constant to better than ¼ cycle per second.

---

7. T. D. Jacot, "Notes on Interferometer Phase Measuring Systems," JHU/APL MED-SR/200 (1 Oct 1969).
8. O. J. Baltzer (DRL/UT), "A Radar Interferometer for Homing Purposes," JHU/APL CM-260 (15 May 1946).
9. C. R. Rutherford (DRL/UT), "Double Modulation Radar Interferometer," JHU/APL CF-505 (3 Dec 1946).

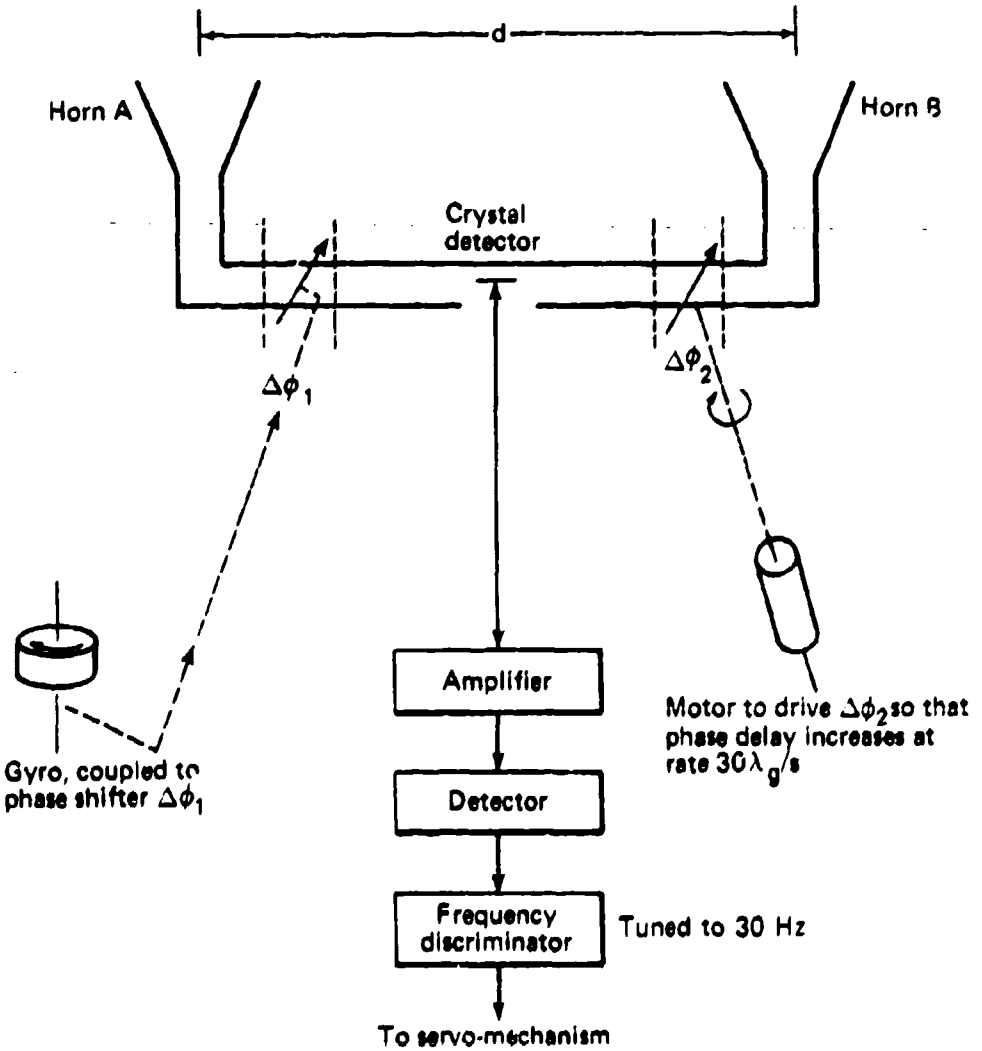

1. If output frequency = 30 Hz, on collision course.
2. If frequency >30 Hz, discriminator gives positive polarity signal for counterclockwise turn.
3. If frequency <30 Hz, discriminator gives negative polarity signal for clockwise turn.

Fig. 11 Block diagram of a frequency deviation scheme to detect change in true bearing.

Rutherford's report describes a double modulation system that eliminates any error cause by variations in motor speed. A local oscillator acts as the frequency reference for the frequency discriminator by making the frequency changes caused by changes in true bear-

ing of the target to be manifest as variations from the local oscillator frequency. One modulator is a mechanical single-sideband modulator that makes a low frequency filter unnecessary. The frequency discriminator acts as its own filter for the second modulator.

Figure 12 shows a block diagram of Rutherford's proposal. He suggested that the 50-Hz oscillator be frequency modulated by a signal from a rate gyro to provide body-motion decoupling. This scheme was the basis for the first homing systems that were built and flight tested in the Talos Missile Program. The activity of DRL/UT in the interferometer development program continued for many years in conjunction with developments at JHU/APL. Additional early DRL/UT reports of interest are included in the bibliography.

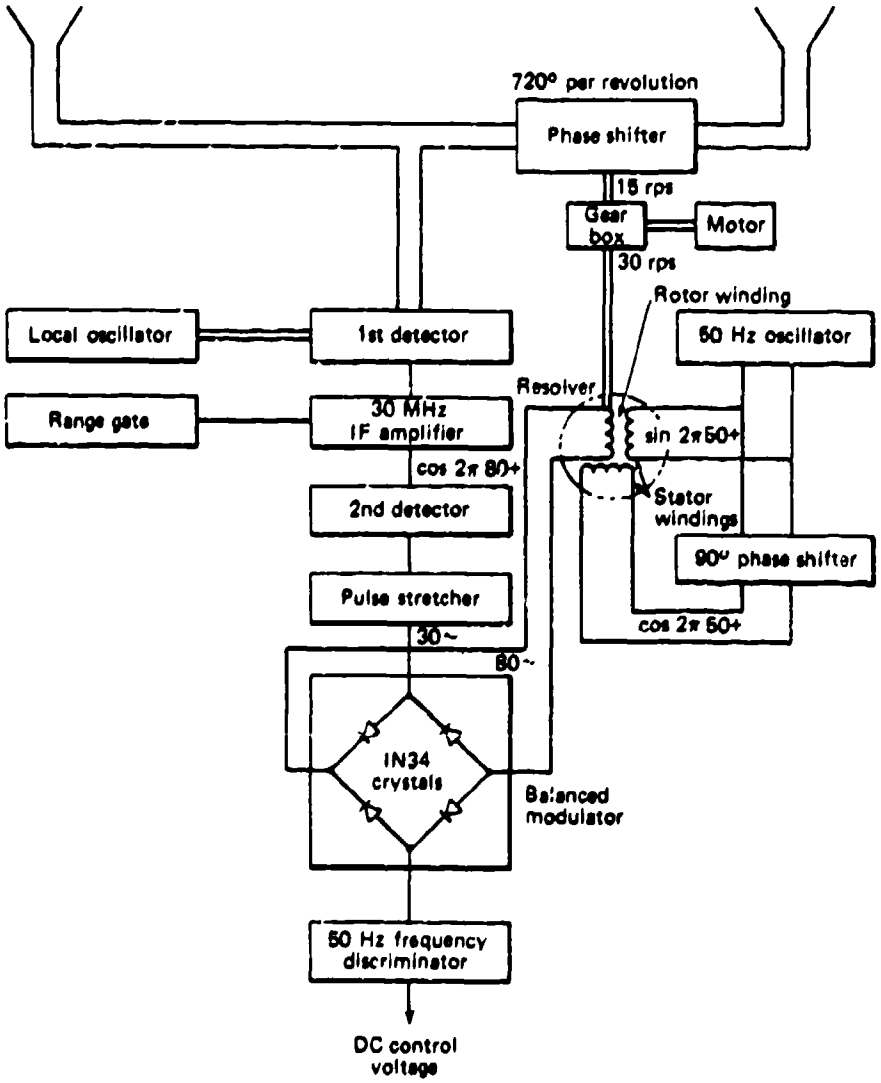

Fig. 12 Rutherford's radar interferometer system (from Ref. 9).

4.0 INTERFEROMETER ANGLE MEASUREMENT

4.1 INTERFEROMETER THEORY

4.1.1 Angle Measurement

Figure 13 is a single-plane illustration of the use of an RF interferometer to measure the look angle, β, between a missile centerline and the LOS to a target. Two interferometer antennas, A and B, are separated by a distance d. The interferometer receives RF energy emitted or reflected from the target. Since the distance between the missile and the target is much greater than the separation between the interferometer antennas, it is a very good approximation to consider the RF wavefronts to be planar, as shown in the figure. The wavelength of the RF signal is represented by λ.

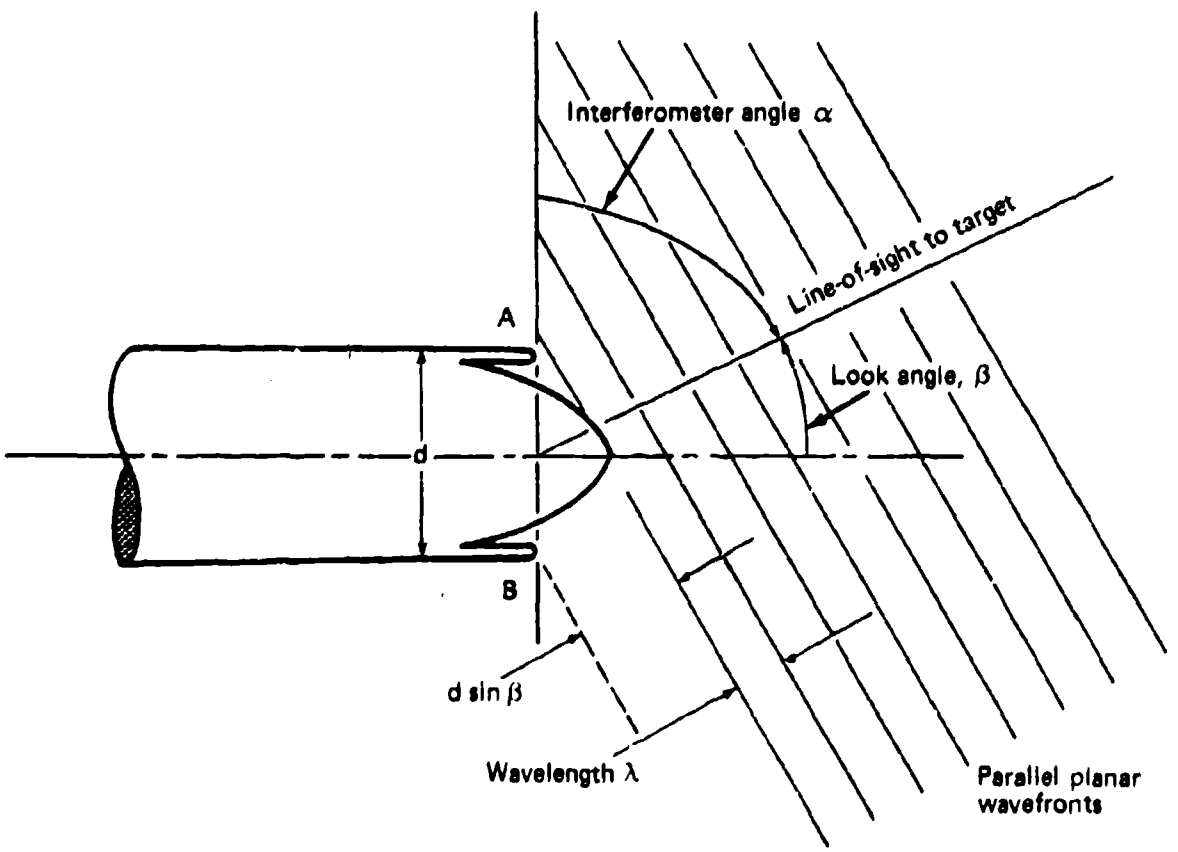

Fig. 13 Body-fixed RF interferometer.

For the look angle shown in Fig. 13, any given wavefront will arrive at antenna A before it arrives at antenna B. In particular, when a wavefront arrives at antenna A, it will still have to travel a distance $d \sin \beta$ before it arrives at antenna B.

The output signal of antenna B will, therefore, lag the output signal of antenna A by an absolute phase angle that is proportional to $d \sin \beta$. If the distance $d \sin \beta$ were equal to a full RF wavelength, λ, the absolute phase angle would be 2π radians. In general, the phase angle between the output signal of antenna A and output signal of antenna B is

$$\theta = \frac{2\pi d}{\lambda} \sin \beta \tag{4}$$

If the wavelength were known and the absolute phase angle could be measured, Eq. 4 could be used to determine the look angle, β. Unfortunately, there is no simple way to measure the absolute phase angle.

4.1.2 Angular Ambiguities

Subsection 4.1.1 has shown that an interferometer measurement of look angle is based on measurement of the phase angle between the signals received by two interferometer antennas. Figure 14a is a plot of the absolute phase angle, θ, as a function of the look angle,

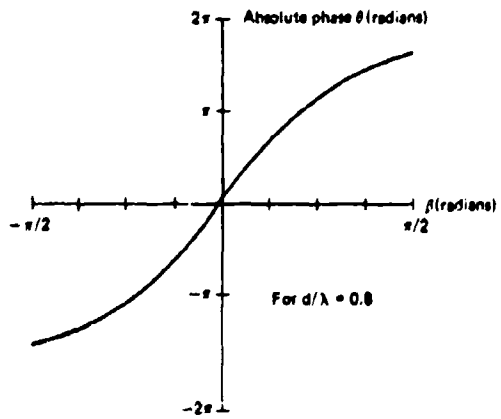

(a) Absolute

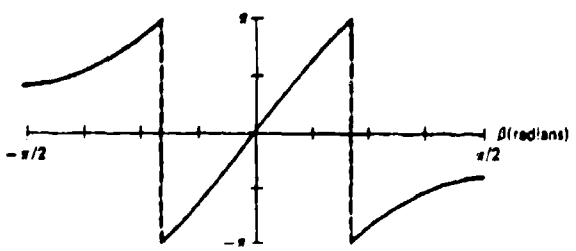

(b) Measured

Fig. 14 Phase versus look angle.

β, for the particular case of $d/\lambda = 0.8$. For this case the range of θ is greater than 2π; it extends from -1.6π to $+1.6\pi$, a range of 3.2π. However, for any practical phase measurement scheme the range of measured values will not exceed 2π. Therefore, the relation between the look angle and the measured or relative phase angle, denoted by θ_m, is shown in Fig. 14b. If the actual value of β is $\pi/8$, the measured value of θ will be 0.61π radians. However, an actual value of β equal to -0.34π radians would produce the same measured value of β. Therefore, an interferometer measurement based on the measured phase angle cannot determine that the look angle is $\pi/8$ or -0.34π radians; it can only determine that the look angle is one of those two values, illustrating the angular ambiguity of interferometer measurements. In this example, the distance between the ambiguities is 0.91π radians.

The distance between interferometer ambiguities depends on the ratio d/λ. This is illustrated by Figs. 15a and 15b, which are plots of look angle versus measured phase angle for d/λ ratios of 1.6 and 3.2. As the d/λ ratio increases, there are more values of β corresponding to each measured value of the phase angle, and the ambiguities are closer together.

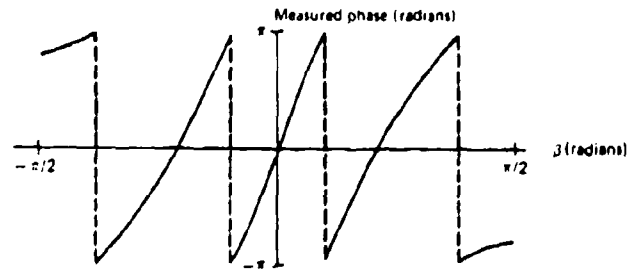

(a) For d/λ = 1.6

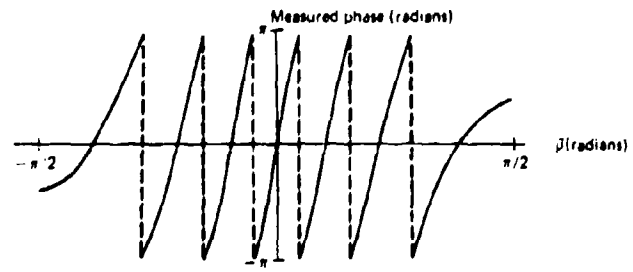

(b) For d/λ = 3.2

Fig. 15 Measured phase versus look angle.

Although it is disconcerting to realize that the interferometer angle cannot be measured unambiguously, the ambiguity does not significantly affect the use of interferometers for proportional navigation that does not require a measurement of the angle. Instead, proportional navigation is based on a measurement of the angular rate of the LOS, which can be measured unambiguously. The angular ambiguity would be significant only for systems re-

quiring a direct measurement of the LOS angle, for example, missiles in which the interferometer measurements are used to point a second seeker at the target for inflight acquisition and handover to a second guidance mode, or for systems where the gain variation of the rate measurement is seriously affected by the terms associated with absolute angle ($\cos \beta$).

4.1.3 Angular-Rate Measurement

Since implementation of proportional navigation requires a measurement of the LOS rate, an interferometer guidance system must measure the phase rate between the two interferometer signals, rather than the phase angle. The following discussion describes a phase scanning technique for performing this measurement.

The significance of body-motion rotation is treated in detail in Chapter 5, and will not be considered here. Temporarily assuming no missile-body rotation reduces the measurement of the LOS rate to a measurement of $\dot{\beta}$, the derivative of the look angle. Figure 16

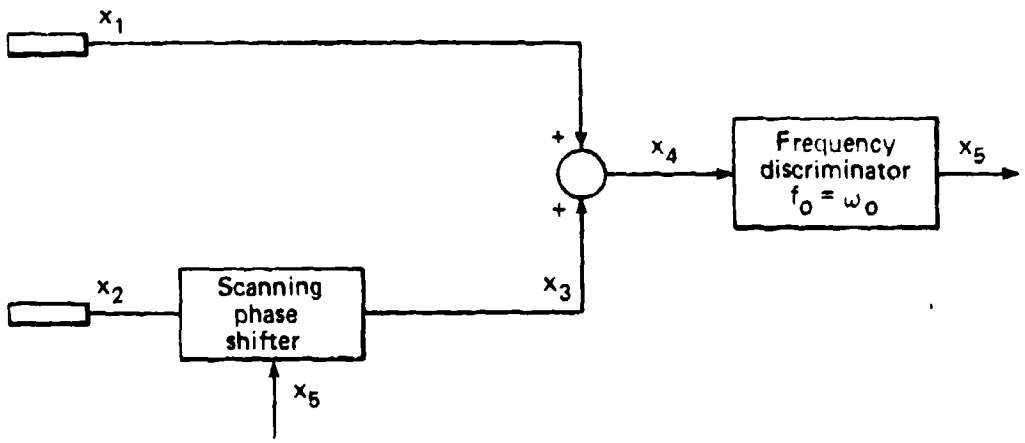

Fig. 16 Measurement of angle rate.

shows a phase scanning approach for this measurement. The signals received by each interferometer are:

$$X_1 = A_1 \sin \omega t$$
$$X_2 = A_2 \sin (\omega t + \theta) , \tag{5}$$

where ω is the frequency, and θ is the electrical phase between the two received signals. Two different amplitudes, A_1 and A_2, represent any possible difference in the gains of the two interferometer antennas, but ultimately the scanning measurement of phase rate is very insensitive to the amplitude of the received signals.

The angle β and consequently θ can change with time, but during a small interval about any time t_o the variation can be linearly approximated as

$$\theta(t) = \theta(t_o) + \dot{\theta}(t_o)(t - t_o) \tag{6}$$

An expression for $\dot{\theta}$ can be obtained by differentiating Eq. 4 and solving Eq. 6:

$$\dot{\theta} = \frac{2\pi d}{\lambda} \dot{\beta} \cos\beta \tag{7}$$

so that

$$\theta(t) = \theta(t_o) + (t - t_o) \frac{2\pi d}{\lambda} \dot{\beta} \cos\beta . \tag{8}$$

Equations 7 and 8 can be used to write a new expression for X_2.

$$X_2(t) = A_2 \sin\left[(\omega + \frac{2\pi d}{\lambda} \dot{\beta} \cos\beta)t + \theta(t_o) - t_o \frac{2\pi d}{\lambda} \dot{\beta} \cos\beta\right] . \tag{9}$$

A scanning phase shifter advances the phase of X_2 by ϕ according to the following schedule:

$$\phi(t) = \omega_s t + \phi(t_o) , \tag{10}$$

where ω_s is the scan frequency. The output of the phase shifter is

$$X_3 = A_2 \sin\left[\left(\omega + \omega_s + \frac{2\pi d}{\lambda} \dot{\beta} \cos\beta\right)t + \theta(t_o) - t_o \frac{2\pi d}{\lambda} \dot{\beta} \cos\beta + \phi(t_o)\right] \tag{11}$$

If $\dot{\beta} \cos\beta$ is assumed to be constant over the small time interval of interest, then X_3 can be written as follows:

$$X_3 = A_2 \sin\left[\left(\omega + \omega_s + \frac{2\pi d}{\lambda} \dot{\beta} \cos\beta\right)t + \Phi\right] , \tag{12}$$

Where Φ is a constant.

The next step in the signal processing is to add X_1 and X_3 to generate X_4, which is simply

$$X_4 = A_1 \sin\omega t + A_2 \sin\left[\left(\omega + \omega_s + \frac{2\pi d}{\lambda} \dot{\beta} \cos\beta\right)t + \Phi\right]. \tag{13}$$

Figure 17 is a phasor representation of X_4. It indicates that X_4 is an amplitude modulated signal at a carrier frequency ω. The frequency of the amplitude modulation is the frequency difference between X_1 and X_3, which is

$$\omega_m = \omega_s + \frac{2\pi d}{\lambda} \dot{\beta} \cos\beta. \tag{14}$$

In a phase scanning system, X_4 is processed to determine the frequency of the amplitude modulation and to measure the difference between ω_m and the scan reference, ω_s. This produces a signal, X_5, as follows:

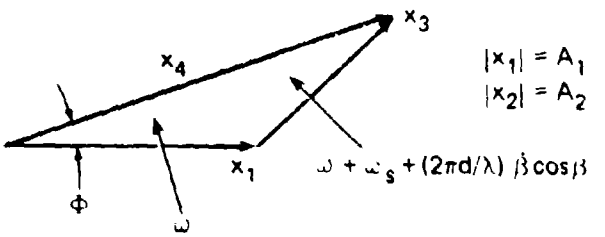

Fig. 17 Phasor diagram.

$$X_\zeta = \left(\frac{2\pi d}{\lambda}\cos\beta\right)\beta. \tag{15}$$

X_ζ is an unambiguous measure of $\dot{\beta}$ in that it is proportional to β. It does, however, have a scale factor that is proportional to $\cos\beta$, which may or may not be known. This scale factor is the $\cos\beta$ term introduced in Subsection 2.4.2 and mentioned again in Subsection 4.1.2.

4.2 ELIMINATION OF COSINE β FACTOR

In Section 4.1 it was shown that angle measurements in a single plane are contaminated by a $\sin\beta$ factor, and angle rate measurements are contaminated by a $\cos\beta$ factor.

One possible solution to the $\cos\beta$ factor problem was to devise an antenna system where the $\sin\beta$ factor was not generated in the angle measurement process. Two possible configurations to accomplish this (CHU I and CHU II antennas) were proposed by Chu Associates (Littleton, MA). Reference 10 is the final report covering their work. The $\cos\beta$ factor is not a problem when the ratio of missile velocity to normal target velocity is large, and consequently β is small. When β becomes large, other factors in addition to the $\cos\beta$ become significant if homing with three-dimensional geometry is considered. This problem occurs because the LOS rates measured by the interferometer antennas are not on the two orthogonal axes of the missile for large look angles of β.

Reference 11 is a critique on the CHU I antenna and its problems. Figure 18 from Ref. 11 shows the planes of interferometer measurement. Section 2.2 discussed body decoupling of a missile motion from the interferometer signals in a single plane. It can be seen from Fig. 18 that missile motion sensors in the body axes of the steering planes will not measure rates in the planes of the interferometer measurements. This will be discussed more completely in Chapter 5.

The normal interferometer treats three-dimensional homing as two orthogonal two-dimensional cases. The two guidance signals in the pitch and yaw channels are:

10. "Final Engineering Report: Improved Interferometer Antenna System," prepared for JHU/APL Subcontract 7733 by Chu Associates, Littleton, MA, JHU/APL Accession No. 142788 (30 Oct 1959).
11. A. G. Rawling, "On the Undesirability of the CHU I Type Interferometer Antenna in Homing," JHU APL BBD-458 (Jul 1958).

$$-\frac{d}{dt}(\cos\alpha) + Nq, \qquad \frac{d}{dt}(\cos\gamma) + Nr. \tag{16}$$

The angles α and γ between missile axes and the LOS are shown in Fig. 18. The conventions for positive sense of rotation of the missile angular rates in the pitch (q) and yaw (r) channels is also shown. The factor N, which is ideally equal to cos β, was found by simulation for Talos to be approximated adequately by a constant equal to 0.9.

From Fig. 18 it can be seen that while the rotation of the LOS is measured in two non-orthogonal planes YOT and ZOT, the missile must steer in orthogonal planes YOX and ZOX, and the body motion is measured about axes y and z.

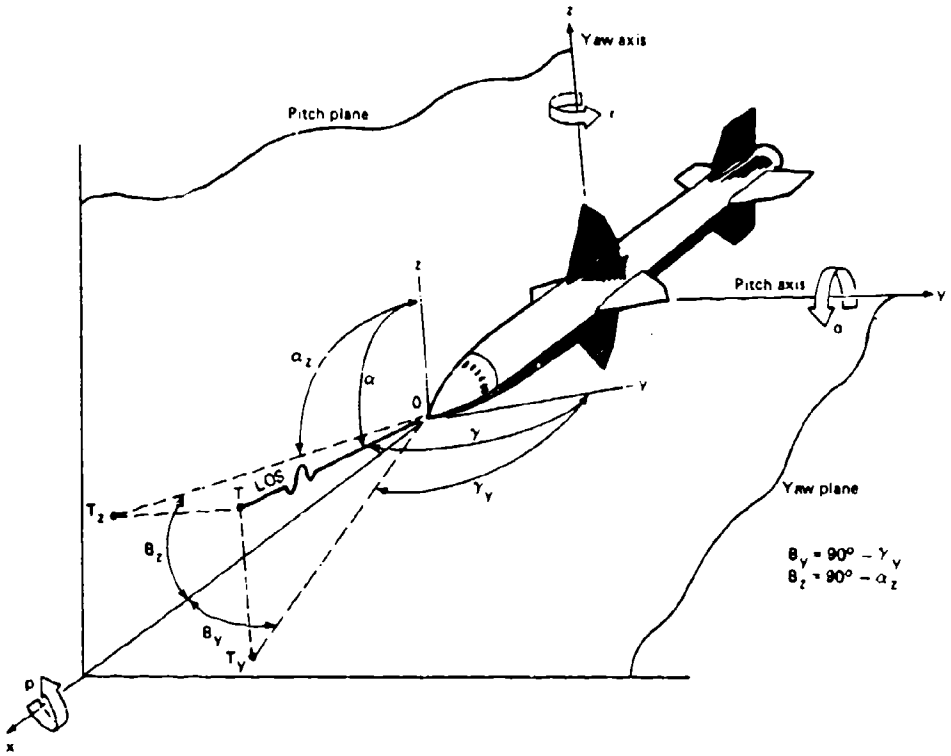

Fig. 18 Interferometer measurement and control axes.

The theoretical deficiencies of a homing system using these equations is discussed in Ref. 12. The CHU I antenna proposed to measure the projections of the angles α_z and γ_y in the steering planes using the expressions:

$$-\frac{d}{dt}(\alpha_z) + Nq, \qquad \frac{d}{dt}(\gamma_y) + Nr. \tag{17}$$

12. G. C. Munro, "Mathematical Discussion of a Device Suggested by J. W. Follin, Jr., for Improving the Performance of the Talos Interferometer Homing System," JHU/APL CF-2654 (1 Jul 1957).

The special array antenna eliminated the cosine factor in the normal antenna configuration. The angles α_z and γ_y measure the projection of the missile-target LOS into the steering planes (see Fig. 18). They are related to the angles β_y and β_z measured in the wing planes from the missile longitudinal axis to the projections of the line of sight by

$$\beta_y = 90^\circ - \gamma_y , \qquad \beta_z = 90^\circ - \alpha_z . \tag{18}$$

However, α_z and γ_y indicate the relationship to the true angles α and γ somewhat better than β_y and β_z.

This was an attempt to convert the three-dimensional homing process into a pair of independent two-dimensional processes with the measurements and steering signals "embedded" in the missile wing planes. Results of simulations of this homing process are discussed in Ref. 11. The conclusions of this report are as follows:

1. The missile equipped with the CHU I type interferometer homing system suffers from degraded performance.

2. Conditions under which the antenna was tested might be considered nonconservative, e.g., no radome aberration and no noise present in the simulation. Missile roll rate was negligible, except for that occurring through aerodynamic coupling in the case of negative heading errors.

3. There was no apparent need to test CHU I further with target maneuver and roll rate biases.

As mentioned previously, the CHU I antenna measured projections of the LOS rates into the steering planes. The antenna design had uniform lobe widths with a planar null surface. In an attempt to correct the deficiencies shown by the simulation, a design was proposed with uniform lobe spacing on a conical surface as opposed to the planar surface of the CHU I antenna. This was known as the CHU II antenna. Reference 10 is the final report on this work. The abstract of this report is quoted below:

> The design objectives under this subcontract were the development and design of an improved interferometer scanning antenna for missile navigation. The project consisted of two (2) phases. Phase I was the development of an interferometer antenna having uniform lobes with planar null surfaces. Phase II was the design of an interferometer scanning antenna having uniform lobe widths and amplitudes but with conical null surfaces. Phase I has been covered in a previous engineering report. This report contains formulations of the solutions to the synthesis problem of producing a conical null surface, uniform lobe, interferometer antenna pattern using (1) linear array designs and (2) modified point source designs in shaped reflector and lens systems. Feasibility of the techniques of modifying the phase pattern of a point source to activate the desired antenna pattern is demonstrated. This report further contains experimental evidence that the location of the present dielectric rod antenna cannot be changed without adverse effect.

Unfortunately the required configuration of the CHU II antenna system was not compatible with the missile airframe design, and there were no further studies on its performance were made.

4.3 AMBIGUITY RESOLUTION

Although it has been demonstrated through many flight tests that the interferometer can be used to successfully intercept a target when only the LOS rate is used in the steering command, there are at least two situations where the measurement of β or $\cos\beta$ is desirable. These are:

1. Missile-target trajectories where computation of $\cos\beta$ is necessary to provide adequate body-motion decoupling, and

2. Direct measurement of β to point a secondary system such as an infrared or short range active seeker.

In a single plane the phase rate signal derived from the interferometer has been shown to be

$$\dot{\theta} = \frac{2\pi d}{\lambda}\,\dot{\beta}\cos\beta\,, \tag{19}$$

where $\dot{\theta}$ is the electrical phase rate, d is the spacing, λ the wavelength, and β the angle between the missile longitudinal axis and the missile-to-target LOS. The interferometer sensitivity is proportional to $\cos\beta$. β is large, and the deviation of $\cos\beta$ from unity is most significant for intercept of high speed crossing targets.

If there is no compensation for the $\cos\beta$ variation in the interferometer sensitivity, body-motion decoupling can be degraded as described in Subsection 2.4.2. The $\cos\beta$ compensation can be based on techniques that measure $\cos\beta$ directly and do not measure β, or on measurement of β and computation of $\cos\beta$.

Reference 13 gives a survey of systems to provide measurements of $\cos\beta$ and β. This report presents analysis of systems proposed for use in an advanced Talos missile. Although the concepts presented may have other applications, the particular methods of instrumenting these concepts, as described in the referenced report, are limited to the signal processing proposed for the particular missile.

Figure 19, taken from the referenced report, illustrates the geometric relations for a three-dimensional analysis of an interferometer system. A pair of interferometer antennas 2 and 4 located along the z axis measure the angle α, and antennas 1 and 3 along the y axis measure γ. Both the α and γ measurements can be ambiguous if the antenna spacing is large with respect to a wavelength of the received signal.

Some useful relationships from Fig. 19 are: If $OA = 1$, then

$$\begin{aligned} OB &= \sin\beta, \\ OD &= OB\cos\psi = \cos\alpha, \\ OC &= OB\cos(90^\circ - \psi) = \cos\gamma\,, \\ \cos\alpha &= \sin\beta\cos\psi, \text{ and} \\ \cos\gamma &= \sin\beta\cos(90^\circ - \psi). \end{aligned} \tag{20}$$

13. "Survey of Systems to Provide an Unambiguous Measure of the Angle of the Target Line of Sight," prepared for JHU/APL by Dunn Engineering Associates, Cambridge, MA (20 Sep 1957).

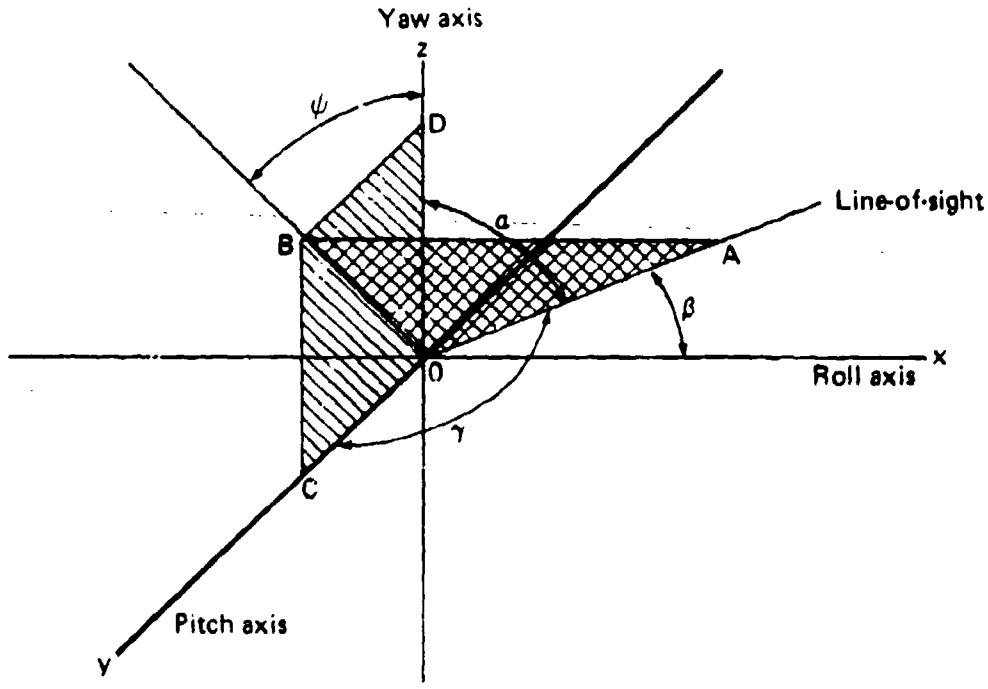

Fig. 19 A coordinate system showing the symbols used to define the three-dimensional guidance problem.

Some of the techniques used to solve ambiguities or to measure cos β address the problem by solving the ambiguity in the α and γ measurements separately and then computing β or cos β. Other techniques provide cos β directly. Subsections 4.3.1 through 4.3.5 describe several techniques for determining β unambiguously.

4.3.1 Multiple Baselines

4.3.1.1 n-Channel Interferometer Systems. The interferometer system represented by Fig. 19 processes signals from two antennas along the z axis to measure α, and processes signals from two antennas along the y axis to measure γ. When a real target is located in any particular direction, the interferometer system's ambiguous measurements of α and γ will define an ambiguous set of directions, one of which will be the true target direction. Given a real target along the missile centerline, the unambiguous field-of-view can be defined as the angle between the centerline and the nearest ambiguity.

The two-channel interferometer system represented by Fig. 19 has an unambiguous field-of-view of λ/d radians. However, without changing the antenna arrangement, two additional channels of interferometer data can be obtained by processing one of the z-axis antennas with each of the y-axis antennas. Use of this information can extend the unambiguous field-of-view to $\sqrt{2}\lambda/d$.

This example suggests that the unambiguous field-of-view could be extended even further if additional antennas were added to provide additional interferometer channels. That is the subject of Ref. 14. In practice, the unambiguous field-of-view depends on the accuracy of the electrical phase measurements as well as on the geometric arrangement of the antennas. Reference 14 is a thorough and rigorous analysis of the ambiguity resolution that can be achieved in the presence of phase measurement errors for arbitrary antenna arrangements in a plane.

4.3.1.2 Three Collinear Antennas. A special case of the multiple baseline antenna system uses closely spaced elements to provide coarse angle information for the unambiguous measurement of α and γ and wide-spaced antennas to provide the angular sensitivity desired for accurate guidance. Figure 20 shows a configuration for this measurement. α is

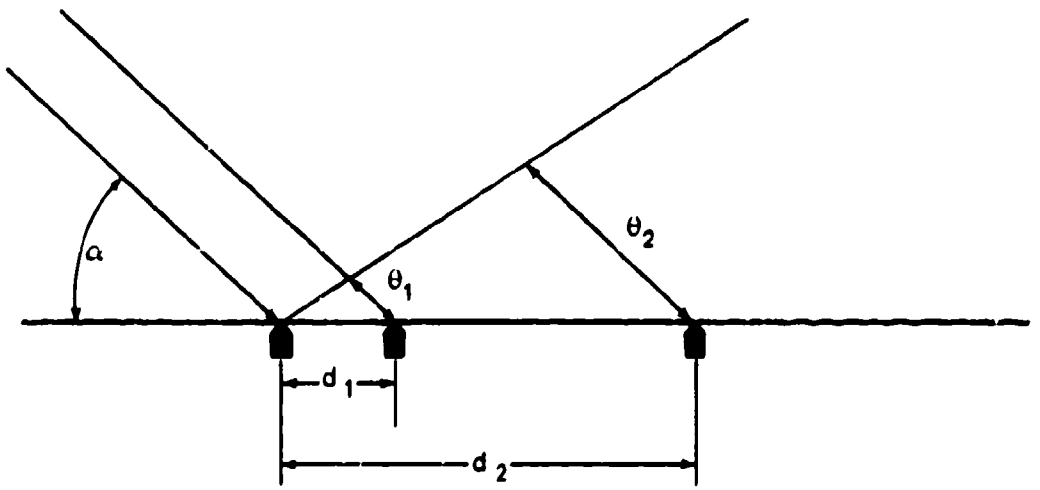

Fig. 20 Wide and narrow spaced antennas. θ = electrical phase difference at two antennas; d_1 = spacing of antennas for ambiguity resolution; d_2 = spacing of antennas for missile guidance; λ = wavelength of signal.

the angle between the LOS and a line joining the two antennas (along the z axis of Fig. 19). In a single plane case or when the target lies in the x-y plane of Fig. 19, the complement of the angle α is β. When the target is out of the plane, the total solution requires taking into account three-dimensional considerations:

From Fig. 20 it is seen that

$$\theta_1 = \frac{2\pi d_1}{\lambda} \cos \alpha , \tag{21}$$

and if

$$\frac{d_1}{\lambda} \leq \frac{1}{2} , \tag{22}$$

14. J. E. Hanson, "On Resolving Angle Ambiguities of n-Channel Interferometer Systems for Arbitrary Antenna Arrangements in a Plane, JHU/APL TG-1224 (Oct 1973).

then

$$\theta_1 \leq \pi \cos \alpha , \tag{23}$$

thus allowing Eq. 21 to be solved unambiguously using the principal value of the arc cosine as follows:

$$\alpha = \cos^{-1} \frac{\theta_1 \lambda}{2\pi d_1} . \tag{24}$$

The angle θ_2 is used for creating the steering signal since it makes use of the maximum aperture d_2. The steering signal is generated from the angular rate obtained from the time derivative of the angle

$$\dot{\theta}_2 = \frac{2\pi d_2}{\lambda} \dot{\alpha} \sin \alpha . \tag{25}$$

This ambiguity resolution technique provides a measurement of α, and thus sin α, so that the proper solution to Eq. 25 is available.

It is often not practical to locate two antennas with half wavelength separation because of physical limitations and mutual coupling problems. An alternative is shown in Fig. 21.

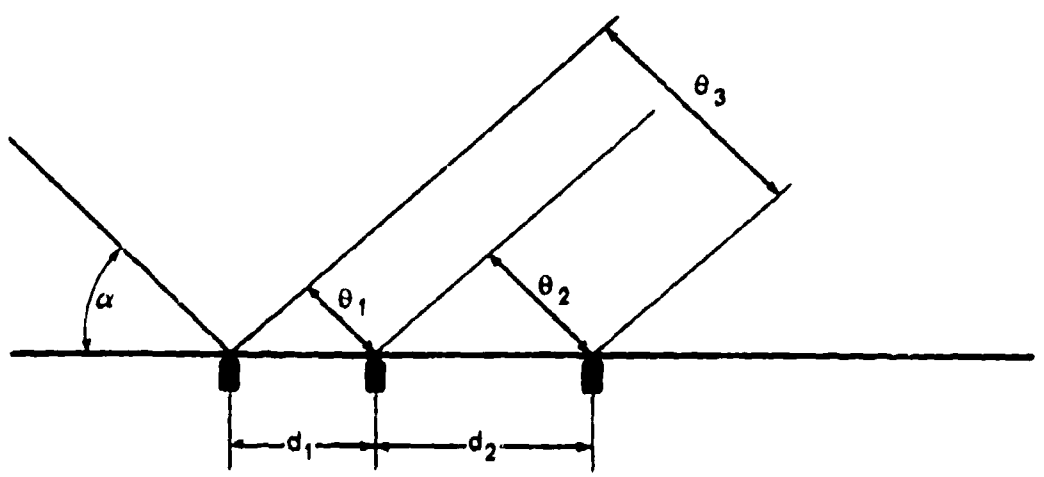

Fig. 21 Alternative antenna configuration using $d_2 - d_1$ for ambiguity resolution.

From this figure, if

$$\theta_1 = \frac{2\pi d_1}{\lambda} \cos \alpha , \tag{26}$$

and

$$\theta_2 = \frac{2\pi d_2}{\lambda} \cos \alpha , \tag{27}$$

then

$$\theta_2 - \theta_1 = \frac{2\pi}{\lambda} (d_2 - d_1) \cos \alpha , \tag{28}$$

If $d_2 - d_1$ is set equal to $\lambda/2$, then

$$\theta_2 - \theta_1 = \pi \cos \alpha \tag{29}$$

and α can be computed again as

$$\alpha = \cos^{-1} \frac{\theta_2 - \theta_1}{\pi} . \tag{30}$$

The spacing $d_1 + d_2$ would be used for guidance, and

$$\theta_3 = 2\pi \frac{d_1 + d_2}{\lambda} \cos \alpha . \tag{31}$$

A separate measurement with antennas along the y axis of Fig. 19 can provide a measurement of γ. β and ψ of Fig. 19 can be computed from the α and γ measurements to point a secondary system, or $\cos \beta$ can be computed. The latter computation will be shown to be necessary in body-motion decoupling as discussed in Chapter 5.

4.3.2 Multiple Frequencies

Use of at least two different frequencies can be shown to be equivalent to using multiple baselines of antennas (see Fig. 22). As shown previously

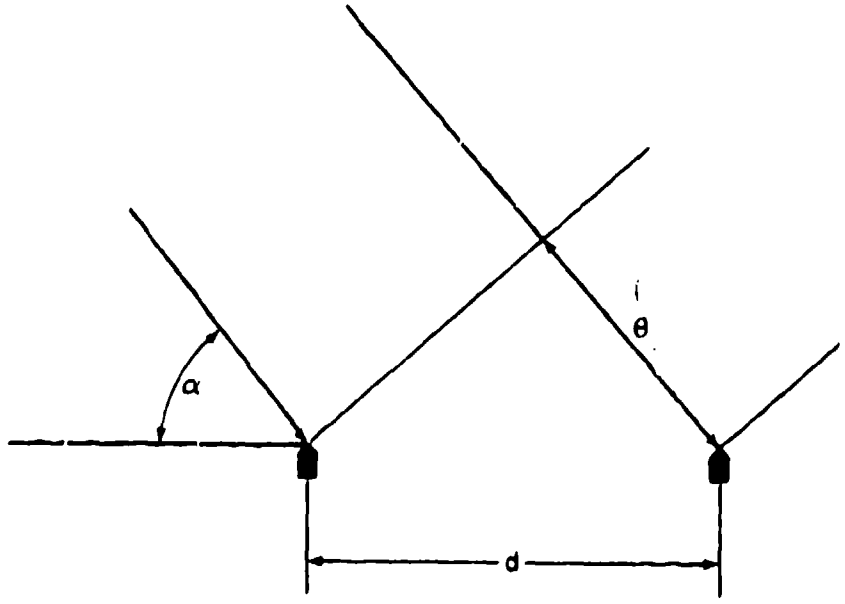

Fig. 22 Interferometer diagram.

$$\theta = \frac{2\pi d}{\lambda} \cos \alpha \, . \tag{32}$$

where λ is the wavelength of the received signal, and θ is the electrical phase difference between the signals in the two antennas and can only be measured from $-\pi$ to $+\pi$ radians. If two frequencies are used with wavelengths λ_1 and λ_2, and the change in θ is measured as a function of the change in λ, then

$$\theta_1 - \theta_2 = 2\pi d \cos \alpha \left(\frac{1}{\lambda_1} - \frac{1}{\lambda_2} \right) . \tag{33a}$$

If λ_1 is approximately equal to λ_2, then

$$\theta_1 - \theta_2 \approx \frac{2\pi d \cos \alpha}{\lambda_1} \left(\frac{\lambda_2 - \lambda_1}{\lambda_1} \right) . \tag{33b}$$

If $(\lambda_2 - \lambda_1)/\lambda_1$ is set equal to $\lambda_1/2d$, then $\theta_1 - \theta_2 = \pi \cos \alpha$, which is unambiguous over the range $\alpha = 0$ to $\alpha = \pi$. Thus the correct value of α can be computed.

4.3.3 Nutating Antennas

An ambiguity resolution technique proposed for use with a Doppler tracking receiver used a separate small antenna driven in a circular motion in a plane normal to the longitudinal axis of the missile. Figure 23, taken from Ref. 13, shows an edge view of the

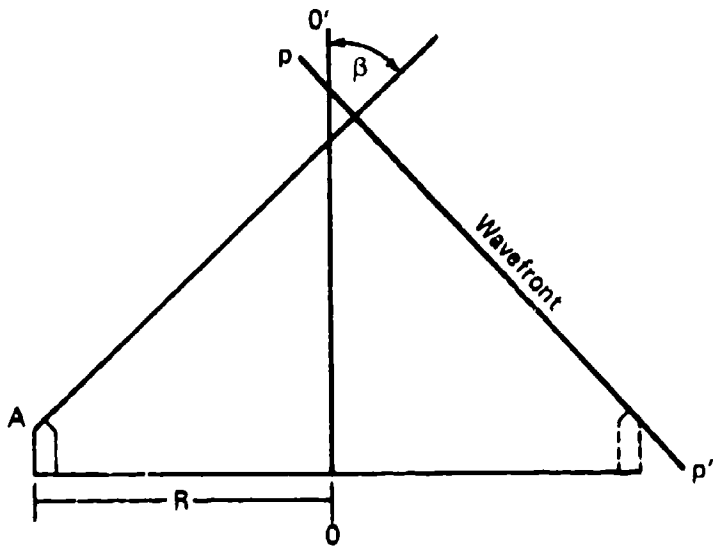

Fig. 23 An edge view of the path of the nutating antenna.

path of the nutating antenna. The Doppler signal received by a stationary antenna on the missile's nose is directly proportional to the missile-to-target closing velocity

$$f_d = \frac{V_c}{\lambda} \, , \tag{34}$$

where f_d is the frequency of the Doppler signal, V_c the missile-target closing velocity, and λ the wavelength of the received signal.

If the missile antenna is not stationary but nutated in a circular path in a plane normal to the missile roll axis as shown in Fig. 23, then the received Doppler signal becomes

$$f_d = \frac{1}{\lambda} \left[V_c + \omega_n R \sin \beta \cos (\omega_n t + \phi) \right] , \tag{35}$$

where ω_n is the angular velocity of the nutation, R the radius of nutation, and ϕ the angle between the target projection in the nutation plane and a missile reference. The deviation of the Doppler signal about its nominal value can be measured with a frequency discriminator producing a signal proportional to

$$\frac{\omega_n}{\lambda} R \sin \beta (\cos \omega_n t + \phi) . \tag{36}$$

The peak amplitude of the sinusoidal signal is a measure of β, and the phase of the signal with respect to a nutation reference signal provides the measurement of the polar angle ϕ.

This technique relies on the use of the phase rate history of a coherent Doppler signal to give the desired measurement. If the received output is not time coherent, e.g., a noise source, the receiver output is only noise, which cannot provide pointing information.

4.3.4 Special Antenna Pattern

4.3.4.1 Skewed Antenna Patterns. In a normal configuration of interferometer antennas the axes of the antennas are parallel. The power differential (as a function of look angle) between the signals from each antenna is essentially zero, and only the time differential is used for angle measurement. However, if the antennas are skewed on the missile such that their beam center is pointed away from the missile centerline by an angle equal to the half angle of the individual patterns, then a coarse unambiguous angle measurement is possible. The differential amplitude measurement can be made through logarithmic amplifiers to provide the necessary dynamic range. Figure 24 shows a conceptual diagram of a system using skewed antennas for ambiguity resolution.

4.3.4.2 Staggered Antenna System. The following discussion of a staggered antenna system for ambiguity resolution is taken directly from Ref. 13. A sketch of the staggered antenna configuration is shown in Fig. 25. Antennas 2 and 4 are in the y-z plane, while antennas 1 and 3 are located in a plane parallel to the y-z plane but a distance s from it. The projection of antennas 1 and 3 upon the y-z plane form, with antennas 2 and 4, the corners of a square of side $d \cos \theta$, where d is the distance between antennas 1 and 2 or 3 and 4, and θ is the angle the line 1-2 makes with its y-z plane projection.

The electrical phase difference between the signals received at antennas 1 and 2 can be calculated thus. First, the centerpoint of the antenna pair is translated to the origin and the antennas projected on the three coordinate axes. Since the translated antenna pair 1-2 is in the y-x plane, only two projected antenna pairs result. One is along the y axis and of length $d \cos \theta$, and the other is along the x axis and length of $d \sin \theta$.

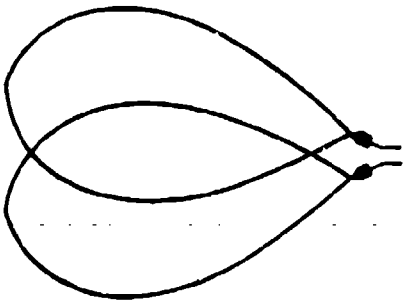

(a) The antenna pattern

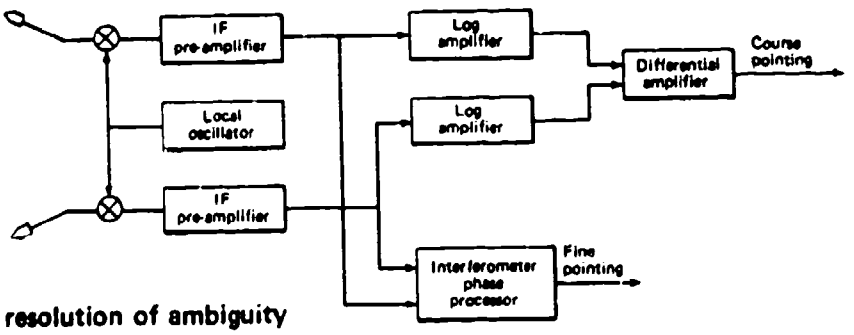

(b) The resolution of ambiguity

Fig. 24 Skewed antennas.

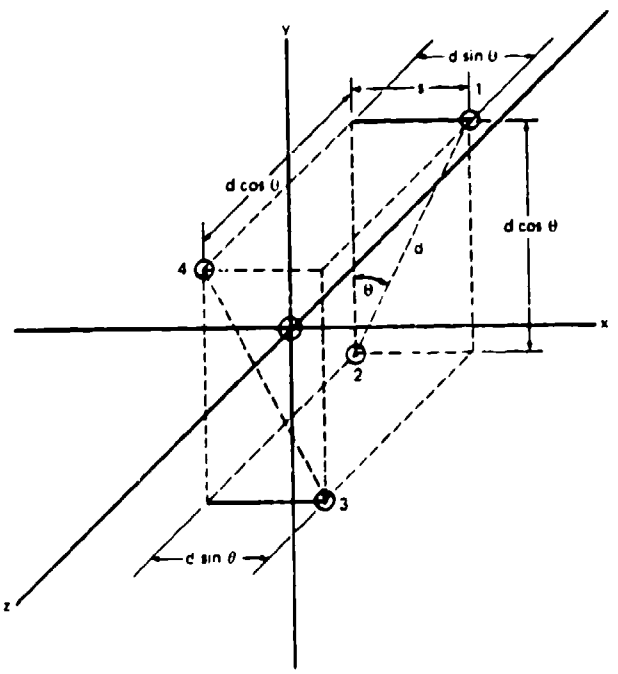

Fig. 25 Sketch of a staggered antenna configuration.

In Fig. 26 the LOS of the target and the projected antenna pairs are shown. The electrical phase difference between the vertical pair of projected antennas 1′-2′ is, according to well-known interferometer theory, equal to $(2\pi d/\lambda)\cos\theta\cos\alpha$, while that between pair 1″-2″ is $(2\pi d/\lambda)\sin\theta\cos\beta$. The differences indicated are the phase at 2′ minus the phase at 1′, and the phase at 2″ minus the phase at 1″. If θ_{21} is the electrical phase difference between antenna 1 and antenna 2, then

$$\theta_{21} = \frac{2\pi d}{\lambda}(\cos\theta\cos\alpha + \sin\theta\cos\beta) \ . \qquad (37)$$

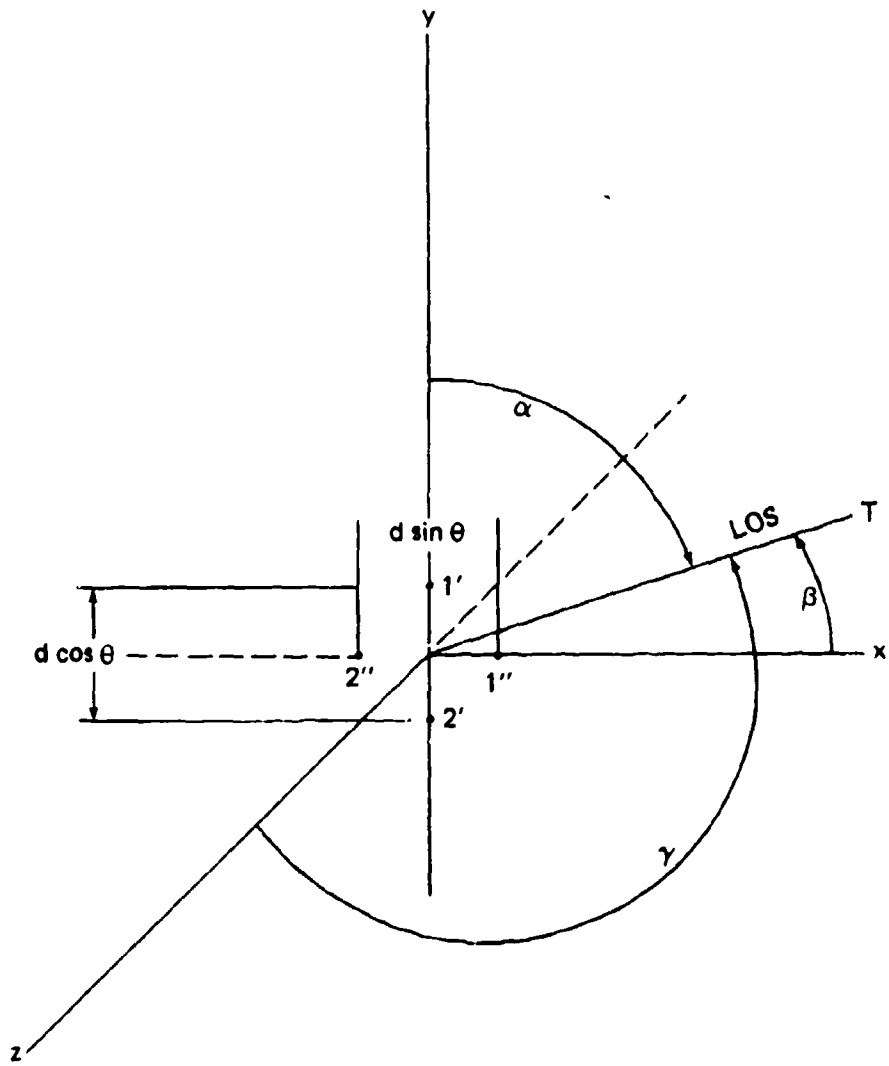

Fig. 26 Line-of-sight and the projected antenna pairs.

Examination of antenna pair 4-3 indicates that its projected antenna pairs will differ from those of 1-2 only in the respect that the angle θ should be changed to $-\theta$.

Therefore, if θ_{34} is the difference between the electrical phase received at 3 and that received at 4, then

$$\theta_{34} = \frac{2\pi d}{\lambda} (\cos\theta \cos\alpha - \sin 6 \cos\beta) . \tag{38}$$

By a similar analysis for pairs 1-4 and 2-3

$$\theta_{14} = \frac{2\pi d}{\lambda} (\cos\theta \cos\gamma + \sin\theta \cos\beta) , \tag{39}$$

and

$$\theta_{23} = \frac{2\pi d}{\lambda} (\cos\theta \cos\gamma - \sin\theta \cos\beta) . \tag{40}$$

Examination of Eqs. 37 through 40 shows that

$$\theta_{21} - \theta_{34} = \frac{4\pi d}{\lambda} \sin\theta \cos\beta , \tag{41}$$

$$\theta_{21} + \theta_{34} = \frac{4\pi d}{\lambda} \cos\theta \cos\alpha , \tag{42}$$

$$\theta_{23} - \theta_{14} = \frac{4\pi d}{\lambda} \sin\theta \cos\beta , \tag{43}$$

and

$$\theta_{23} + \theta_{14} = \frac{4\pi d}{\lambda} \cos\theta \cos\gamma . \tag{44}$$

Thus by taking differences of the phase differences θ_{21}, θ_{34}, θ_{23}, and θ_{14} in pairs one may evaluate cos β. The sums of the phase differences Eqs. 42 and 44 provide the interferometer signal used for guidance.

The preceding analysis, taken from Ref. 13, does not point out that the staggered antenna system measures cos β, not β, and that it can only be used to modify the gain terms of the interferometer equations. It does not provide a β measurement for pointing a secondary system.

4.3.5 Missile-Motion Techniques for Ambiguity Resolution

4.3.5.1 Roll Dither. Roll dither can be used to resolve ambiguity. Reference 13 provides an analysis of a method of computing the unambiguous LOS direction to a target with a scanning interferometer on a missile that is dithered in roll.

Figure 19 provides the nomenclature for this discussion. Figure 27 displays a view of the front of the missile showing the antenna configuration. Antennas 1 and 3 along the y axis measure a function of γ, and antennas 2 and 4 along the z axis measure a function of α.

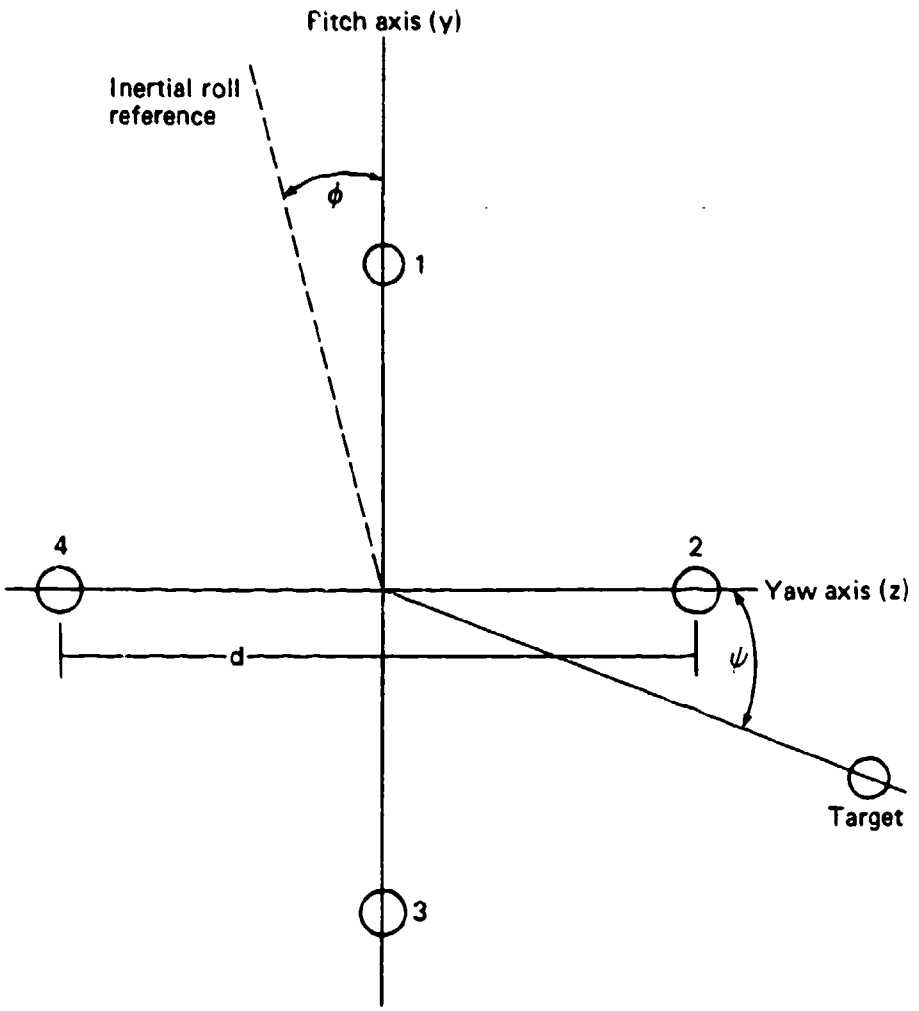

Fig. 27 View looking at front of missile, showing antenna target configuration.

The electrical phase difference between antennas 1 and 3 yields a measurement of γ that is ambiguous every 2π radians of phase, that is

$$\theta_{13} = \frac{2\pi d}{\lambda} \cos\gamma \text{ or } \frac{2\pi d}{\lambda} \sin\beta \sin\psi \,, \tag{45}$$

and for antennas 2 and 4

$$\theta_{24} = \frac{2\pi d}{\lambda} \cos\alpha \text{ or } \frac{2\pi d}{\lambda} \sin\beta \cos\psi \,. \tag{46}$$

If the missile is rolled through a small angle $\Delta\phi$ and phase measurements made again, then

$$\theta'_{13} = \frac{2\pi d}{\lambda} \sin\beta \sin(\psi + \Delta\phi) \tag{47}$$

and

$$\theta'_{24} = \frac{2\pi d}{\lambda} \sin\beta \cos(\psi + \Delta\phi) . \tag{48}$$

Taking the difference between Eqs. 45 and 47 gives

$$\theta_{13} - \theta'_{13} = \frac{2\pi d}{\lambda} \sin\beta [\sin\psi - \sin(\psi + \Delta\phi)] \tag{49}$$

and the difference between Eqs. 46 and 48 gives

$$\theta_{24} - \theta'_{24} = \frac{2\pi d}{\lambda} \sin\beta [\cos\psi - \cos(\psi + \Delta\phi)] . \tag{50}$$

This can be written as

$$\Delta\theta_{13} = \frac{2\pi d}{\lambda} \sin\beta (\sin\psi - \sin\psi\cos\Delta\phi - \cos\psi\sin\Delta\phi) . \tag{51}$$

Since $\Delta\phi$ is a small angle

$$\Delta\theta_{13} \approx -\frac{2\pi d}{\lambda} \sin\beta\cos\psi\sin\Delta\phi = -\frac{2\pi d}{\lambda} \sin\Delta\phi\cos\alpha , \tag{52}$$

and similarly

$$\Delta\theta_{24} = \frac{2\pi d}{\lambda} \sin\beta(\cos\psi - \cos\psi\cos\Delta\phi + \sin\psi\sin\Delta\phi) . \tag{53}$$

Again assuming $\Delta\phi$ to be small

$$\Delta\theta_{24} \approx \frac{2\pi d}{\lambda} \sin\beta\sin\psi\sin\Delta\phi = \frac{2\pi d}{\lambda} \sin\Delta\phi\cos\gamma . \tag{54}$$

If the absolute value of $\sin\Delta\phi$ is less than $\lambda/2d$, then the absolute values of $\Delta\theta_{13}$ and $\Delta\theta_{24}$ are less than π. Therefore they can be measured unambiguously for $\cos\alpha$ and $\cos\gamma$.

In a practical use of roll dither to solve ambiguities, several points must be considered:

1. If the roll dither is continued throughout the homing phase, the frequency of the dither must be sufficiently high to allow a filter to separate the dither from the guidance signal.
2. If the dither is used only for initial angle acquisition, some form of signal is required to indicate that angle acquisition is complete.
3. The frequency selected for roll dither must be well removed from the natural pitch and yaw weathercock frequencies.
4. If the measurements of $\Delta\theta_{13}$ and $\Delta\theta_{24}$ are continuous as a function of roll position, and the instrumentation of the measurements can follow phase changes of greater than 2π radians, then there is no restriction on the amplitude of the roll motion $\Delta\phi$.
5. Increasing the amplitude of the roll dither will improve the S/N of the angle measurement.

4.3.5.2 Rolling Interferometer. Rolling interferometers measure β and ψ directly. Referring to Figure 27, assume a pair of antennas 2 and 4 located on the z axis. As shown earlier, the phase difference between these antennas is given by

$$\theta_{24} = \frac{2\pi d}{\lambda} \cos\alpha = \frac{2\pi d}{\lambda} \sin\beta \cos\psi \ . \tag{55}$$

If the missile is rolled 2π radians about the x axis of Fig. 19, and θ_{24} is measured continuously including changes of more than 2π radians, then $\cos\psi$ varies from $+1$ to -1 with two positions of $\cos\psi = 0$ ($\pi/2$ and $3\pi/2$). The peak-to-peak deviation of θ_{24} is $(4\pi d/\lambda) \sin\beta$ and

$$\beta = \sin^{-1}\left[\frac{\lambda}{4\pi d} \text{ (peak-to-peak deviation of } \theta_{24})\right], \tag{56}$$

which is unambiguous; ψ can be determined by the roll position where $\theta_{24} = 0$.

A method of instrumenting this technique is shown in Fig. 28. The signals at points 1 and 2 are the signals directly from the interferometer antennas or by way of a conversion and intermediate amplifier. The phase changes are transferred to a low frequency carrier (ω_0) without loss of phase sensitivity. The carrier signal ω_0 at point 8 has a sinusoidal peak-to-peak phase deviation of $(4\pi d/\lambda_2) \sin\beta$ radians. Since this deviation is sinusoidal, the phase rate is given by point 9, and an unambiguous measurement of β is given by point 10 as the peak-to-peak amplitude of a signal at the frequency ω_r (roll rate). A more complete description of this process is given in Refs. 15 and 16.

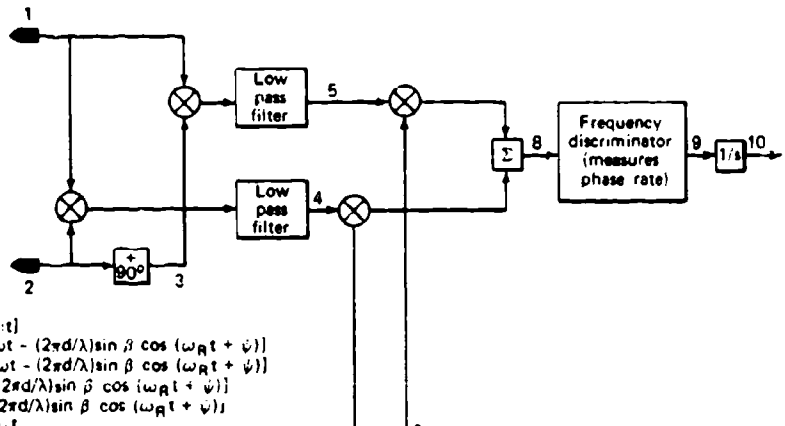

1. $\sin[\omega_0 t]$
2. $\sin[\omega t - (2\pi d/\lambda)\sin\beta \cos(\omega_R t + \psi)]$
3. $\cos[\omega t - (2\pi d/\lambda)\sin\beta \cos(\omega_R t + \psi)]$
4. $\cos[(2\pi d/\lambda)\sin\beta \cos(\omega_R t + \psi)]$
5. $\sin[(2\pi d/\lambda)\sin\beta \cos(\omega_R t + \psi)]$
6. $\cos\omega_0 t$
7. $-\sin\omega_0 t$
8. $\sin[(2\pi d/\lambda)\sin\beta \cos(\omega_R t + \psi)] \cos\omega_0 t - \cos[(2\pi d/\lambda)\sin\beta \cos(\omega_R t + \psi)] \sin\omega_0 t$
   $= \sin[(2\pi d/\lambda)\sin\beta \cos(\omega_R t + \psi) - \omega_0 t]$
   $= -\sin[\omega_0 t + (2\pi d/\lambda)\sin\beta \cos(\omega_R t + \psi)]$
9. $-\omega_R(2\pi d/\lambda)\sin\beta \sin(\omega_R t + \psi)$
10. $(2\pi d/\lambda)\sin\beta \cos(\omega_R t + \psi) + K$

Fig. 28 Rolling interferometer signal processing.

15. J. F. Gulick, Jr. and J. E. Hanson, "Interferometric Rolling Missile Body Decoupling Guidance System," United States Patent No. 3,897,918 (5 Aug 1975).
16. J. F. Gulick, J. S. Miller, and A. J. Pue, "Broadband Interferometer and Direction Finding Missile Guidance System," United States Patent No. 4,204,655 (27 May 1980).

A significant advantage of this technique is the use of the full antenna separation for ambiguity resolution as well as steering. This provides a continuous measure of the LOS with the best available S/N, and it will be shown later that body decoupling techniques are available to provide an inertial measurement of the LOS rate as required for a proportional navigation guidance law.

4.3.6. Broadband Implications

4.3.6.1 Path Length Matching for Broadband Applications. In some applications where an interferometer is used, it is necessary to maintain good angle track on signals that cover a reasonably wide RF spectrum. The angle measurement equations shown in the previous paragraphs show a fundamental relationship between the phase measurement and the wavelength λ of the signal. An error in the known value of λ gives an error in the angle measurement. There is, in addition to this fundamental relationship, another source of error that is sometimes neglected since most of the interferometer applications ultimately depend on phase rate as opposed to absolute phase difference. This additional error source is created by unequal path lengths from the two interferometer antennas to the phase measuring receiver.

Figure 29 shows an interferometer with unequal cable lengths from the antennas to the receiver. The path length difference between antennas 2 and 1 is $d \cos \gamma$, and the electrical difference is $(2\pi d/\lambda) \cos \gamma$ radians. Obviously this can be greater than 2π radians for large values of d/λ. When γ approaches $\pi/2$, then the term $(2\pi d/\lambda) \cos \gamma$ approaches zero, and the sensitivity to changes in λ approaches zero. Unfortunately, the phase difference

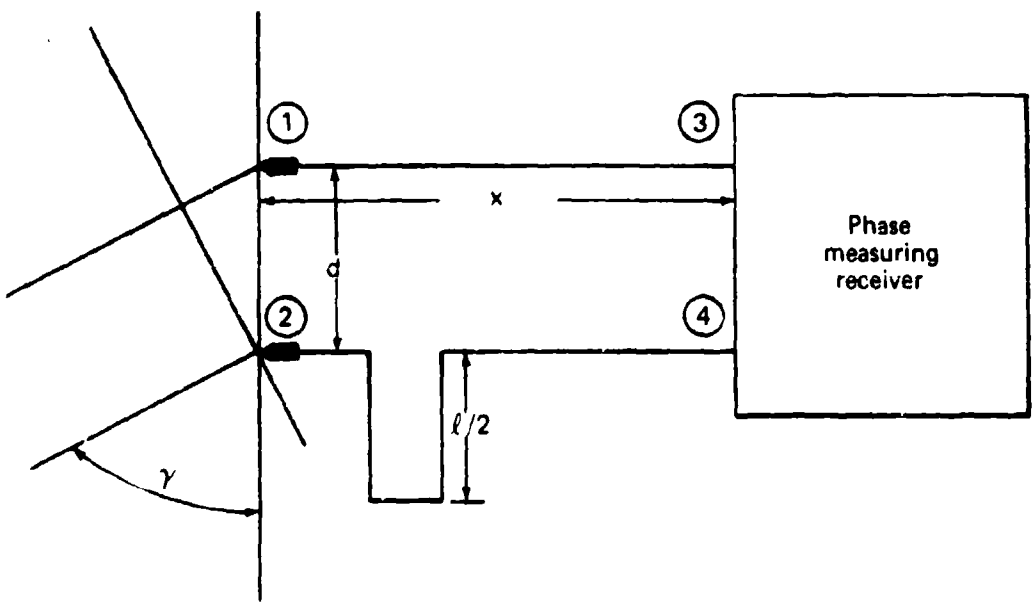

Fig. 29 An interferometer with unequal line lengths.

measurement is not made at the antennas but is made at the end of cables of some length. If the cable from 1 to 3 is length x and the cable from 2 to 4 is length x + ℓ, then the phase difference between 4 and 3 is given by

$$\theta_{43} = \frac{2\pi d}{\lambda} \cos\gamma - \frac{2\pi}{\lambda}(x + \ell - x)$$
$$= \frac{2\pi d}{\lambda} \cos\gamma + \frac{2\pi \ell}{\lambda} \text{ radians} . \qquad (57)$$

In a particular missile application where this path length difference was ignored, the physical layout resulted in a cable length difference of 12 wavelengths. A receiver with an instantaneous bandwidth of 1% operating on a broadband signal had phase noise that was intolerably large until the line lengths were adjusted.

4.3.6.2 Microwave Trombone. One application of interferometer guidance used frequency agility over a 10% RF bandwidth and required a look angle up to 60° off the roll axis of the missile. Since the phase measurement is actually a time difference measurement contaminated by changes in microwave frequency, a development shown in Fig. 30 was attempted that was inherently immune to frequency changes. This development used an adjustable length microwave trombone to internally match the external time difference between the signals at the two antennas. The adjustable line must be set to within one-half wavelength of the proper position by the coarse unambiguous cos β measurement — then the interferometer phase measurement can maintain a fine track. From Fig. 30 it can easily be seen that the total range of travel of the adjustable line must be equal to $2d$ times the absolute value of cos γ_{max}.

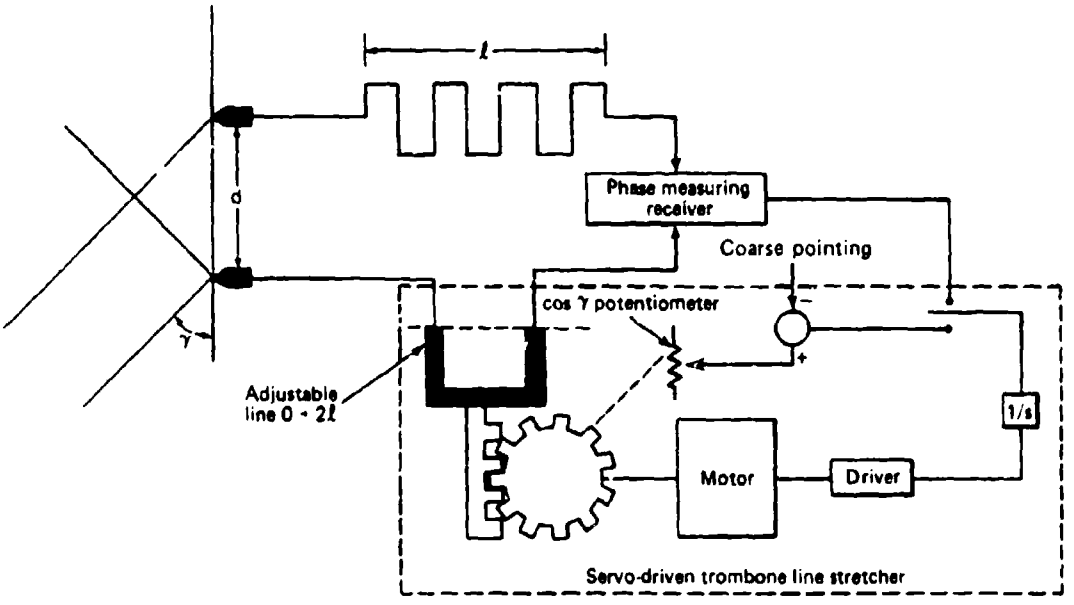

Fig. 30 Interferometer with mechanical line stretcher.

It is also readily apparent that if the line stretcher is adjusted to have zero phase difference at the receiver for any microwave frequency, it is also zero for all frequencies and is therefore frequency independent. It will be shown later that body-motion decoupling can occur via the line stretcher. Although the concept of a mechanically adjusted line was sound, the practical implementation was extremely difficult. The most severe problems were:

1. The VSWR caused by impedance mismatch varied with both frequency and position. The changing VSWR created a changing phase shift and angle error.

2. The mechanically sliding contacts created noise in the system.

3. The servo time delay was a critical factor when the body motion decoupling was inserted via the line stretcher.

4.3.6.3 Digital Line Stretcher (UHF). An application of interferometer guidance using radio frequencies in the 100 to 200 MHz band employed a variable line length produced by using diodes to switch in or out various line lengths. The changes in line lengths were binary ratios to provide a simple method of control. Figure 31 shows a conceptual diagram of this system. The diode switches were driven by signals from a body-mounted gyro to provide data stabilization or body decoupling. This will be discussed in detail in Chapter 5.

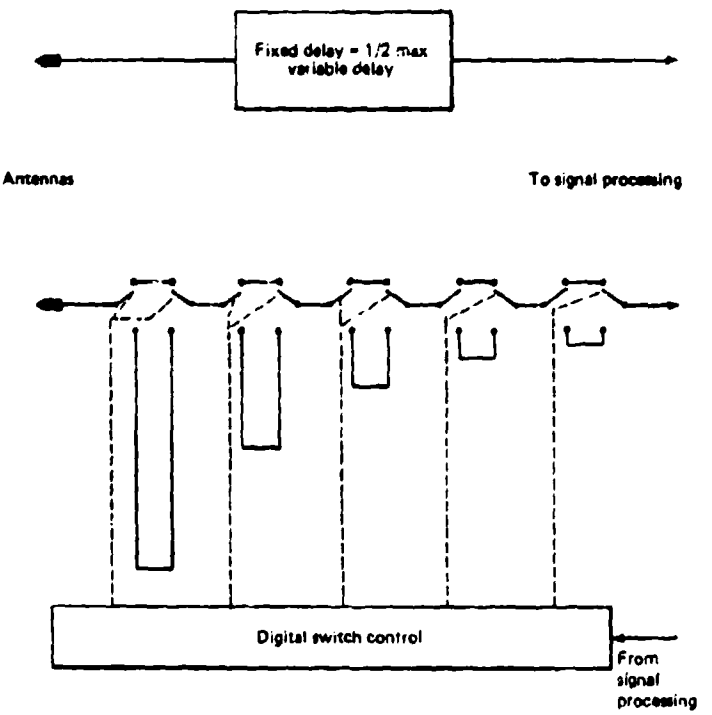

Fig. 31 Interferometer with digital line stretcher.

4.3.6.4 Microwave Digital Line Stretcher. A missile using continuous roll to eliminate angular ambiguities (as discussed in sub-subsection 4.3.5.2) also uses a digitally controlled microwave line stretcher. Figure 32 from Ref. 16 shows a diagram of an interferometer seeker using these techniques.

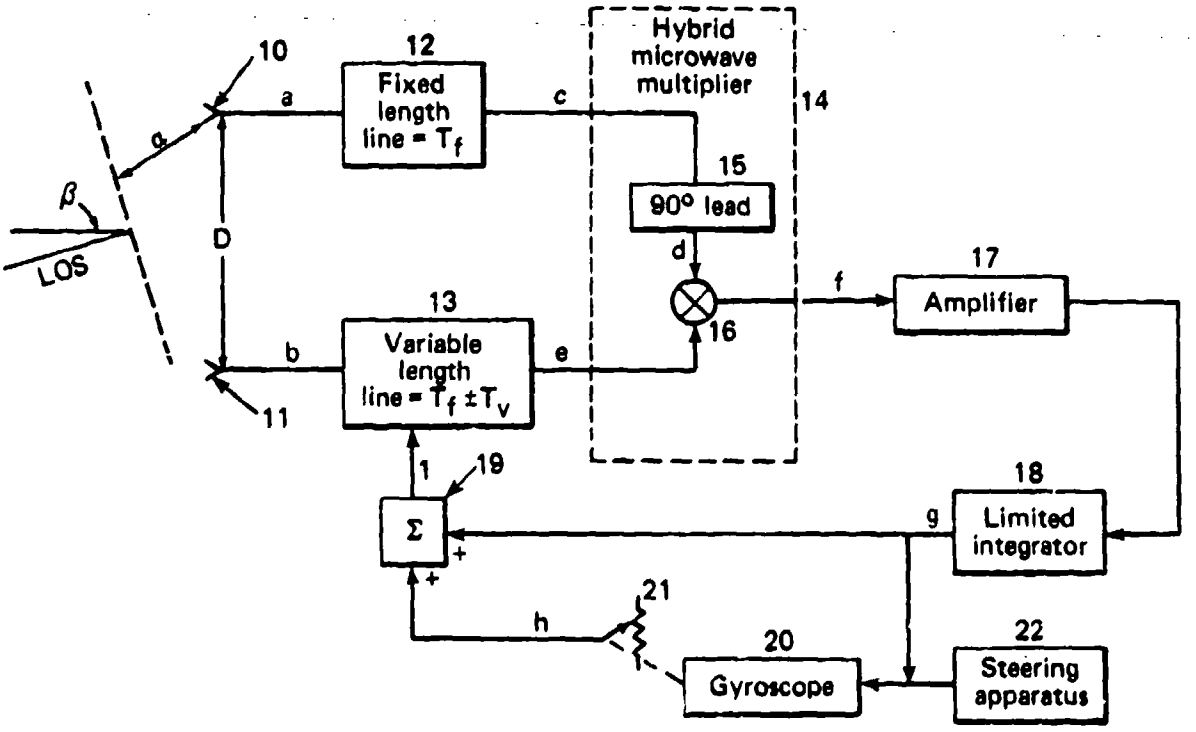

Fig. 32 Rolling interferometer using digital line stretcher.

A digital line stretcher for this application is currently in development. The upper frequency limit of the experimental unit is above 15 GHz while the lower frequency limit is probably below 2 GHz although no attempt was made to determine the lower limit. A schematic of the experimental line stretcher is shown in Fig. 33 and a typical set of test data is shown in Fig. 34, taken from Ref. 17. Detailed measurements on the experimental unit are also given in that reference.

4.3.7 Phase Measurement

Interferometer guidance depends on the measurement of the phase difference of signals entering two widely spaced antennas. As mentioned previously, the relative position or rate of the target with respect to the airframe is measured by the interferometer receiving system. The airframe motion with respect to inertial space is subtracted from the in-

17. D. K. Larson, "Performance of the Microwave Associates MPM-258 Line Stretcher," JHU/APL FIB79U-137 (26 Nov 1979).

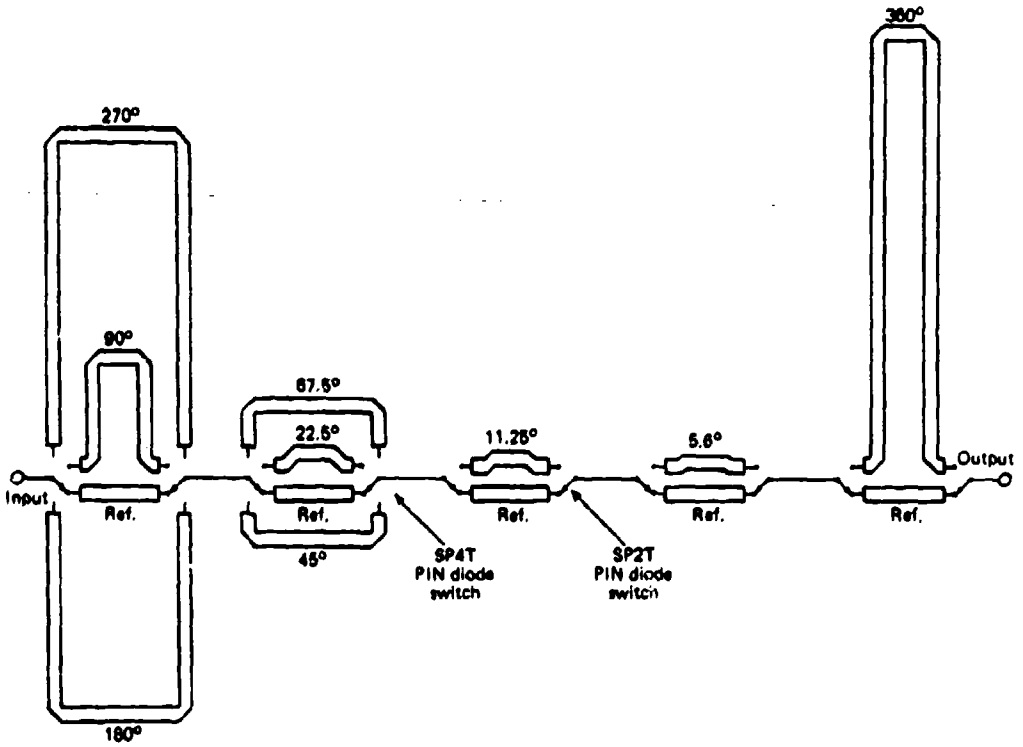

Fig. 33 Schematic diagram of 7-bit line stretcher (from Ref. 14).

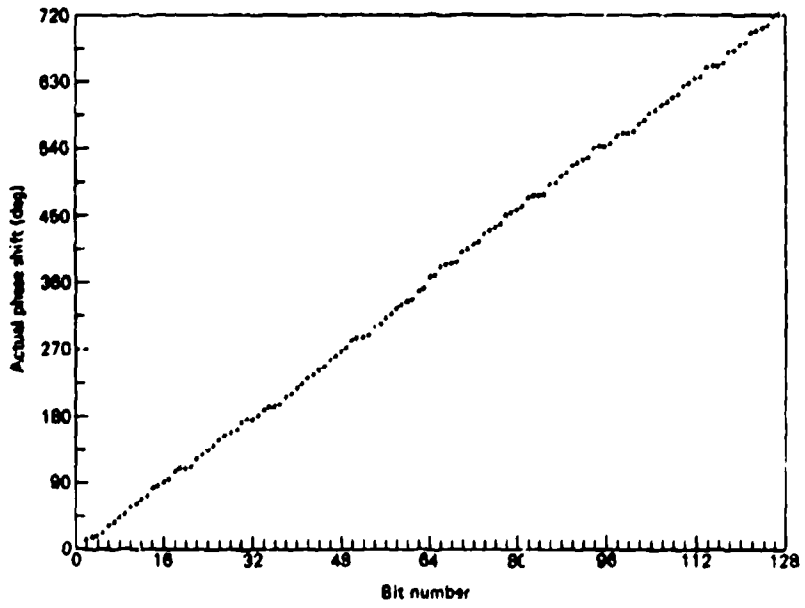

Fig. 34 Phase shift versus bit number (from Ref. 14).

terferometer signal to provide the missile-to-target LOS rate in inertial space. Small errors in the measurement of relative position or rate of the target with respect to the missile body result in large errors in the measurement of the LOS rate.

There are two primary sources of errors that affect the interferometer process. These are:

1. Multipath reflections from other portions of the missile airframe that distort the wave front as it reaches the antennas; and
2. Signal processing that produces an output proportional to the electrical phase difference between two microwave inputs at the antenna.

A detailed discussion of both of these errors is given in Ref. 1. This reference discusses the allowable error due to both causes as a function of the antenna separation, measured in wavelengths of the signal.

4.3.7.1 Multipath Errors. A simple example taken from Ref. 1 shows how a multipath signal leads to boresight error and error-slope values that change with target aspect angle β. The peak boresight error slopes are determined by the relative level of the multipath signal (ρ), but the angle rate at which the error slope varies and its effect on the guidance loop are determined by the interferometer separation in wavelengths.

To illustrate this dependence, consider an interferometer with a scatterer, such as a nosecone tip, located between the two antennas as shown in Fig. 35a. Assume that the scattered signal received at each antenna is the same and does not vary with β. While this is an over-simplified assumption, it still allows a valid comparison to be made of the results of different d/λ spacings.

In the phase diagram of Fig. 35b, one antenna is advanced in phase, and one is retarded by the maximum amount. This may happen very easily as the multipath geometry changes. According to the diagrams, the maximum interferometer phase error is

$$\epsilon = 2\psi = 2\sin^{-1}\rho \,. \tag{58}$$

This phase error may be used to show the resulting boresight as a function of multipath level; that is,

$$\text{boresight error} = \frac{\sin^{-1}\rho}{\pi(d/\lambda)\cos\beta} \,. \tag{59}$$

The error is in spatial degrees and may swing plus or minus by this amount as the multipath geometry changes. Boresight errors, calculated with Eq. 59 are plotted in Fig. 36 for various multipath levels. These errors are at $\beta = 0°$, and the off-boresight errors will increase. The errors may also be calculated as a function of d/λ and β for a fixed value of ρ using Eq. 59.

The boresight errors and boresight error slopes for an interferometer with $d/\lambda = 4$ and a multipath level of -30 dB are plotted in Fig. 37. Both the errors and their periods increase with β. Boresight error slopes are plotted in Fig. 38 for d/λ equal to 1, 2, 4, and 8. The peak slopes remain the same (0.036 when $\rho = -30$ dB), while the period decreases with increasing d/λ.

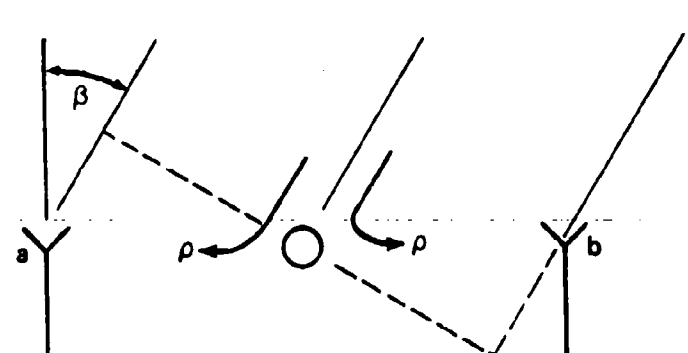

(a)

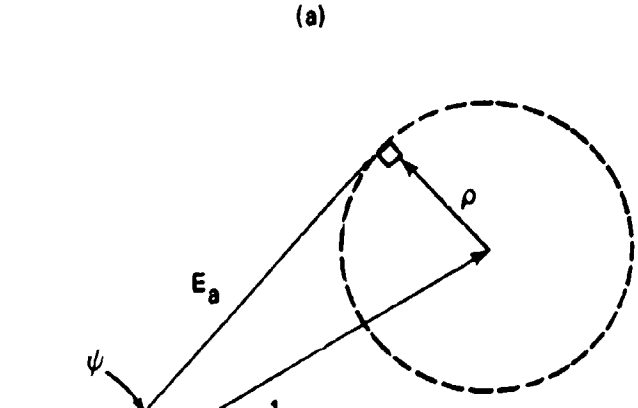

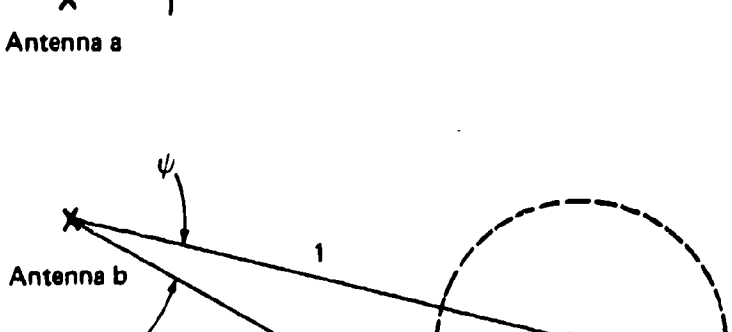

(b)

Fig. 35 Phase errors from multipath reflections.

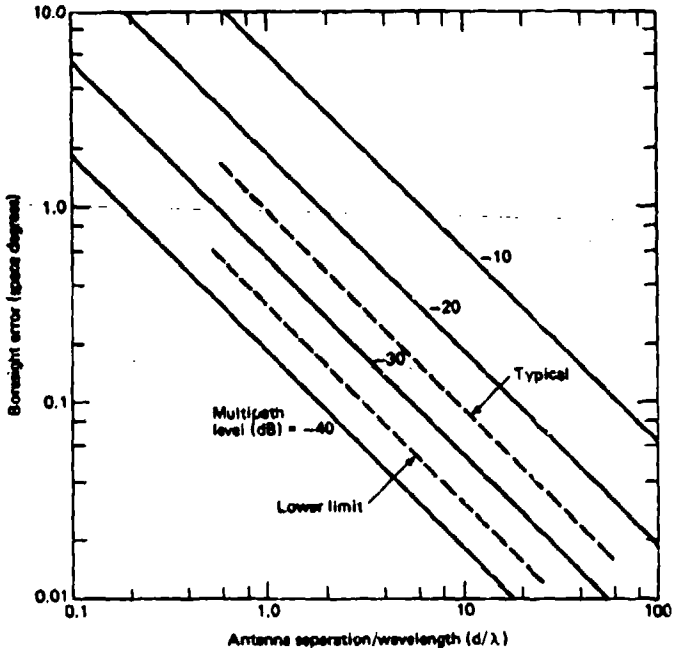

Fig. 36 Interferometer angle error caused by multipath, $\beta = 0°$.

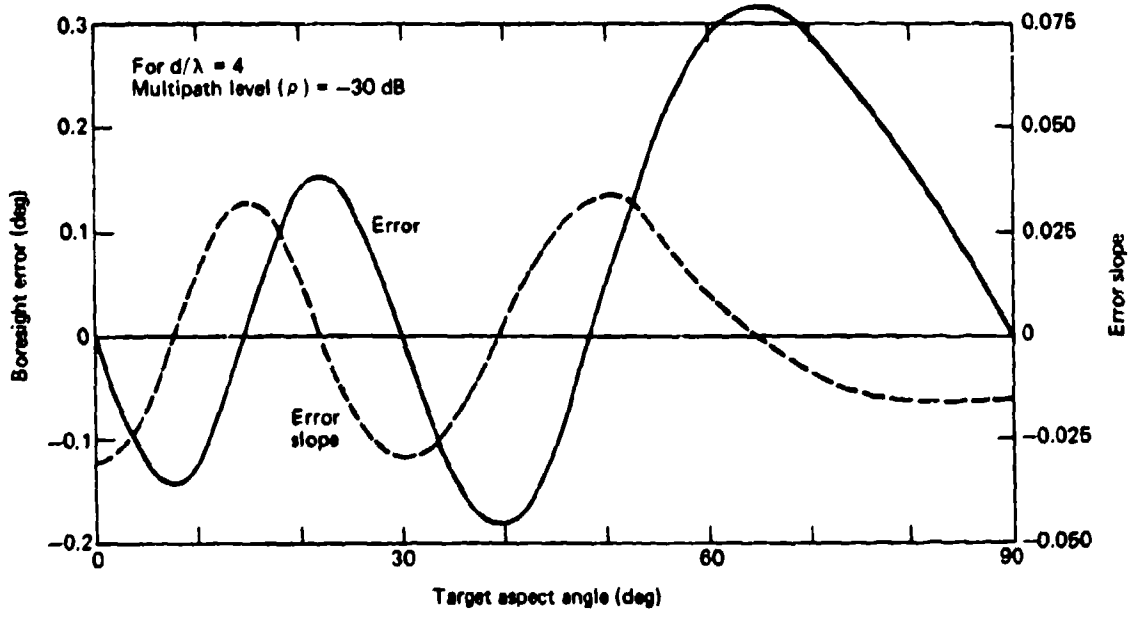

Fig. 37 Interferometer boresight error and error slope caused by multipath from the nose-cone tip.

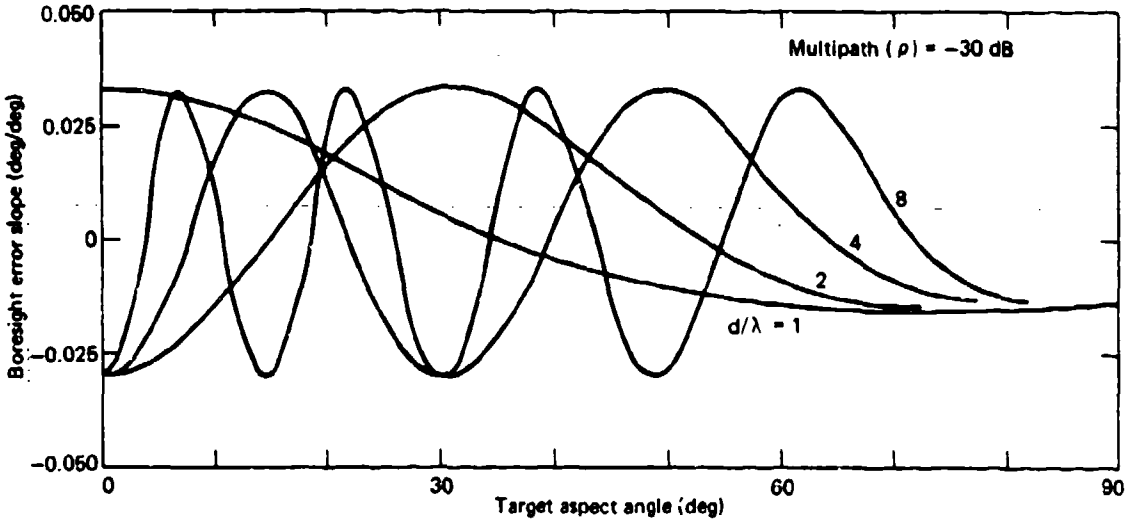

Fig. 38 Interferometer boresight error slope caused by multipath from the nose-cone tip.

4.3.7.2 Polarization Errors. In a missile where the incident polarization is controlled by the missile user, such as active or semiactive receivers, the polarization of the receiving antennas can be matched to that of the incident radiation. There are, however, some situations such as passive mode homing where the missile user neither knows nor controls the polarization to be received. Furthermore, the polarization may be changing slowly or rapidly. Reference 18 provides an analysis of the effects of mismatched polarization on an interferometer system. This analysis assumes that the only radiation received by the antennas comes directly from the target. When conditions approaching cross polarization exist for the direct signal, the multipath signal from a reflection on the missile airframe (as discussed in the previous section) may be more significant.

One conclusion from Ref. 18 is as follows:

> When the incident polarization is predominantly linear, but with an unknown tilt angle, a circular polarized receiving antenna is preferable, and if the incident polarization is predominantly circular but with unknown sense, a linear receiving antenna is preferable.

Another conclusion that may be drawn is that in the absence of any hard intelligence information on a radar target it is probably best to use circularly polarized receiving antennas for an ARM since most radars transmit linear polarization.

In some applications it may be necessary or desirable to operate interferometer antennas behind a radome. Reference 19 discusses the effects of this type of operation. The particular configuration that prompted this analysis was a gimballed interferometer behind a nonsymmetrical aircraft radome.

18. D. R. Marlow, "Interferometer Phase Errors Caused by Receiver Antenna Polarization Mismatches — For Plane Waves of All Polarization Types," JHU/APL MED-SF/220 (10 Sep 1968).
19. R. C. Mallalieu, "The Effect of Incident Polarization on an Interferometer Antenna Behind a Radome," JHU/APL MED-SR/160 (20 May 1969).

4.3.7.3 Phase Measurement Errors. In Ref. 1 a discussion of phase measurement shows some of the sources of error. It has been shown that the electrical phase difference between the signals at the two antennas is given by

$$\theta = \frac{2\pi d}{\lambda} \sin \beta \, . \tag{60}$$

Differentiation with respect to β gives the phase slope or "interferometer gain"

$$\frac{d\theta}{d\beta} = \frac{2\pi d}{\lambda} \cos \beta \, . \tag{61}$$

If ϵ represents the interferometer phase error measurement in radians, then the angle error in the interferometer system is given by:

$$\text{angle error} = \frac{\epsilon}{d\theta/d\beta} = \frac{\frac{360}{2\pi}\epsilon}{\frac{2\pi d}{\lambda} \cos \beta} \text{ space degree} \tag{62}$$

and

$$\text{error slope} = \frac{d}{d\beta}\left(\frac{\epsilon}{d\theta/d\beta}\right) \text{degrees/degree} \, . \tag{63}$$

The methods used to measure phase difference require the use of I (in phase) and Q (quadrature) phase comparators as well as a method of reconstructing the angle from these comparator outputs. Figure 39 shows the signals available at the output of the I and Q comparators. The phase angle of interest (θ) is obtained by circuits that solve the equation

$$\theta = \tan^{-1} \frac{V_1 \sin \theta}{V_2 \cos \theta} \, . \tag{64}$$

The assumption is, of course, that the 90° lag is precisely 90° and that $V_1 = V_2$. In practical circuits neither the angle nor the amplitudes are precise, and a cyclical error is produced that is a function of θ. If we assume that the amplitudes are related as $V_1/V_2 \approx 1 + \delta$, and the 90° phase lag can be expressed as $90 + \alpha$ degrees, then an expression can be derived to provide the measurement error as a fuction of θ:

$$\epsilon \text{ (radians)} \approx \frac{\delta}{2} \sin 2\theta + \alpha \cos^2 \theta \, . \tag{65}$$

For values of δ less than 0.2 and values of α less than 0.2 radians, Eq. 65 will approximate the error in phase measurement. The effect of this phase measurement error on boresight error and boresight error slope was computed using values that are characteristic of an excellent measurement system, i.e., $\delta = 0.06$ (0.5 dB), $\alpha = 0.088$ radians (5°), and d/λ ratios of 0.5, 1.0, 2.0, and 3.0. These errors are typical of the capability of good laboratory test equipment such as the Hewlett-Packard Microwave Network Analyzer. The representative boresight error curves in Fig. 40 show that for a given phase error the boresight errors vary with d/λ (antenna separation in wavelengths). Reference 1 discusses these effects in greater detail; however, it has been shown that greater error magnitudes can be tolerated if the period with respect to aspect angle is small.

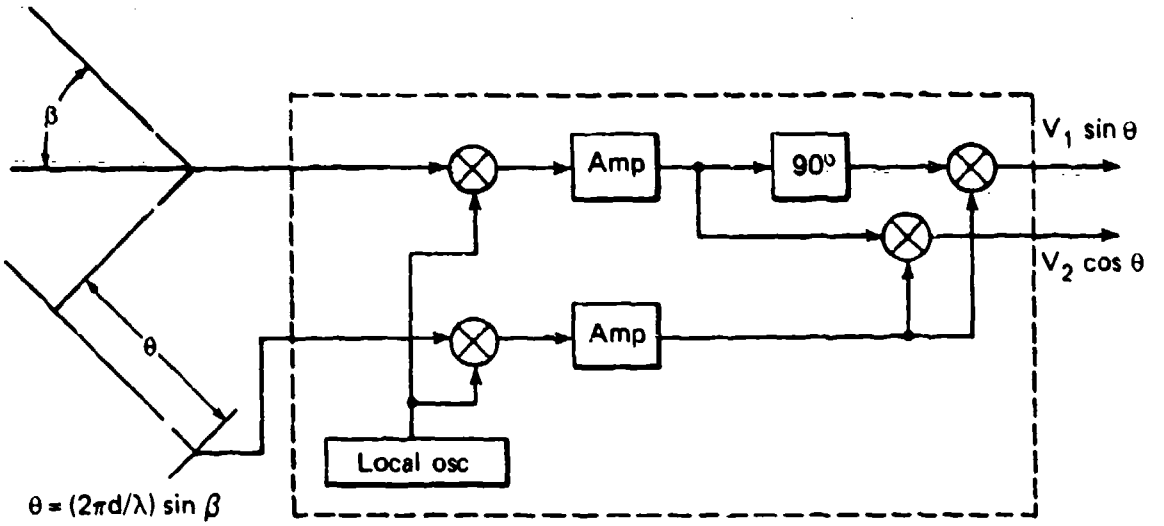

Fig. 39 Diagram of interferometer signal processing.

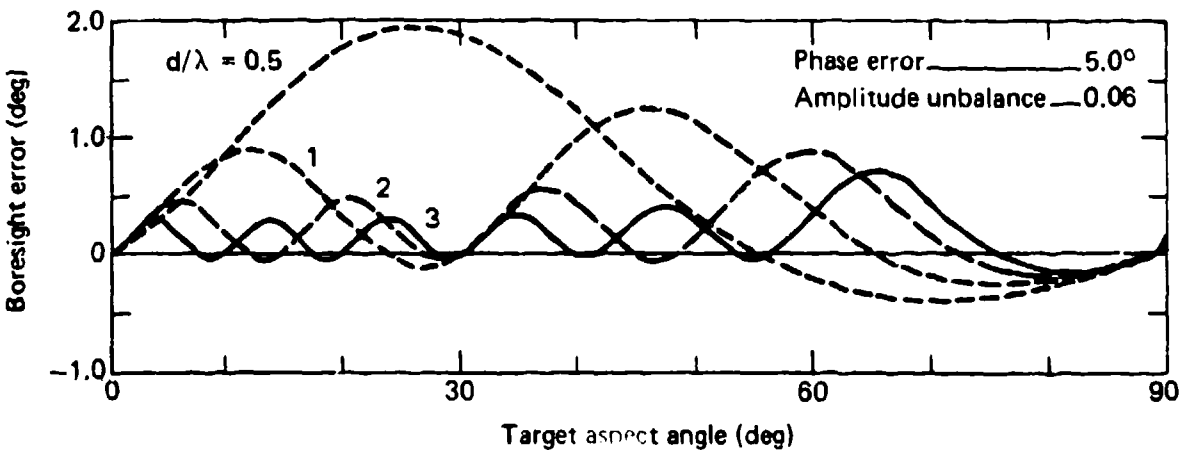

Fig. 40 Boresight error versus look angle for various values of d/λ.

Figure 39 shows a simplified diagram of interferometer signal processing. As shown in that figure, the signals from each antenna may be amplified separately prior to the phase comparison. Obviously any differential change in phase between the two amplifiers as a function of amplitude, or Doppler frequency in continuous wave (CW) systems, creates an apparent target motion. With proper attention to the phase shift vs. amplitude or automatic gain control (AGC) level, it is possible to provide adequate performance. In some applications in an ARM mode of operations, commutating techniques have been employed that interchanged the channels on a pulse-to-pulse period. This effectively eliminates errors due to amplifier differences.

4.3.7.4 Early Scanning Interferometer System (pre-1955). Figure 12 shows the block diagram of a scanning system. In an effort to avoid some of the problems associated with the I and Q phase measuring process and the differential phase shift between amplifiers, the early interferometer systems used a continuously scanning phase shifter in one antenna line. This was actually a form of multiplexing the two antenna signals into a single amplifier. The multiplexing eliminates errors due to differential phase shift that would occur in separate amplifiers The particular technique used by DRL had a significant advantage that may not have been recognized by the originators. During countermeasures tests against a broad-band noise source, it was discovered that scanning phase shifters located in the antenna or local oscillator lines (Figs. 41a and 41b) will provide the same steering sense for

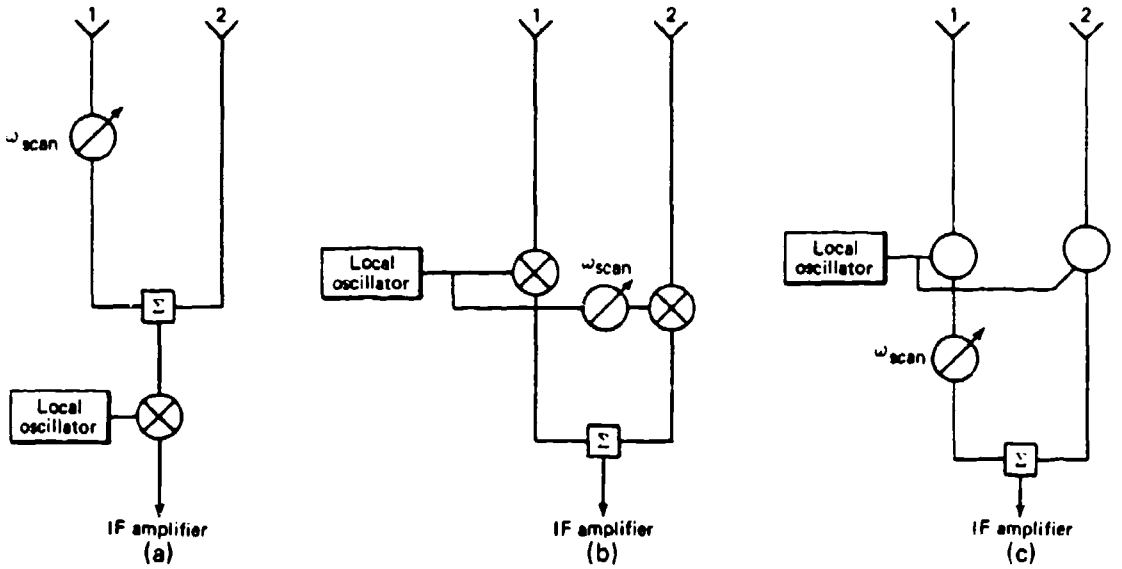

Fig. 41 Phase shifter locations for scanning interferometers.

input RF signals above or below the local oscillator at the IF frequency difference, but the configuration of Fig. 41c has reversed steering sense for signals above or below the local oscillator frequency. A complete analysis of this pehenomena is given in Ref. 7. A brief description of each configuration is as follows: In all three configurations assume that the scanning phase shifter adds phase continuously. Therefore, the frequency at the output of the phase shifter is the input frequency plus the scan frequency and a target moves from left to right such that the frequency seen by antenna 2 is incrementally higher than the frequency seen by antenna 1. It is necessary that the resulting scan frequency detected by the amplitude modulation of the signal in the IF amplifier be independent of the relationship between the input signal and the local oscillator, i.e., above or below the local oscillator by an amount equal to the IF amplifier center frequency.

In Fig. 41a, if we assume ω_s = 200 Hz, a target rate such that ω_{ant2} = 10 Hz above ω_{ant1}, ω_{LO} = 10 GHz, and ω_{ant1} = 10.060 GHz; then the signal in the IF from antenna 1 is 10.06 GHz + 200 Hz − 10 GHz = 60.0002 MHz. The signal from antenna 2 is 10.06 GHz + 10 Hz − 10 GHz = 60.000010 MHz. The amplitude modulation detected at the output is 60.0002 MHz − 60.000010 MHz = 190 Hz.

Again using Fig. 41a, assume the same ω_{s}, target rate, and ω_{LO}, but with ω_{ant1} = 9.94 GHz; then the signal in the IF for antenna 1 is 9.94 GHz + 200 Hz − 10 GHz = 59.999800 MHz and for antenna 2 is 9.94 GHz + 10 Hz − 10 GHz = 59.999990 MHz. The amplitude modulation difference frequency is 190 Hz — the same as in the first example. If we use Fig. 41b, a numerical example will yield the same results as those obtained with Fig. 41a.

Using Fig. 41c, if we assume ω_{ant1} = 10.06 GHz, ω_{ant2} = 10.06 GHz + 10 Hz, and ω_{LO} = 10 GHz; then the signals in the IF are: for antenna 1, 10.06 GHz − 10.0 GHz + 200 Hz = 60.000200 MHz, and for antenna 2, 10.06 GHz − 10 GHz + 10 Hz = 60.000010 MHz. The amplitude modulation detected at the output is 60.000200 − 60.000010 = 190 Hz. Again assuming the above conditions but with ω_{ant1} = 9.94 GHz and ω_{ant2} = 9.94 GHz + 10 Hz, then the signals in the IF are for antenna 1, |9.94 GHz − 10.0 GHz| + 200 Hz = 60.000200 MHz, and for antenna 2, |9.94 GHz + 10 Hz − 10 GHz| = 59.999990 MHz. The amplitude modulation detected at the output is now 210 Hz. It can be seen that a discriminator centered at 200 Hz (scan frequency) would provide opposite polarity voltage for the same target motion as a function of RF signal frequency above or below the local oscillator. This would result in reversed interferometer sense.

One problem that occurs with a system that multiplexes two signals into a single amplifier is the susceptibility to interference at the frequency of multiplex or scan. If the scan detection process derives information from the amplitude modulation at frequencies near the scan frequency, the error signals can be contaminated. The problems with the result are similar to those associated with a conical scan receiver, though not quite as acute. The interferometer scanning process produces essentially 100% modulation regardless of the error magnitude, whereas the conical scan receiver has zero modulation on boresight. Therefore, a given level of modulation will perturb the conical scan receiver more than the scanning interferometer.

Tests were performed at the Naval Ordnance Laboratory at Corona, California with missile hardware in closed-loop simulations to study these effects. Special IF amplifiers were developed in an attempt to reduce some of the effects by successive limiting, but improvements were so slight that they were abandoned.

Electronic scanning circuits were developed that allowed a high frequency scan. The signals from each antenna were filtered separately by a pass band less than the scan frequency before combining. Amplitude modulations of the RF signals in the frequency band of the scan were then filtered out and had no adverse effect.

The early scan system used by the Talos missile is shown in Fig. 42. It uses Rutherford's double modulation (Ref. 9). The scan frequency used was 44 Hz and the nominal center frequency of the voltage-controlled oscillator was 54 Hz. The rate gyro used a DC pickoff with a tailored output characteristic to provide a linear transfer of frequency shift vs body angular rate. The actual circuit used was a multivibrator type of oscillator where the period between pulses was directly proportional to the voltage applied. Therefore, the transfer of the gyro output vs rate input was an inverse function. The antenna spacing and frequency of this system provided an interferometer gain ($2\pi d/\lambda$) of approximately 90. An LOS rate of 1°/s was considered adequate resolution (at that time) and translated to a frequency shift of 0.25 Hz to be measured by the discriminator. This was considered a difficult but not insurmountable job when the center frequency of the discriminator was 54 Hz.

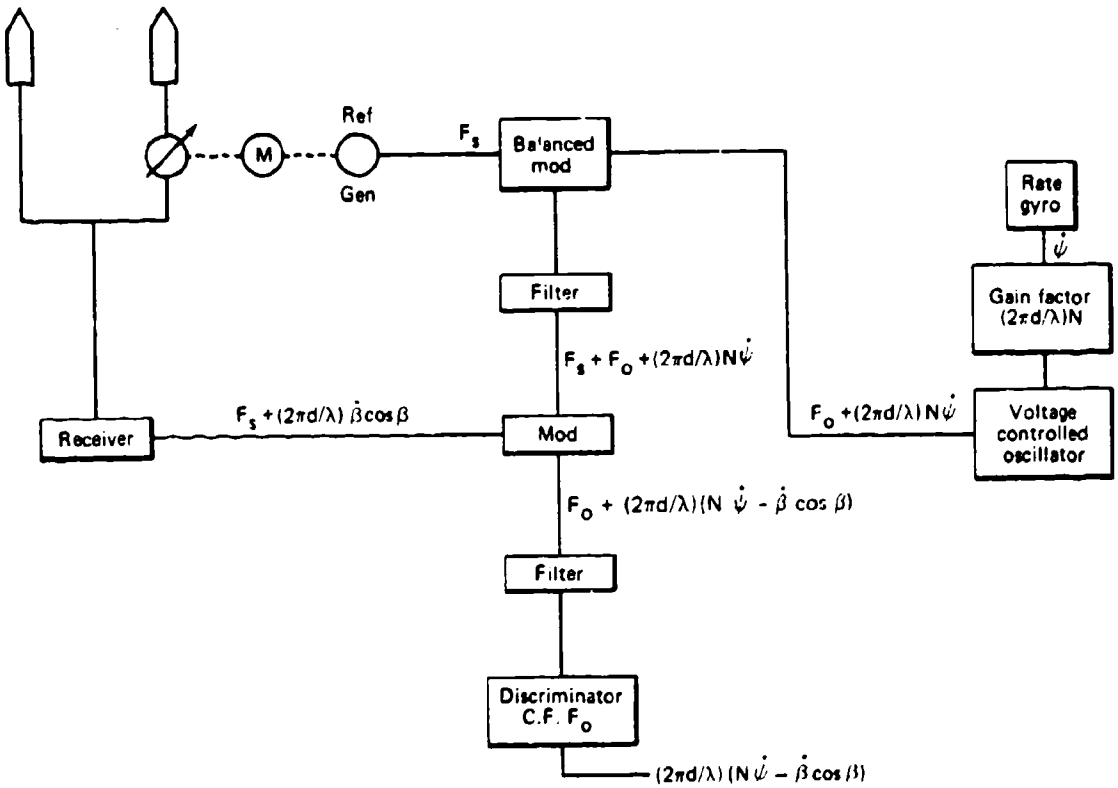

Fig. 42 Early Talos interferometer (1950).

Unfortunately, tests on aircraft targets showed a rather sizeable signal modulation in the scan frequency band because of propeller modulation. This required a shift of the scan frequency to the maximum value consistent with the pulse repetition rate, in this case approximately 300 Hz.

Figure 43 shows the first attempt at a seeker designed for the higher scan. It was felt that a motor with a constant speed could be used, eliminating the scan cancellation circuits. The voltage-controlled oscillator was driven by a gyro with an AC pickoff. The gyro pickoff excitation was a portion of the oscillator output shifted in phase 90°. The pickoff output then was applied to the oscillator input as a quadrature signal, thus causing a frequency deviation proportional to the amplitude of the gyro output and essentially proportional to the missile-body rate. Several factors combined to make this impractical. The higher scan frequency caused the discriminator to be more critical. At the same time, the wavelength of the microwave signal was increased from 0.1 ft to 0.166 ft, reducing the interferometer gain from 90 to 54.

Various systems were employed to attempt to reduce the bias caused by errors among the frequency of the scan generator, the voltage controlled oscillator and the discriminator center, but it became so complicated that this block diagram was abandoned.

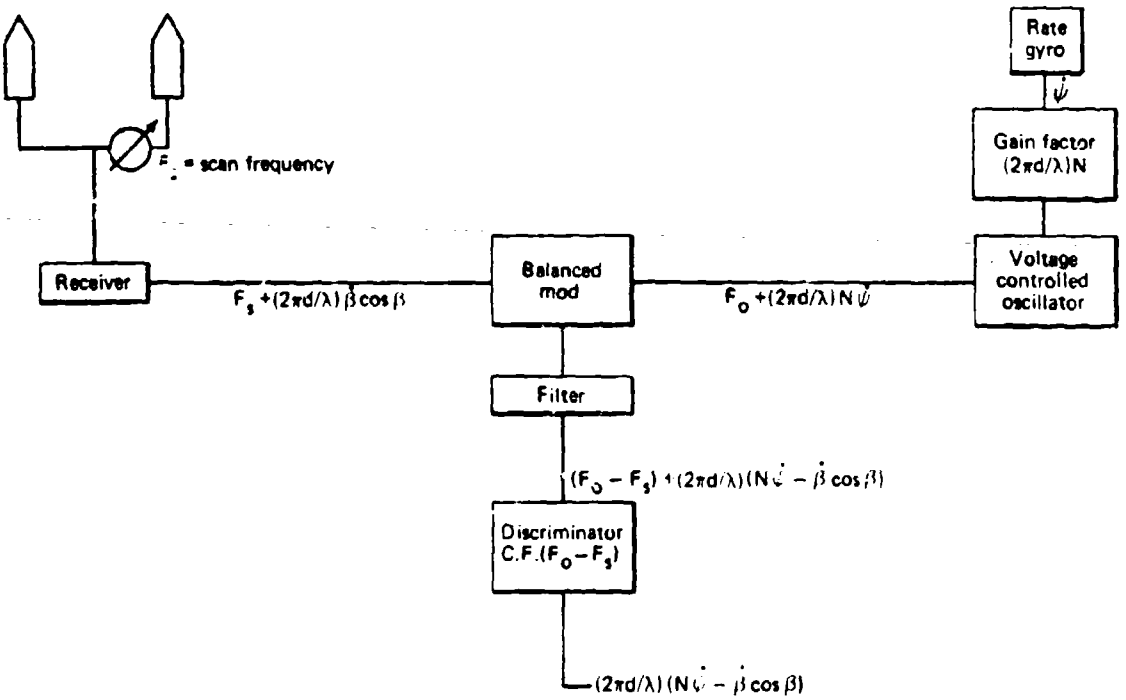

Fig. 43 Modified Talos receiver (1953).

Subsequently, a second scan cancellation system using a mechanical single sideband modulator as suggested by Rutherford (Ref. 9) was built with the frequencies in the area of 250 Hz and 1300 Hz for the voltage-controlled oscillator driven by the body-rate gyro. This seeker was used as the production version of Talos in the late 1950's and was aboard the early Talos ships. The continued problems with bias, transients, gyro linearity, and ability to set the gain of the body decoupling portion of the seeker were the driving force to develop a new design that was to become the operational system for two decades. This is described in detail in sub-subsection 4.3.7.5.

4.3.7.5 Post-1955 Scanning Interferometer. The pre-1955 scanning systems used the electrical phase rate of the scan signal as a measure of relative target rate. It used an oscillator, frequency-modulated by a gyro measuring missile body rate, to provide a signal with a phase rate proportional to missile motion. The frequency of the difference between these signals was used as a measure of LOS rate.

In 1954 a device known as STAPFUS (Stable Platform Phase Follow Up System) was developed (Ref. 20). This device employed electromechanical devices to combine the phase of the scan signal with the phase of a phase-modulated scan reference signal. Figure 44 shows a diagram of STAPFUS as it was used in production. A brief description of its operation follows.

20. J. F. Gulick, T. D. Jacot, H. H. Knapp, and H. H. Nall, "An Electromechanical Comparator for Use with the Scanning Interferometer Homing System," JHU/APL CF-2303 (3 Nov 1954).

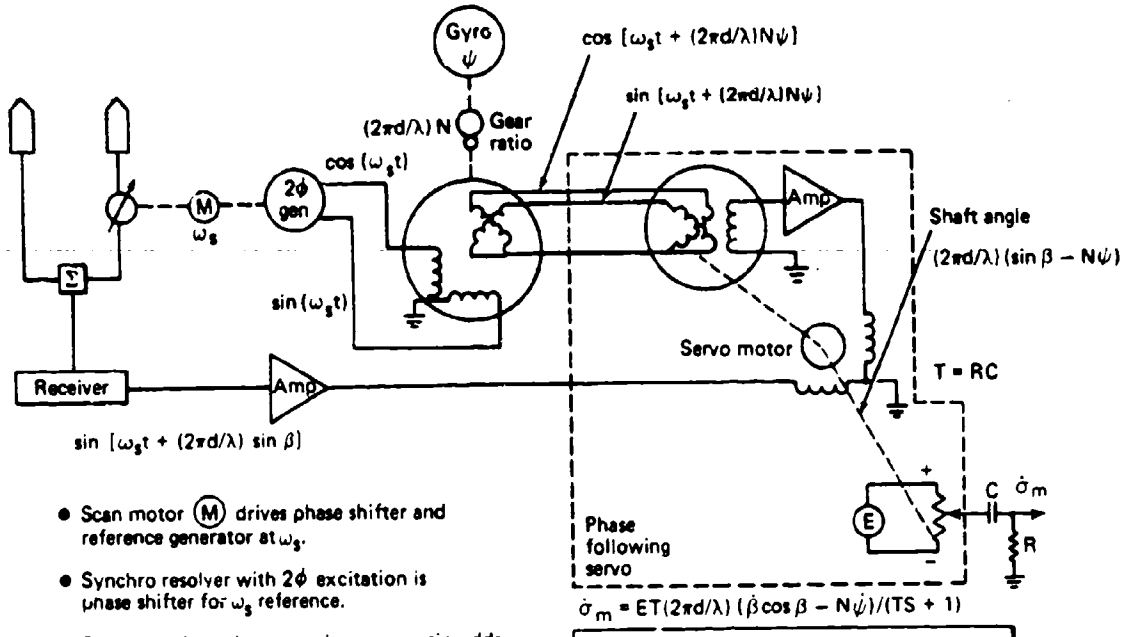

- Scan motor (M) drives phase shifter and reference generator at ω_s.
- Synchro resolver with 2ϕ excitation is phase shifter for ω_s reference.
- Free gyro through appropriate gear ratio adds phase compensation to reference.
- Servo provides phase difference in form of shaft angle.
- Potentiometer and network provide $\dot{\sigma}_m$.

Fig. 44 Scanning interferometer using STAPFUS.

A scan motor M drives the microwave shifter and a 2ϕ reference generator at ω_s. A synchro resolver with 2ϕ excitation provides a phase shift of its output signal directly proportional to the shaft position. A free gyro driving the resolver shaft through the proper gear ratio adds or subtracts the proper phase from the reference. The position of the phase-following servo-output shaft is a measure of the phase difference between the interferometer scan signal and the phase-shifted reference. A potentiometer on the output shaft and a derivative network provides a voltage proportional to the phase rate of the difference. Initial conditions and biases are eliminated by differentiation. The gyro portion of this system will be described in detail in Chapter 5 of this report.

As seen in Fig. 44, the interferometer and the gyro channels have some independent signal processing prior to the subtraction process. This is more apparent in the mathematical block diagram of Fig. 45, where it can be determined that

$$\dot{\sigma}_m = \left[\dot{\sigma} + \dot{\psi}\,\frac{(G_G - G_I)}{G_I}\right]\frac{G_I/G_G}{(S/kG_G) + 1} \tag{66}$$

and if $G_G = G_I$, there is no coupling of body motion (ψ) into the measured LOS rate. The terms G_G and G_I are not simple gain terms but are transfer functions that include phase and gain. If they are not equal, it can also be seen from Eq. 66 that the sign of the body motion

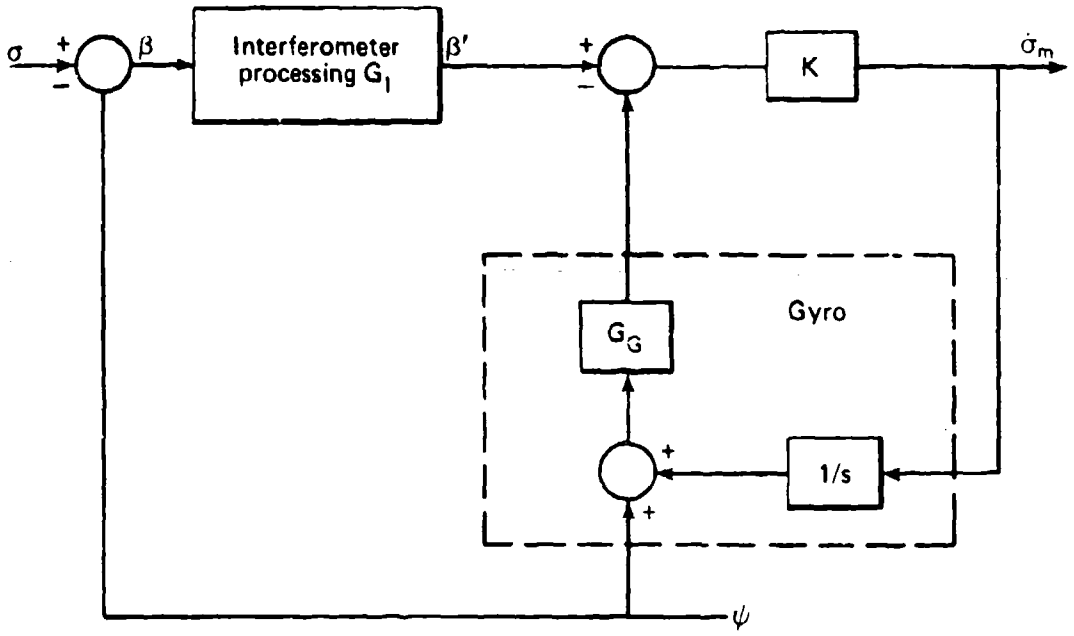

Fig. 45 How body decoupling errors contaminate guidance signals.

coupling changes as a function of the sign of their differences. If these transfer functions are sufficiently mismatched, the guidance loop will become unstable.

It has been shown previously that the phase gain θ of the interferometer is:

$$\frac{2\pi d}{\lambda} (\cos \beta)\dot{\beta} , \tag{67}$$

where d/λ is the antenna separation measured in wavelengths of the frequency, and β is the LOS measured from the missile centerline. In a particular missile where the control surfaces were nearly at the missile center of gravity, it was determined by simulation that a gain ratio of G_G/G_I + 0.925 was a good compromise over the range of cos β encountered in most situations. It was also determined that a delay mismatch of up to approximately 0.007 second in the gyro channel was acceptable, but an excess delay in the interferometer channel was unacceptable. Other airframe configurations that used more or less body angle of attack for lift would have different requirements. This delay restriction put some limitations on the allowable filter bandwidth in the interferometer channel and some instrumentation limitations on the method used for providing the gyro subtraction. One of the first studies in this area is discussed in Ref. 21.

Section 4.5.3 discussed the phase measurement errors caused by imperfections in the I, Q process. The scanning interferometer has precisely the same problems. The scan phase shifter can be considered a single-sideband modulator where the frequency of the

21. D. Young and E. A. Ripperger (DRL/UT), "Effect of Time Lags and Aerodynamic parameters on the Stability of the DRL Homing System," JHU/APL CM-495 (12 Aug 1948).

microwave input signal is shifted above or below the input carrier by an amount equal to the phase rate of the phase shifter. This process requires a 90° equal amplitude split in the microwave signal. If there are errors in the 90° phase shift or amplitude ratio, the same errors occur as were described in sub-subsection 4.3.7.3. An analysis of the errors caused by nonlinearities in the phase shifter is given in Ref. 22.

4.3.7.6 Signal Processing with Nonscanning Interferometers. The scanning interferometers described in sub-subsection 4.3.7.5 had two major limitations, one associated with pulse radars and the other associated with countermeasures vulnerability. One application of interferometer guidance used a pulse radar signal where the pulse repetition rate was essentially the same as the scan rate of the system described in sub-subsection 4.3.7.5. A modification of that system that operates without scanning is shown in Fig. 46. The errors caused by differential phase delay in the two receiver channels were minimized by a transfer switch that interchanged the channels on a pulse-by-pulse basis. An I, Q phase comparator and a holding circuit provided a DC voltage that was proportional to the cosine and sine of the interferometer angle, and that was then converted to a 400 Hz amplitude modulated carrier by a balanced modulator. These two signals when applied to a synchro resolver allowed the interferometer angle to be shifted by a gyro connected to the resolver shaft. The same servo described in sub-subsection 4.3.7.5, with slight circuit modifications, was used to measure the difference angle.

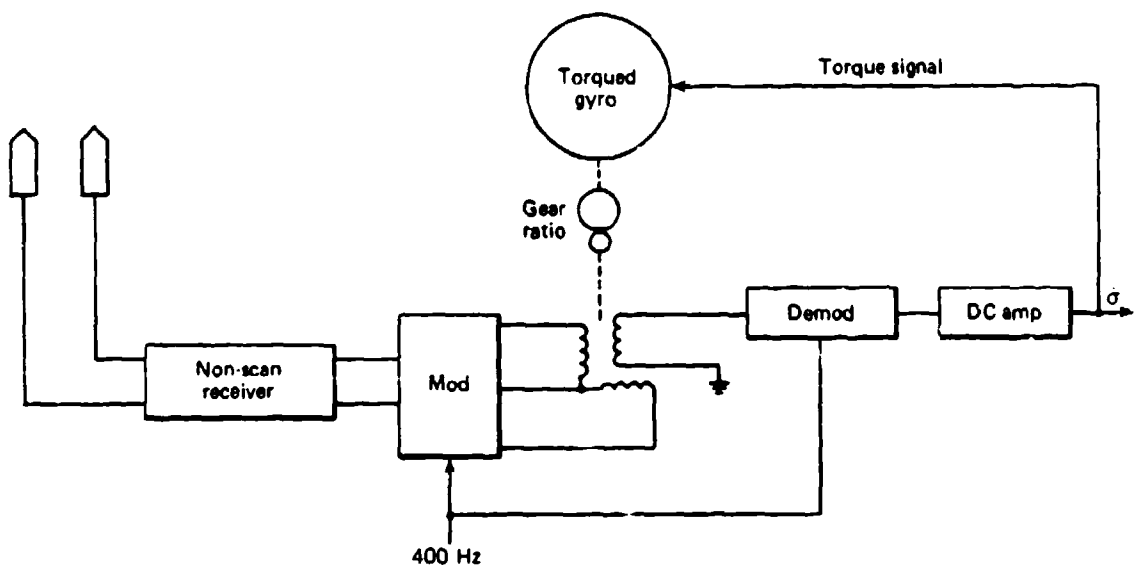

Fig. 46 Nonscanning interferometer using STAPFUS.

22. C. E. Akerman, "Analysis of the Undesired Beta Signals (Squiggles) in the CWI Homing System," JHU/APL CF-2661 (22 Jul 1957).

A different form of receiver without the effects of scan was developed for use with the CW system as a result of countermeasures vulnerability tests. A technique used the simplifications associated with scanning seekers and the countermeasures immunity of nonscanning systems. This was known as hidden scan because the point in the system where the scan frequency was apparent was "hidden" behind narrow-band filters. A block diagram of a hidden scan system is shown in Fig. 47. It can be seen from the figure that modulations at the scan frequency ω_s on the input signal ω_i are filtered by the narrow-band filter following the first mixer. The filter remains centered on the desired signal by a Doppler tracking loop associated with a reference receiver.

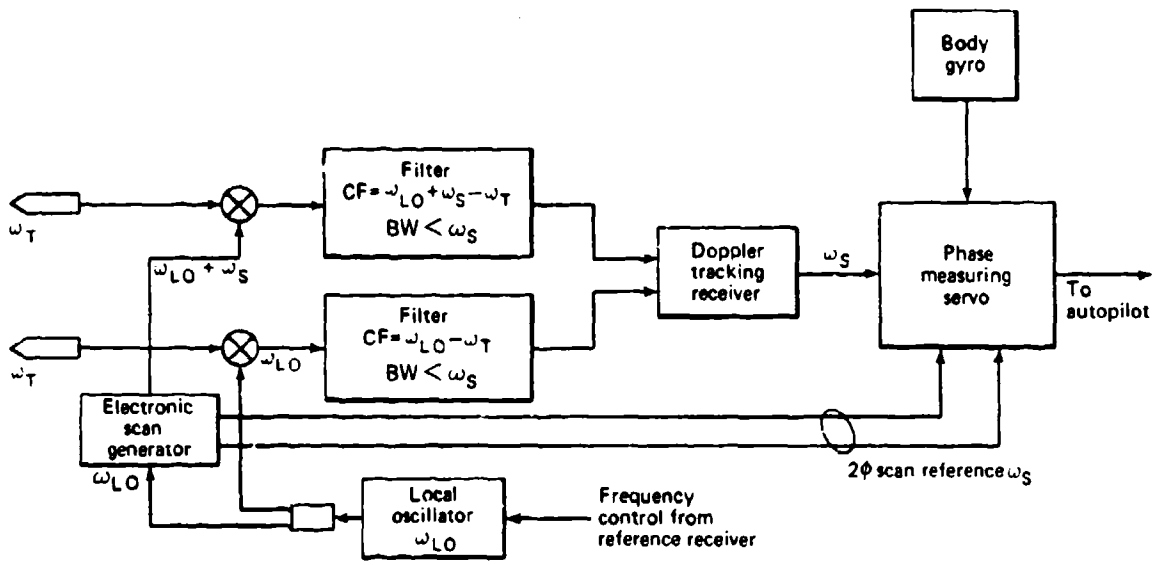

Fig. 47 Hidden scan seeker.

4.3.7.7 Multiple Target Performance. The multiple target performance of an interferometer seeker against Gaussian noise sources has been evaluated by both experiment and analysis. Reference 23 provides an analysis that solved some previous disagreement between experiments and the theory of Ref. 24. The disagreement occurred when the analysis showed that it was impossible to track one of two closely-spaced Gaussian noise sources, and the experiments showed that one of the two sources could clearly be tracked if there was a small difference in power level. This was demonstrated both in laboratory tests and missile flight tests. The reason for the disagreement lies in the analysis assumptions of "two closely-spaced targets." The analysis was based on linear theory and did not consider the trigonometric nonlinearities associated with a steering system using phase comparison

23. W. P. Bishop, L. B. Childress, J. S. Florio, J. E. Hanson, and H. H. Nall, "Agreement Between Theory and Recent Multiple Jammer Tracking Experiments with the CWI System," JHU/APL BBD-794 (15 Apr 1960).
24. J. E. Hanson, "On the Impossibility of Passive Angular Discrimination of Two Closely Spaced Gaussian Noise Barrage Jammers," JHU/APL BBD-764 (3 Feb 1960).

techniques. The linear theory is applicable for target spacing where the electrical phase difference between the two targets is less than 90°. When the phase difference is 90 to 180°, there is much more suppression of the weak target by the strong target than would be predicted by linear theory. In fact, for a separation equivalent to a 180° phase difference, the weaker target is completely suppressed both mathematically and experimentally.

Figures 48 and 49 show experimental flight test configurations. The test represented in Fig. 48 involved an aircraft carrying an operational noise jammer and four targets located on the ground. The missile was not equipped with a warhead. After a close miss on the air target the missile guided toward the array of ground targets. The center of the ground target array was located 3 km off the original flight line, requiring some maneuvering. The missile selected a single target in the terminal phase and guided toward it. Figure 49 shows a two-target case with close spacing. The impact point was adjacent to one of the targets which clearly would have been destroyed with a warhead.

Another scenario that was considered and examined was the case where it was possible to "burn through" jamming and see semiactive return from one target. If a second jamming target is within the field of view of the missile antenna, the guidance errors are corrupted. Reference 25 discusses a method used to reduce or eliminate guidance signal contamination caused by an off-target noise source. The technique makes use of the coherent

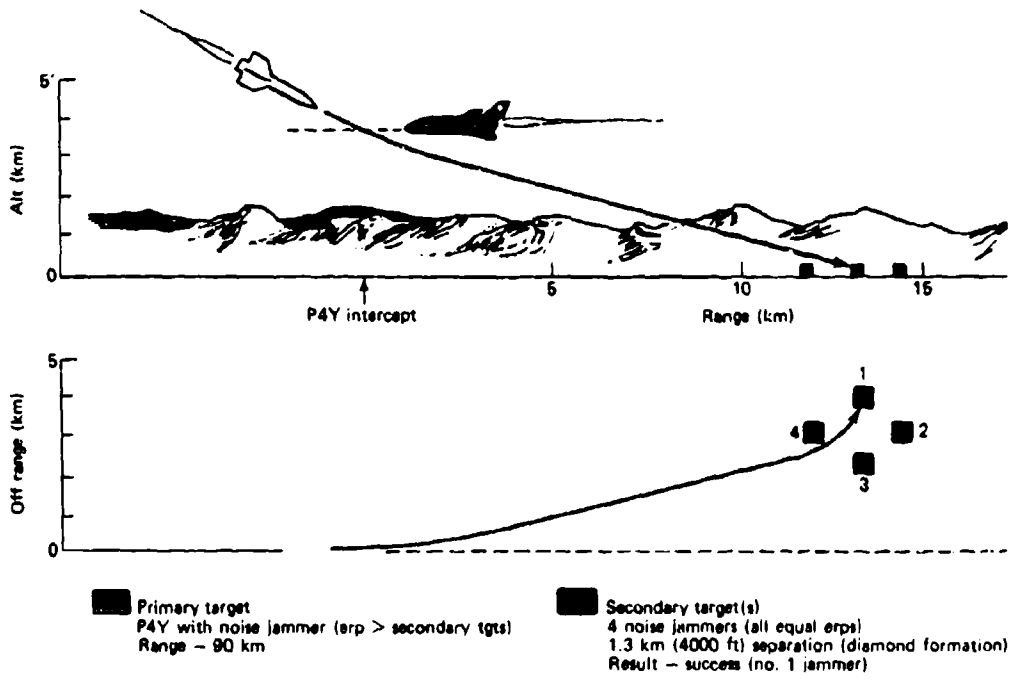

Fig. 48 Multiple jammer test.

25. J. E. Hanson "A Note on the Non-Simultaneous Gating of Front End Pulses in the Typhon LR Interferometer System," JHU/APL BBD-1036 (Aug 1961).

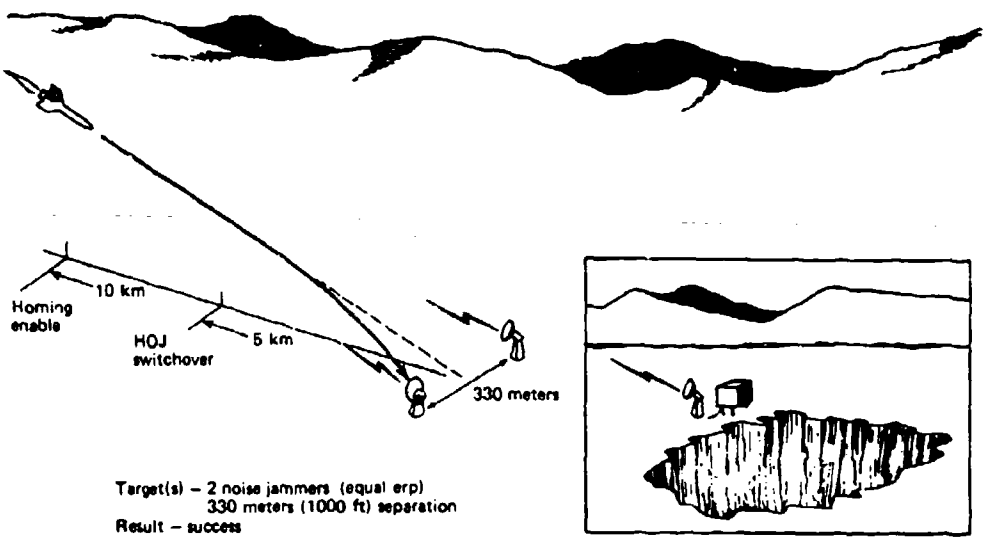

Fig. 49 Multiple jammer test.

characteristics of a semiactive pulse Doppler target return signal while a noise signal is incoherent. The antenna pairs of the interferometer were sampled nonsimultaneously. A coherent target signal can provide angle information in this mode, but the noise from an off-target source is decorrelated and does not bias the angle information.

A version of the interferometer is used in a foreign-built operational missile. It combines the interferometer and a gimballed-dish seeker. The dish is slaved to the interferometer and is used for the acquisition and Doppler tracking signal. The narrow beam of the dish suppresses signals from other targets. Another version of the dish interferometer, which used the dish in the angle channels as well, was suggested by Dr. A. Kossiakoff while he was Director of JHU/APL. The intent was to reduce the noise in the angle channels due to sources outside of the dish beamwidth by correlation techniques where each interferometer element was multiplied by the dish signal. This concept is described in Ref. 26 and analyzed by Refs. 27 and 28.

4.3.7.8 Track-Loop Bandwidth Requirement for Glint Noise. The phase-following servo is a feedback electromechanical device and consequently has delays. The transfer can be expressed in the form of a quadratic expression as

$$\frac{1}{T^2S^2 + 2\zeta TS + 1}, \tag{68}$$

where T is essentially the time constant, and ζ is the damping factor.

26. A. Kossiakoff, "Advanced Missile Guidance," JHU/APL AK-009-70 (13 Jan 1970).
27. R. E. Gingas and J. F. Hartranft, "Investigation of Triple Sensor Missile Guidance," JHU/APL MCM-SR/638 (8 Jul 1970).
28. R. L. McDonald "Two Target Tracking Error Expressions for a Combined Dish Interferometer Receiver," JHU/APL MPA-1-233 (12 Aug 1970).

An early task in the development process was to determine the effect of various values of T and ζ on performance and to select a range of appropriate values. The original specifications were determined empirically with flyover tests at DRL/UT. A missile receiver with appropriate microwave systems and a target illuminator were located on the ground at a test site. Targets were flown over the site, and tape recordings of receiver scan output and the reference generator output were made for many different flight conditions and target types. The targets varied from single engine aircraft to B29 and B36 aircraft passing to within 100 to 200 ft above the simulated missile antennas. The recorded data were then used as input to the phase servo in a wide range of gain and damping conditions. The criterion used for selecting suitable values was the minimum range between the aircraft target and the ground based system before the received signal disintegrated to noise. Many conditions were examined resulting in a specification range for both T and ζ. The results showed that with T greater than or equal to 0.017 or less than or equal to 0.03 and ζ greater than or equal to 0.8 or less than or equal to 1.2, good pointing information would be provided at ranges as close as a few hundred feet on the large multiple engine aircraft. These values of T and ζ were then specified for the system.

At a later date, computer simulations were run to verify these values. Reference 29 reports on one of these simulations. Figure 50 from the referenced report shows a range of ac-

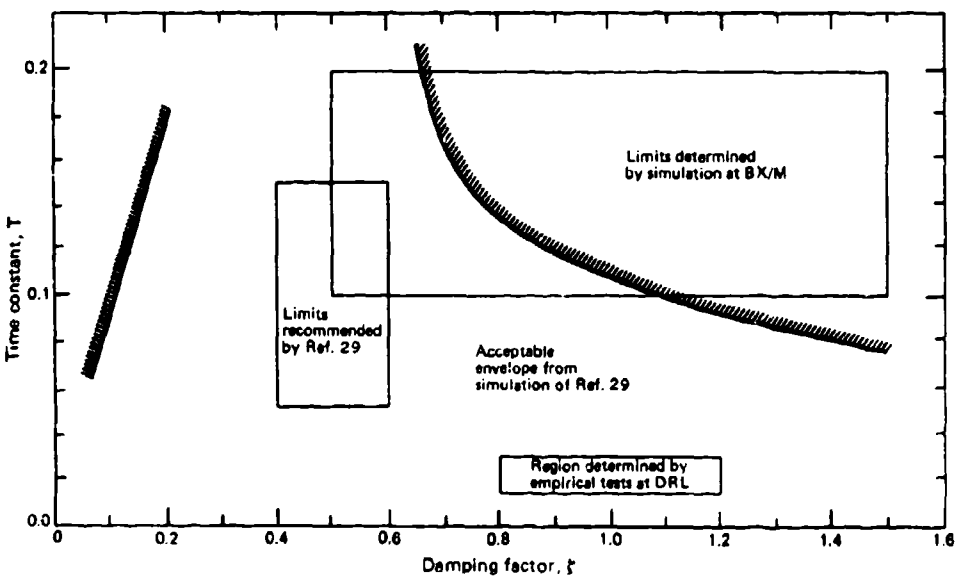

Fig. 50 Performance envelope for acceptable homing for Talos 6B1, showing limits determined for STAPFUS phase servo (adapted from Ref. 29).

ceptable values from this simulation and also the limits established by a simulation at the Bendix Mishawaka missile division. The values determined by the empirical tests at DRL/UT and later used as the production specifications appear to be unnecessarily tight

29. R. E. Christenberry, "An 1103 Evaluation of the Effects of STAPFUS Parameters on the Talos 6B1 (STAPFUS) Missile in the Homing Phase," JHU/APL BBD-675 (17 Aug 1959).

when examined with this simulation; however, fortunately, the tight specification was maintained, and the short time constant was extremely valuable when the multiple target performance was evaluated. Reference 30 shows that a time constant should be on the order of 0.02 second for a multiple blinking jammer encounter. In tests against extended targets such as large surface ships the fast response servo followed the point of reflection from various target points, and the autopilot provided the filtering. During some of the experiments against extended targets, tests were made where the time constant was increased by a factor of three with the intent that glint noise would be filtered with the servo. Performance was drastically reduced. A series of tests to determine the tracking point associated with large ships, small patrol craft, and multiple ship targets was carried out at the Chesapeake Bay Bridge and Navy test ranges. For the bridge tests a missile seeker was located in a test station suspended below the roadway 230 ft above the water. Ships coming up the channel were illuminated by a source located at the water level and the semiactive return was received by the elevated seeker. Figures 51 and 52 are photographs of the ship targets with the corresponding track points superimposed. The details of the tests are described in Ref. 31. The Navy test range tests were performed with a seeker located in a P2V aircraft. A TV camera was also located in the aircraft, with the interferometer track point electronically superimposed on the TV picture. The targets were illuminated by a land based source. The results are described in Ref. 32. Data on the amplitude of glint noise from various aircraft targets were obtained in tests at DRL/UT. These are reported in Refs. 33, 34, and 35. Figure 53 from Ref. 35 shows the typical distribution of angle noise from various aircraft.

In addition to the frequency response requirements of the servo, it was necessary to determine the angular rate resolution requirements. It was determined by simulation and flight tests that a measurement resolution of 0.1°/s space rate was required, and furthermore, if resolution of that order were achieved, the result was a high percentage of direct hits on the target. The allowable filtering on the angular rate measurement depends on the homing time available. An acceptable rule has been that the homing time must be at least 5 and preferably 10 missile time constants. The angular rate filter is a part of the total missile time constant. An acceptable value for some surface-to-air missions was found to be 0.5 second.

30. G. C. Munro, "Narrow Beam Interferometer Homing in the Presence of Multiple Blinking Jammers," JHU/APL BBD-1395 (15 Dec 1964). (Also, BBD-1395-1 "Supplement to 1395.")
31. R. Ostrander, "Evaluation of the Antiship Capability of the Talos Missile," Final Report, JHU/APL TG-749 (Dec 1965).
32. "Final Report: Surface Target Tracking and Radar Characteristics Test, D/S 491 Event 2," JHU/APL SMS-FS-346 (May 1970).
33. J. R. Wright and R. M. Adams (DRL/UT), "DRL Noise Measurements Report No. 1," JHU/APL CF-1701 (7 Dec 1951).
34. J. R. Wright (DRL/UT), "Performance of Interferometer Tracker Against Large Target Aircraft," JHU/APL CF-1808 (11 Dec 1952).
35. J. R. Wright (DRL/UT), "Measurement with Scanning Interferometer of Angle Noise for Head-On Aspect of Six Aircraft," JHU/APL CF-1809 (6 Jan 1953).

Fig. 51 Ship target with corresponding track points superimposed.

Fig. 52 Ship target with corresponding track points superimposed.

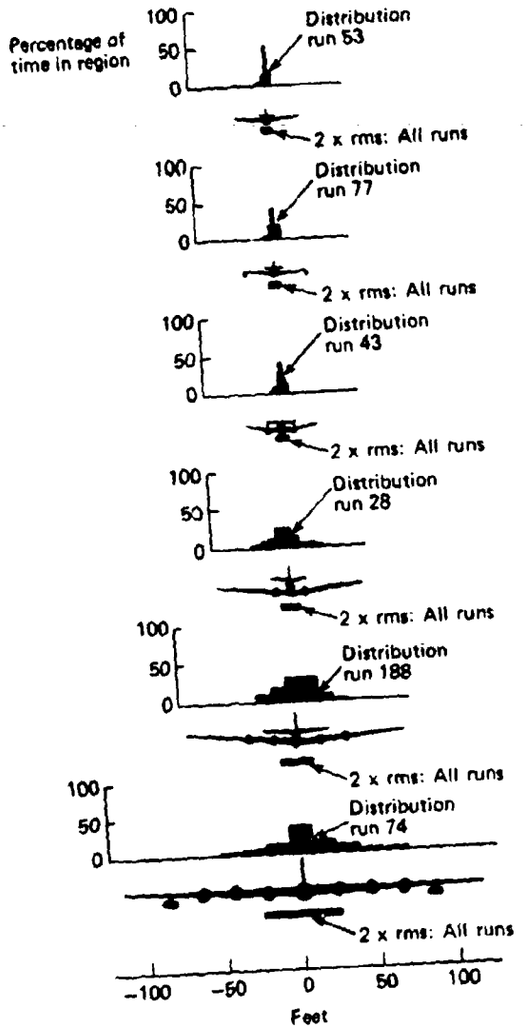

Fig. 53 The rms noise amplitute in relation to aircraft size and distribution plots from typical noise samples.

5.0 BODY-MOTION DECOUPLING

5.1 THEORY OF BODY-MOTION DECOUPLING

Sub-subsection 4.3.7.4 discussed the early scanning systems. Figures 42 and 43 are block diagrams showing both the phase-measuring and body-motion subtraction processes. These systems use body-mounted rate gyros for measurement of missile body motion in the yaw and pitch planes. The subtraction process involves the difference between the apparent target rate and the body rate. Figure 42 shows the frequency of the scan signal from the receiver to be proportional to the interferometer gain, $2\pi d/\lambda$, the apparent rate $\dot{\beta}$, and cos β. The body gyro, through an appropriate gain, frequency modulates an oscillator such that the frequency change, as a function of missile body motion around the yaw or pitch axis, is essentially the same as the change in scan frequency seen by the receiver for the apparent target rate measured by the interferometer. In the diagram of Fig. 42 the true LOS rate, if the gains are correct, is proportional to the change in the frequency F as measured by a frequency discriminator centered at F_o. A serious problem with this system is the inability to set and maintain the discriminator center frequency equal to the modulated oscillator nominal center frequency. Any discrepancy between these frequencies shows up as a direct bias in the measurement of the LOS rate. A problem unique to the use of small spring-restrained rate gyros is that of linearity over a wide dynamic range. Body rates, due to weathercock, could be as high as 40°/s peak when true LOS rates on the order of 0.1 to 0.5° were to be measured. Obtaining gyros that could meet these critical linearity requirements along with other requirements such as minimum delay, spin-up time, and scale factor stability was a serious and almost unsolvable problem.

Sub-subsection 4.3.7.5 discussed a different form of body-motion subtraction. Figure 44 shows a block diagram of that system. The primary difference between this figure and Fig. 42 is the subtraction of phase angles as opposed to subtraction of phase rates. This is accomplished by using a form of free gyro to change the phase of the scan reference signal by an appropriate amount. The gain factor between body motion and phase change was precisely controlled by a known gear ratio between the resolver and gyro platform shaft. The phase angle difference was measured by a phase-following servo with a potentiometer connected to the shaft for an output. The LOS rate is obtained by the derivative of the potentiometer output. Proper selection of the values for the derivative network also provide the first order filter at the autopilot input. Improved performance was obtained with a penalty in size and weight of the gyro and servo system over the electronic system. However, the improved performance was well worth it.

In either system the gain through the gyro channel must be adjusted to match the interferometer gain. Since the interferometer gain is directly proportional to microwave frequency ($1/\lambda$), any change in operating frequency must be accompanied by a change in the setting of the gyro gain.

If there were no provision for body-motion decoupling, the signals in each interferometer channel would, in general, have a component caused by missile-body motion. The basic phase angle output of the two interferometers, θ, can be written using the geometry of Fig. 54:

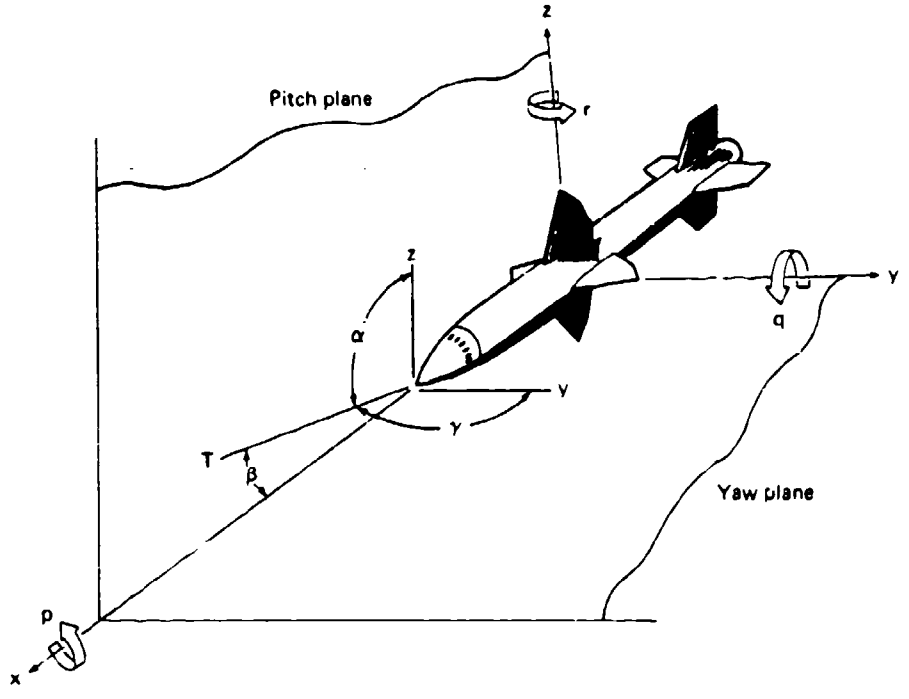

Fig. 54 Interferometer measurement and control axes.

$$\theta_\gamma = \frac{2\pi d}{\lambda} \cos\gamma \tag{69a}$$

and

$$\theta_\alpha = \frac{2\pi d}{\lambda} \cos\alpha \tag{69b}$$

or

$$\theta_\gamma = \frac{2\pi d}{\lambda} (\hat{T} \cdot \hat{y}) \tag{70a}$$

and

$$\theta_\alpha = \frac{2\pi d}{\lambda} (\hat{T} \cdot \hat{z}) , \tag{70b}$$

where carets are used to indicate unit vectors. If rate processing is performed to measure angular rates, the results are

$$\dot{\theta}_\gamma = \frac{2\pi d}{\lambda} [\dot{\hat{T}} \cdot \hat{y} + \hat{T} \cdot \dot{\hat{y}}] \tag{71a}$$

and

$$\dot{\theta}_\alpha = \frac{2\pi d}{\lambda} [\dot{\hat{T}} \cdot \hat{z} + \hat{T} \cdot \dot{\hat{z}}] . \tag{71b}$$

The $\dot{\hat{T}}$ terms are due to motion of the LOS relative to inertial space. The second terms are the body-motion contributions. Expanding these two terms gives:

$$\text{Body-motion term in } \dot{\gamma} \text{ channel} = \frac{2\pi d}{\lambda} [\hat{T} \cdot \dot{\hat{y}}]$$

$$= \frac{2\pi d}{\lambda} [\hat{T} \cdot (p\hat{z} - r\hat{x})] \qquad (72)$$

$$= \frac{2\pi d}{\lambda} (p \cos\alpha - r \cos\beta)$$

and

$$\text{Body-motion term in } \dot{\alpha} \text{ channel} = \frac{2\pi d}{\lambda} (\hat{T} \cdot \dot{\hat{z}})$$

$$= \frac{2\pi d}{\lambda} [\hat{T} \cdot (-p\hat{y} + q\hat{x})] \qquad (73)$$

$$= \frac{2\pi d}{\lambda} (-p \cos\gamma + q \cos\beta) .$$

For pe ect body-motion decoupling, these components have to be subtracted from the signals in the two interferometer channels.

5.2 BODY - MOTION DECOUPLING TECHNIQUE WITHOUT GYROS

It was first proposed by MIT in Ref. 5 that body rotation could be measured by a dual interferometer system. Figure 55, taken from that reference, shows the proposed connec-

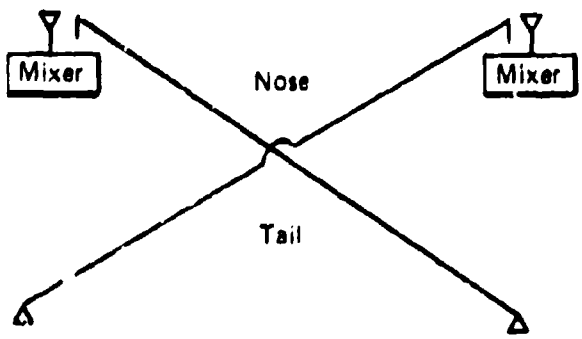

Fig. 55 Body rotation measured by a dual interferometer system.

tion. It was also suggested by Baltzer (Refs. 36 and 37) that dual interferometer might be used in conjunction with a command system. The dual interferometer used forward-looking antennas for target measurement and rear-looking antennas as body-motion references with energy from the illuminators. This form of guidance was considered for a version of Talos called JANUS until simulations showed serious flaws in the fundamental guidance concept with targets having a crossing component. Reference 38 provides a detailed discussion of the problem.

5.3 NONRIGID AIRFRAME

When body-motion gyro signals are subtracted from interferometer signals to obtain the LOS rate, it is usually assumed that the gyros and interferometers are measuring the same motion. This is not always the case. Figure 56 shows a nonrigid airframe bending in its fundamental mode. A gyro located at body station A measuring missile motion will give entirely different results from that of one at body station B. Since the interferometers are measuring the body bending, station A is the more desirable location for decoupling gyros. For weathercock damping in the autopilot, station B is the better choice. If the decoupling gyros are not located near the antennas, a signal at the fundamental body-mode frequency appears on the measured LOS rate. High attenuation notch filters to suppress the body frequencies are also critical in the frequency domain. The body bending frequency is not a constant but rather depends on remaining fuel, altitude, speed, and many other variables.

The early version of the Talos missile experienced a serious maneuver-induced, slow-bending coupling caused by both the location of the gyro near body station B and the compliance of the airframe. This is discussed in Ref. 39.

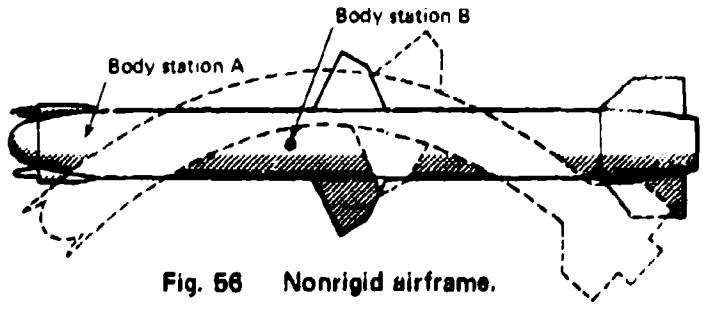

Fig. 56 Nonrigid airframe.

5.4 IMPLEMENTATION TOLERANCES

5.4.1 Sensor Characteristics

The body-motion sensor must maintain linearity of the output vs. input curve over a broad dynamic range. The missile weathercock nonlinearities create a residual signal at the weathercock frequency, which can be destabilizing. The total gyro transfer function must be repeatable as a function of time and temperature to within a few percent. It was found by

36. O. J. Baltzer (DRL/UT), "Command Homing Guidance with the Scanning Interferometer," JHU/APL CM-592 (31 May 1950).
37. O. J. Baltzer, "Missile Guidance System," U. S. Patent No. 3,001,186 (19 Sep 1961).
38. G. C. Munro, "Effects of Missile Angular Velocity on the Janus Interferometer Systems," JHU/APL CF-1680 (11 Sep 1951).
39. N. A. Brigham, "Recommended TALOS Fixes for Slow Bending Discriminator Weaknesses, and the Differentiating Network," JHU/APL CF-1945 (17 Dec 1952).

simulation for the Talos missile that peak weathercock rates to 40°/s could be expected, and a threshold of about 0.1°/s was necessary to ensure satisfactory miss distance.

5.4.2 Establishment of Tolerance Limits

Most of the experience in interferometer guidance has been gained with an airframe whose control surfaces are near the center of gravity, and most of the lift is from the control surfaces instead of body angle of attack. The allowable tolerances may vary widely as a function of airframe configuration and nature of the aerodynamic control, e.g., lift at c. g. vs. tail or canard control where angle-of-attack is used to obtain body lift.

5.4.3 Manufacturing Tolerances

The problem of adjusting the gain of the gyro channel has historically been one of the most difficult parts of the manufacturing process. In the early systems using body-mounted rate gyros several schemes were tried, with various levels of success. They are described briefly as follows:

Each gyro was calibrated on a precision rate table and an output vs. input curve was drawn. The average slope of the curve was determined. A DC voltage representing a known fixed rate was substituted for the gyro signal, and the gain was adjusted to provide the proper frequency deviation of the modulated oscillator.

A second scheme combined a microwave phase shifter in the signal path with a gyro rate table. The proper gear ratio, $2\pi d/\lambda$, was connected between the two. The gain control in the gyro output was adjusted for an output null while the table and phase shifter were oscillating. Local nonlinearities in the gyro curve or nonlinearities in either the equipment phase shifter or missile phase shifter made the null difficult to detect. If the time delays between the two paths were not equal, the output would not reduce to a null, and a quadrature component would remain. A number of test techniques were attempted, using the phase relation of the remaining signal with respect to the gyro table motion. These techniques were only moderately successful because of nonlinearities.

The development of the STAPFUS system mentioned in sub-subsection 4.3.7.5 included a means for precisely calibrating and adjusting the gain between the body gyro and the phase-shifting resolver. The gyro platforms contained both yaw and pitch gyros mechanically displaced at 90° to each other within machining tolerances of a few minutes of arc. A mechanical reference in the form of a pair of holes in the mounting flange plate parallel to one gyro axis allowed the unit to be aligned precisely with one antenna pair. The use of mechanical references established in gyro manufacture allowed more precise alignment with the antennas than had been possible by any means of electrical adjustment previously attempted.

5.5 MEASUREMENT INSTRUMENTS

5.5.1 Strapdown Rate Gyros

A single-degree-of-freedom spring-restrained rate gyro consists of a spinning wheel of angular momentum vector, H, which receives angular rate vector, ω, about the input axis perpendicular to the angular momentum vector. Reacting with the input ω, the gyro

generates a torque L about the output axis, which is orthogonal to the ω and H vectors. Because of mass unbalance, there is usually a mass-unbalance torque vector, L_d, also about the output axis. Referring to the output axis, the gyro wheel, its gimbal assembly, the rotor of the microsyn signal generator, and the rotating part of the damping element mounted on the output shaft constitute the moment of inertia, I, about the output axis. The damper furnishes a damping (torque) coefficient, C. The output shaft is restrained by a spring sensitive to angular displacement of the shaft. The angular stiffness of the spring is K. Thus, with input ω, the gyro output shaft will produce an angular displacement θ from its equilibrium or reference angular position and

$$I\ddot{\theta} + C\dot{\theta} + K\theta = L + L_d \,, \tag{74}$$

where

$$L = \omega H \,. \tag{75}$$

If the microsyn signal generator has a sensitivity, K_s, the output voltage of the rate gyro unit would be V, which is

$$V = K_s\theta \,. \tag{76a}$$

If the microsyn has an offset caused by misalignment between the microsyn null and the spring null, the output voltage will be

$$V = K_s(\theta + \theta_B) \,, \tag{76b}$$

where θ_B is the offset bias. By letting

$$\omega_{gn}^2 = \frac{K}{I} \,, \tag{77}$$

$$\frac{2\zeta}{\omega_{gn}} = \frac{C}{K} \,, \tag{78}$$

and

$$\omega_d = \frac{L_d}{H} \,, \tag{79}$$

Eqs. 74, 75, and 76a can be combined into the following equation:

$$V = \frac{1}{1 + \frac{2\zeta}{\omega_{gn}}s + \frac{1}{\omega_{gn}^2}s^2} \frac{HK_s}{K}(\omega + \omega_{il}) + k_s\theta_B \,, \tag{80}$$

where

ω_{gn} = natural angular frequency of the rate gyro assembly,

ζ = damping ratio of the rate gyro assembly,

s = Laplace operator = d/dt, and

ω_{il} = magnitude of drift caused by mass-unbalance torque L_d.

Several factors associated with the spring-restrained gyro are critical. The maximum angular displacement of the output shaft θ must be limited to a small value to prevent cross-coupling effects. The spring constant, K, must be appropriate to allow full-scale deflection of θ at the maximum required rate to reduce the offset effects of the microsyn bias, θ_B. The values of K (for sensitivity) and I (from the physical characteristics of the gyro wheel) determine the natural frequency of the second-order system ω_{xn}. This natural frequency has an associated delay that is not necessarily compatible with the allowable gyro channel delay. Several other critical factors should also be mentioned:

1. The spring constant, K, is assumed to be a constant over its operating range,
2. The microsyn pickoff is assumed to have a linear output-vs.-θ characteristic, and
3. The calibration sensitivity is directly proportional to H (angular momentum of wheel), which assumes precise control of wheel speed.

Another form of rate gyro is a single-degree-of-freedom integrating gyro. This gyro usually consists of a gimballed gyro wheel enclosed in a cylindrical shell. The output shaft of the gyro assembly extends from both ends of the shell. Rotors of a torque generator and a signal generator are mounted on the extended portions of the shaft. The ends of the output shaft rest on jewel bearings. The shell and all its attached microsyn rotors float within another cylindrical container filled with damping fluid. Two microsyn stators for the torque and signal generators are attached internally to the container. The damping (and flotation) fluid can be temperature controlled to maintain its viscosity constant and density, providing perfect flotation, eliminating any pressure on the jewel bearings. Tight temperature control may be relieved if some residual pressure on the bearing can be tolerated. The major physical and functional difference between rate and integrating gyros are that the latter is not equipped with torsional restraint springs. The only restraining torque comes from the damping fluid. The damping torque is proportional to the rate of the relative motion between the output axis and the housing. Therefore, the output axis position is a measure of the integral of the input torque.

For comparison purposes, let the angular momentum of the gyro wheel, the output-shaft moment of inertia, and the angular-rate damping coefficient of the integrating gyro assembly have values identical to those of the rate gyro assembly. (Strictly speaking, for the same angular momentum wheel, the output shaft moment of inertia of the integrating gyro assembly ought to be slightly larger than that of the rate gyro assembly. The damping coefficient of the two assemblies could be different.) By deleting the $K\theta$ term, Eq. 74 can be rewritten for the integrating gyro assembly as

$$I\ddot{\theta} + C\dot{\theta} = L + L_{\theta_u} \tag{81}$$

The θ_u term is also eliminated since it is a function of the null position of the spring.

In Eq. 81, a term for the mass-unbalance torque L_{θ_u} is included for the integrating-gyro assembly as it is in the case for the rate-gyro torque equation. Because of easier adjustment of the mass unbalance in an integrating-gyro assembly, L_{θ_u} is usually an order of magnitude less than L_{θ_u}. Equations 75 and 76a are also valid since an identical angular momentum is

assumed for both gyro wheels and an identical signal generator will be the natural choice for both gyro assemblies. It is assumed that there is no voltage or current input to the torque generator. By letting

$$\tau_i = \frac{I}{C} , \tag{82}$$

Equations 81, 75, and 76a can be combined into the following equations:

$$\theta = \frac{1}{s(\tau_i s + 1)} \frac{H}{C} (\omega + \omega_{di}) \tag{83}$$

and

$$V = \frac{1}{s(\tau_i s + 1)} \frac{HK_s}{C} (\omega + \omega_{di}) , \tag{84}$$

where

$$\omega_{di} = \frac{L_{di}}{H} \tag{85}$$

is the drift rate of the integrating-gyro assembly.

The presence of the Laplace operator, s, in the denominator in Eqs. 83 and 84 means that the output shaft angle as well as the output voltage of the integrating assembly will increase with time if a unidirectional angular rate input, ω or ω_d, is present. The integrating-gyro assembly alone is therefore not suitable for measuring angular rate even if it is not unidirectional, because the drift contribution remains unidirectional, and the output shaft rotation will eventually reach its design limit. However, the use of an integrating gyro where the signal generator is amplified and supplied to the torquer as a restraining torque similar to a spring has some merits. Figure 57 is a block diagram of a rate-integrating gyro with external amplifier K_1. K_T is the gain of the internal torquer. The equation for the voltage out of the gyro can be shown to be:

$$V = \frac{\frac{1}{K_1} (H\omega + L_d)}{\frac{I}{K_1 K_T} + \frac{C}{K_1 K_T} S + 1} \tag{86}$$

The equation for the natural resonant frequency is similar to that of the spring restrained gyro:

$$\omega_{kn} = \sqrt{\frac{K_1 K_T}{I}} , \tag{87}$$

but the product K_1 and K_T allows an additional degree of freedom. The resonant frequency can be increased by increasing K_1 without affecting the DC gain of the systems. The linearity of the torquer, K_T, is essentially the only term affecting the linearity of the output-vs.-input rate. The wheel speed, of course, must remain constant.

5.5.2 Platforms

The previous section described body-mounted gyros with an output signal representing missile angular rate. STAPFUS used a single-degree-of-freedom stabilized platform. The angular motion of the missile is measured as a shaft rotation of a resolver driven by a gear on the stable platform. Figure 58 shows a simplified diagram of the platform.

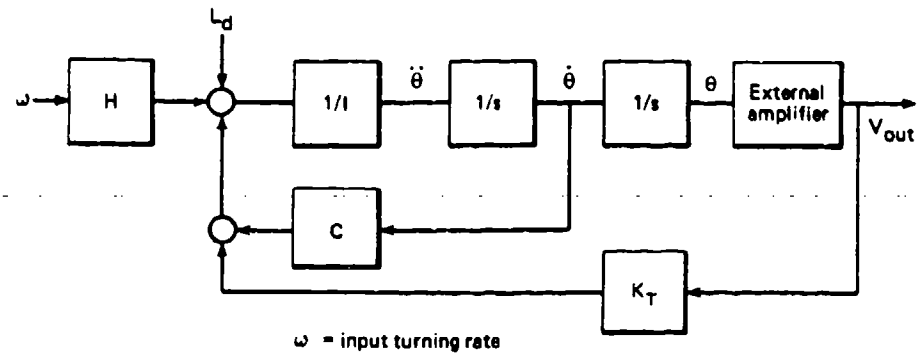

ω = input turning rate
L_d = mass unbalance
H = wheel angular momentum
I = wheel inertia
C = viscous damping coefficient
K_T = torquer gain
K_1 = external amplifier gain
s = Laplace operator d/dt

Fig. 57 Block diagram of a rate-integrating gyro.

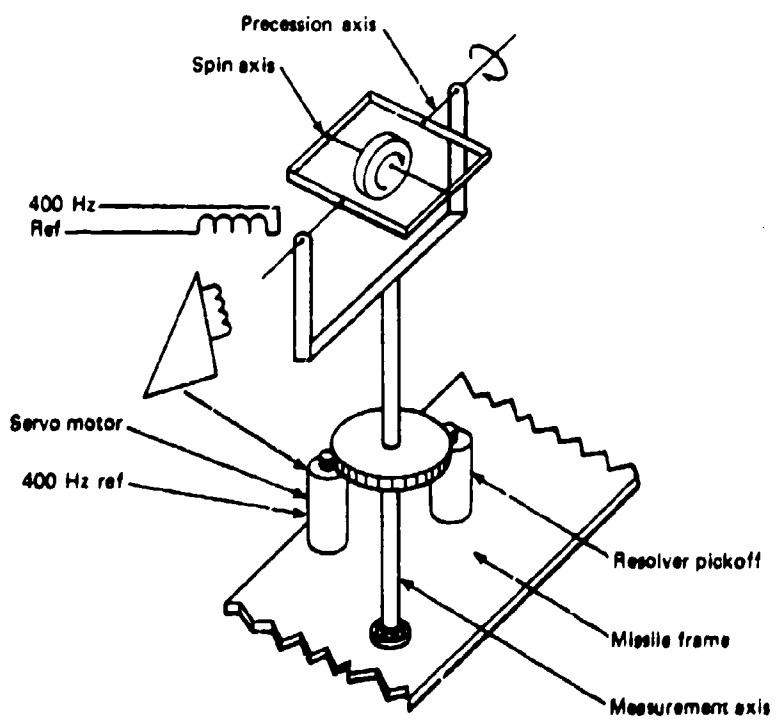

Fig. 58 Single-degree-of-freedom stable platform.

A detailed analysis of the platform used for Talos along with the gyro constants are provided in Ref. 40. The initial development included a calibrated variable gear ratio between the gyro and the phase-shifting resolver. A block diagram of the gear train is shown in Fig. 59. The adjustment range required was 10%. As shown in Fig. 59 the required ratio

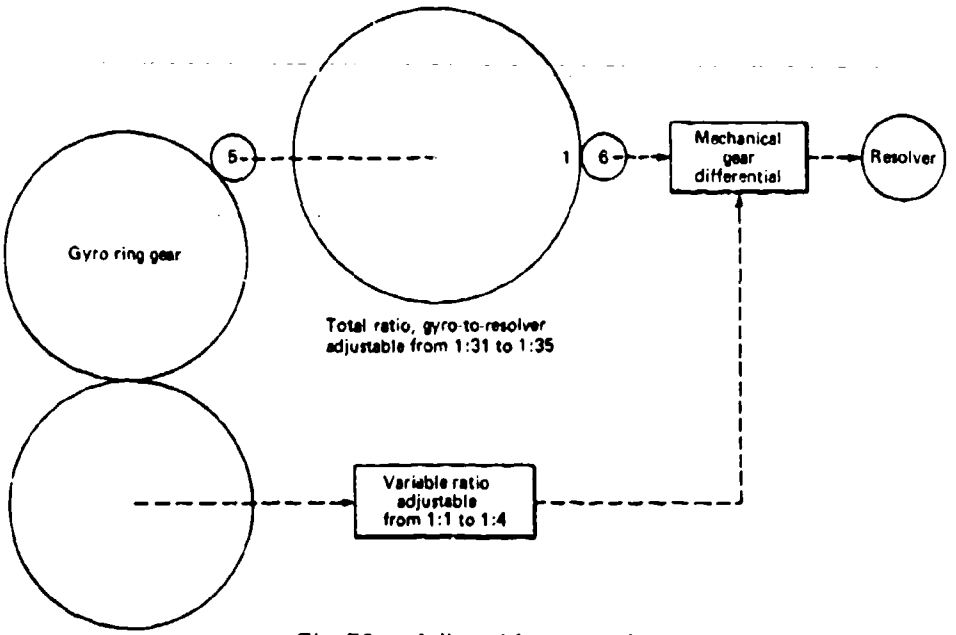

Fig. 59 Adjustable gear train.

was provided by a fixed gear ratio and a parallel variable path added to the fixed path by a mechanical differential gear. The fixed path of 1:30 step-up ratio was combined with a variable path of 1:1 to 1:4. The total was, therefore, a ratio varying from 1:31 to 1:35. The range was adjusted by a calibrated 10-turn control knob, allowing extremely precise and repeatable setting of the gain. Later developments eliminated the need for the adjustment, and two remotely selectable ratios were provided. Figure 60 is a photograph of the initial gyro platform used in test flights.

The body-fixed rate gyros and the STAPFUS platforms involved some assumptions in generating proper decoupling for body motion. The assumptions were valid when the look angle between the missile centerline and the LOS to the target (β) remained less than approximately 30°. When performance at increased altitude against higher performance targets became necessary, control systems operating variable tail surfaces and providing body lift via angle of attack were also necessary. The assumption that β remained small was no longer valid. The body-decoupling gyros mounted to measure motion around the axes of the wing hinges were not adequate. The steering command generated by that system induced missile roll that is not decoupled.

A further problem with the developed system was the assumption that the cos β term that contaminates the interferometer signal could be approximated by a constant on the

40. G. C. Munroe, "The STAPFUS Stabilization Loop," JHU/APL CF-2380 (13 May 1955).

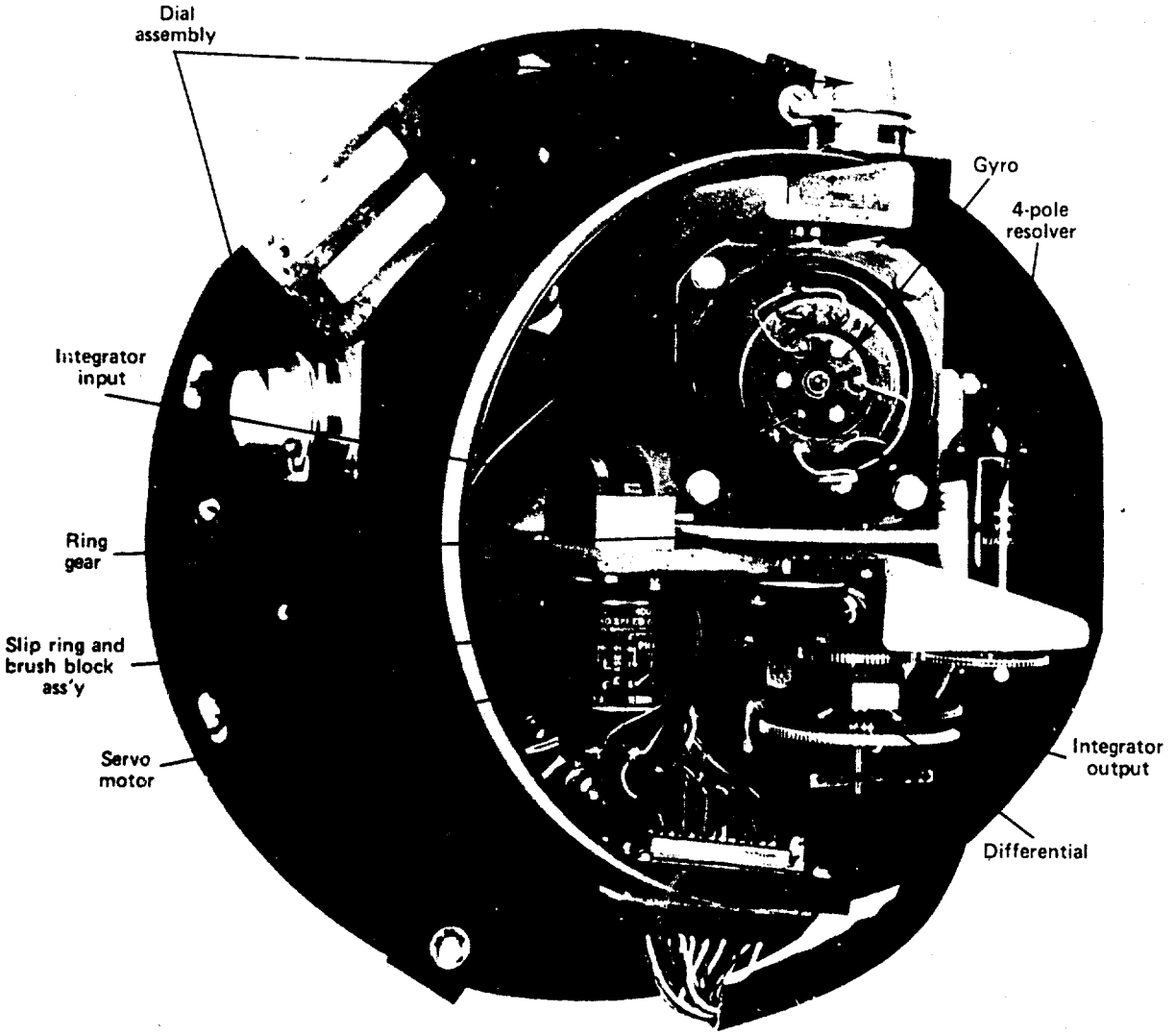

Fig. 60 The original STAPFUS platform.

decoupling gyro gain. A device to solve both of these problems called DIRCOL (Direction Cosine Linkage) was developed. Reference 41 describes the DIRCOL device in detail. A number of additional documents (Refs. 12, 42, 43, and 44) provide simulation results and test results. Figure 61 from Ref. 41 is a diagram defining various angles and axes used in the

41. J. W. Follin, Jr. and G. C. Munro, "Direction Cosine Linkage," U.S. Patent No. 3,215,368 (2 Nov 1965).
42. D. F. Collins, R. P. Borrelli, and A. F. Bassett, "Direction Cosine Linkage (DIRCOL) Homing System Tests," JHU/APL CF-2811 (1 Jun 1959).
43. G. C. Munro, "RFM Study of a Modified Interferometer Homing System," JHU/APL CF-2663 (6 Aug 1958).
44. G. C. Munro and J. W. Follin, Jr., "A Direction Cosine Linkage," JHU/APL CF-2669 (Sep 1958).

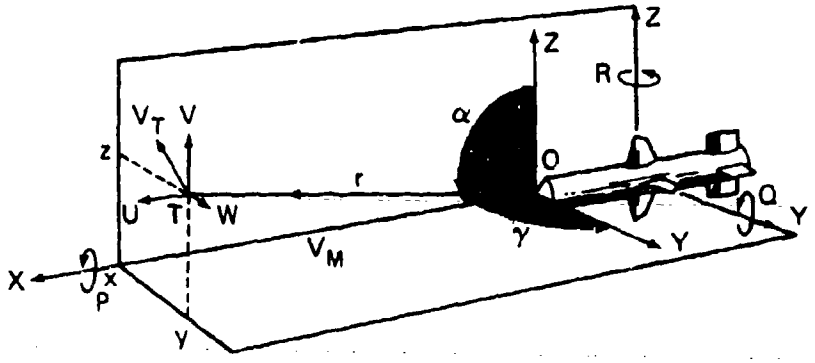

Fig. 61 Angle definitions for DIRCOL.

geometry of the homing system. It has been shown that one pair of interferometers meaures cos α and the other cos γ. The DIRCOL contains a gimbal structure that allows a gyro on the α and γ planes to be used for stabilizing the intersection of these two planes toward the target. The decoupling signals are obtained from measurement of the missile turning rates normal to the α and γ planes. Additional computation is provided to produce the proper steering commands about the missile axes y and z. These steering commands minimize the roll coupling created by the yaw-pitch cross coupling; however, the DIRCOL device does not decouple roll body motion, and a tight roll stabilization loop is still required.

5.5.3 Two-Axis Free Gyro with Torquer

A nonroll stabilized missile uses a single two-axis torqued free gyro to provide body decoupling in yaw, pitch, and roll. Figure 62 from Ref. 45 is a photograph of the gyro. The gyro rotor is a permanent magnet with the poles on the diameter of the rotor. Current in the concentric windings around the diameter of the stator around the rotor are used to supply a torque. The torque signal is an AC signal at precisely the rotation speed of the rotor. The phase of the signal with respect to the rotor position determines the direction of torque. References 45, 46, and 47 describe the concept and test results of a two-axis position pickoff. The rotor position with respect to the missile body is sensed by a two-axis capacity pickoff. The capacitor is formed between the rotor and four plates produced by evaporating a thin film of metal on the inner wall of the stator.

Figure 63 shows the geometry for reference. The plates are shaped to produce the desired output. One pair of capacitive plates provide a signal proportional to sin β cos ϕ and the other pair $-\sin\beta \sin\phi$.

Reference 48 provides an analysis that shows that when the gyro pointing direction is along the missile target LOS, the body motion decoupling is mathematically perfect in all three dimensions, yaw, pitch, and roll.

---

45. C. D. Sayles, "Test Results for the Capacitive Two Axis Pickoff," JHU/APL FIB79U-018 (9 Feb 1979).
46. J. F. Gulick, "A Beta POT Alternative for ASMD," JHU/APL FIB77U-055 (22 Mar 1977).
47. J. F. Gulick, "A Capacitive Two Axis Pickoff for Redeye or Stinger Gyro," JHU/APL FIG-78U-014 (5 Jul 1978).
48. J. S. Miller, "Analysis of Missile Body-Motion Decoupling," Technology Service Corp., W47-190 (26 Mar 1981).

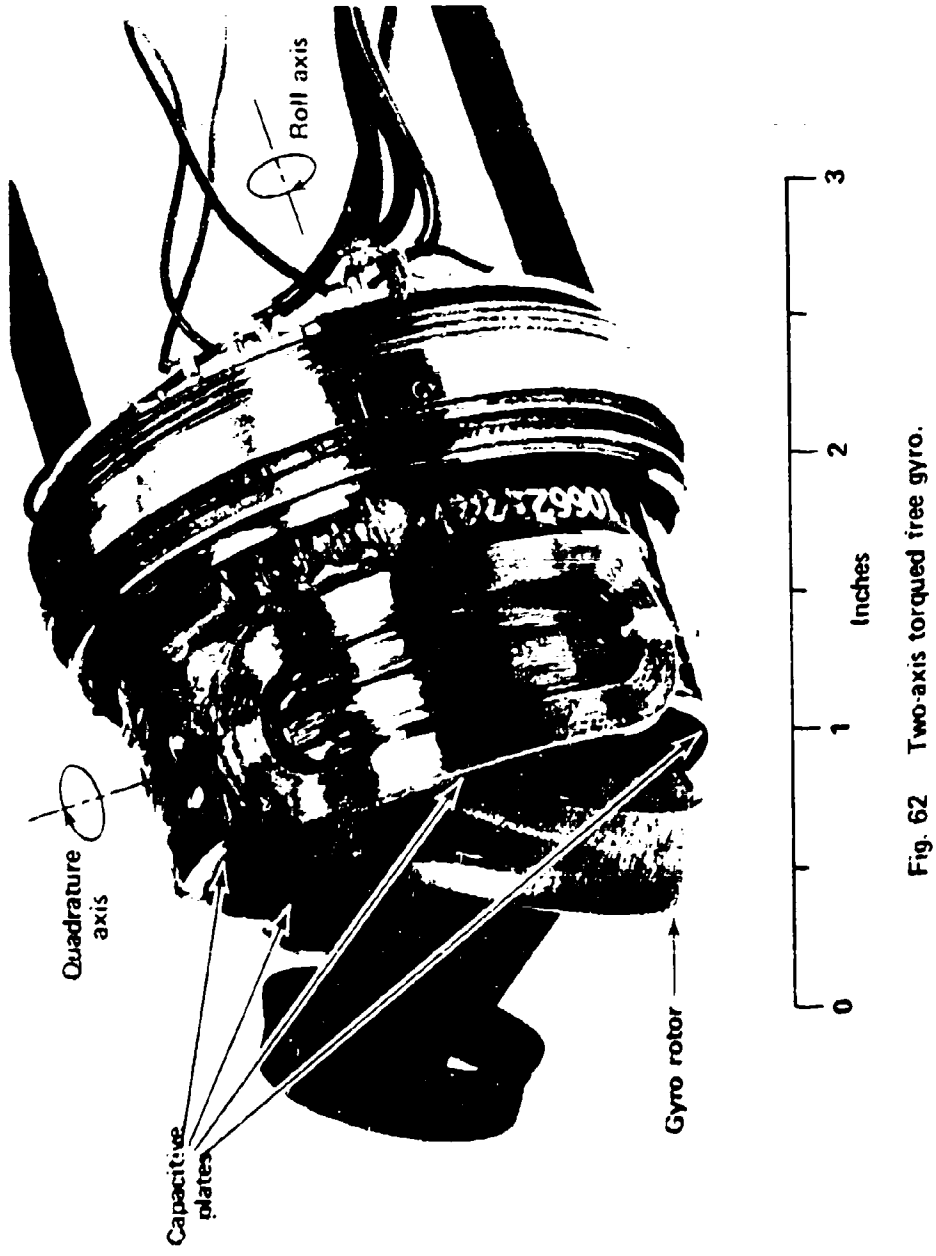

Fig. 62 Two-axis torqued free gyro.

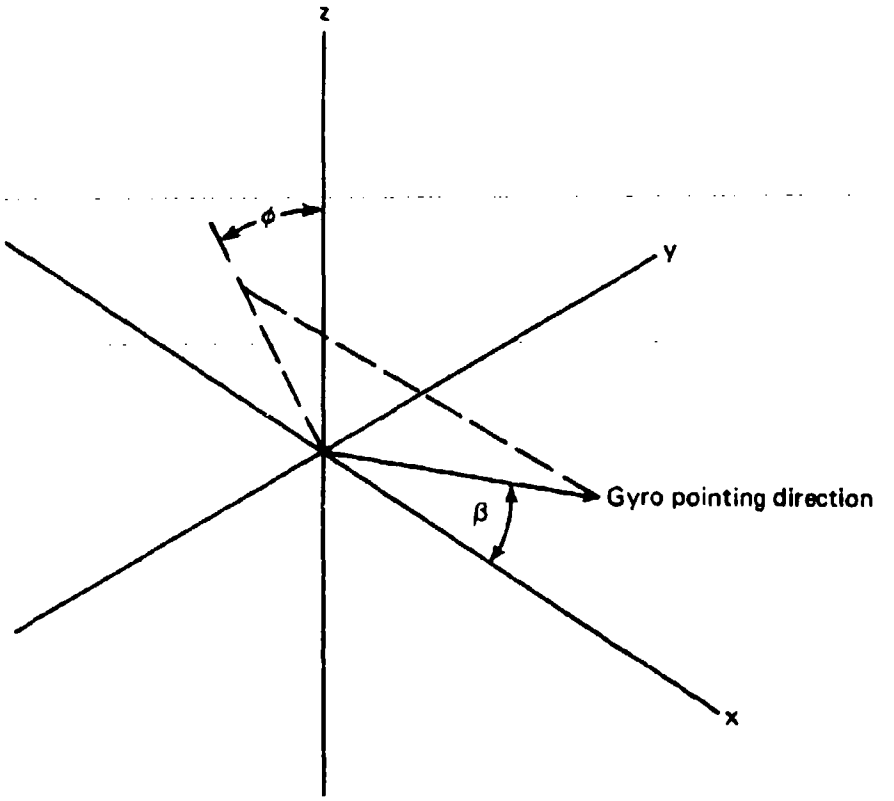

Fig. 63 Two-axis gyro measurement geometry.

5.6 DECOUPLING TECHNIQUES FOR OPERATION OVER A WIDE RF BAND

It has been shown previously that the interferometer electrical phase output is given by:

$$\theta = \frac{2\pi d}{\lambda} \sin \beta \,, \tag{88}$$

where θ is the electrical phase shift, d is the antenna spacing, λ is the wavelength of the signal, and β is the angle between the missile centerline and the LOS to the target.

If the missile-motion decoupling is accomplished by the subtraction of electrical phase, any change in λ requires a change in the gain of the gyro term. Modern digital techniques allow the gyro output to be accurately multiplied by the proper gain factor if λ is accurately known or measured.

It is not unlikely, however, that the received signal can change frequency very rapidly, for example when a chirp signal is received or when the receiver is required to operate over a wide band of noise. In either of these cases, attempting to adjust gain as a function of frequency is not practical.

Subsection 4.4.4 briefly mentioned a technique suitable for broadband applications. The method uses a digitally controlled, adjustable time delay as a part of the microwave line between the antenna and the signal processor. The time delay is controlled by the output of a body-mounted gyroscope as shown in Fig. 64. If a source of radiation, such as a radar signal from a target, lies along the LOS line (at an angle β with respect to the missile centerline), there will be a time difference α between the signals seen by the two antennas.

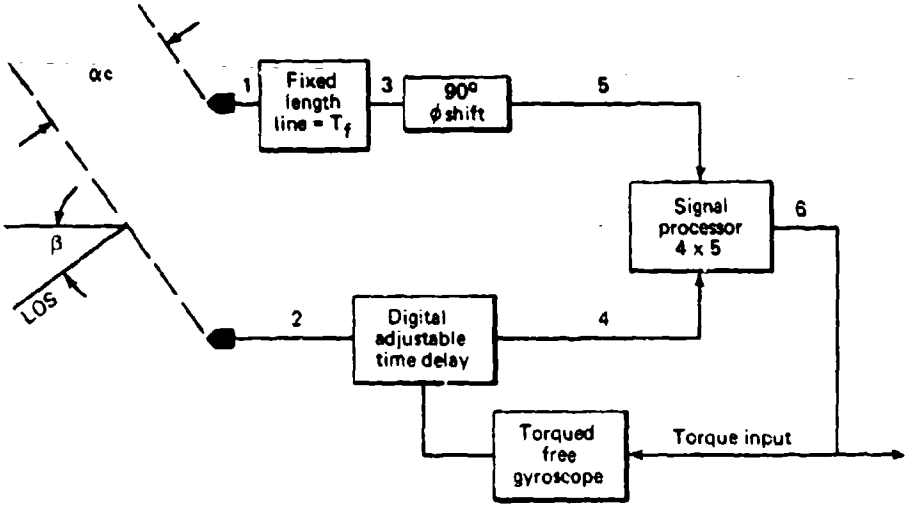

Fig. 64 Body decoupling using digital adjustable time delay.

In Fig. 64, the time delay in the signal at antenna 1 is determined by the equation:

$$\alpha = \frac{(d \sin \beta)}{c} , \tag{89}$$

where c is the velocity of propagation of the signal in the medium. The signal received by antenna 1 is fed to a fixed time delay line of T_f. The signal at antenna 2 is fed to a variable time delay line of delay T_f plus or minus T_t. As a condition of operation, T_t must be less than or equal to T_f.

The signals at various points in Fig. 64 can be described as follows:

$$\begin{aligned}
\text{Signal at point 1} &= \sin 2\pi f_c [t - \alpha] , \\
\text{Signal at point 2} &= \sin 2\pi f_c t , \\
\text{Signal at point 3} &= \sin 2\pi f_c [t - \alpha - T_f] , \\
\text{Signal at point 4} &= \sin 2\pi f_c [t - T_f - T_t] , \\
\text{Signal at point 5} &= \cos 2\pi f_c [t - \alpha - T_f] ,
\end{aligned} \tag{90}$$

where f_c is the input carrier frequency.

The signal processor contains a multiplier whose output includes sum and difference frequencies of the inputs. The sum frequency is a very high microwave signal removed by filtering. The difference frequency is a DC voltage. If

$$\text{Signal at point 6} = \sin 2\pi f_c(\alpha - T_L) \tag{91}$$

is used as a torque signal to the gyro, the loop will null the voltage at point 6. If the gyro is pointed within an interferometer ambiguity, then

$$T_L = \alpha \tag{92}$$

The carrier frequency, f_c, is a gain multiplier on the output signal but is totally eliminated from the decoupling loop. In the steady-state case the torque input is a measure of the LOS rate and is therefore the proper steering signal for proportional navigation. This method has been demonstrated to operate over a bandwidth greater than an octave.

5.7 BODY-MOTION DECOUPLING FOR ROLLING AIRFRAME

Sub-subsection 4.3.5.2 provided the description of the interferometer signal processing for a rolling interferometer. Figure 28 shows a block diagram of that process. Referring to Fig. 28, any phase modulation of oscillator ω_o results in a phase addition or subtraction from the interferometer signals present at points 3 and 4. If the oscillator is phase modulated by a gyroscope measuring missile motion, a method is available for body-motion decoupling.

Figure 65 shows a possible gyro arrangement for this purpose. The gyro pickoff axis

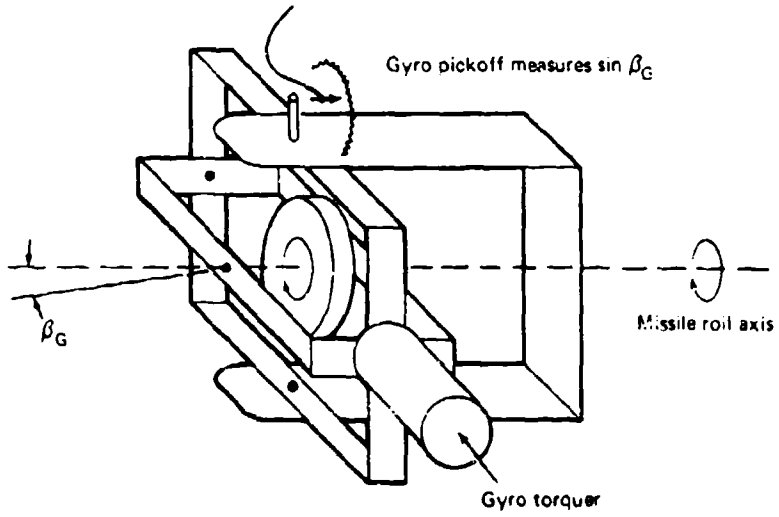

When rolling gyro output = $K_G \sin \beta_G \cos(\omega_R t + \theta_G)$,
where K_G is a gain factor determined by voltage applied to pickoff

Fig. 65 Gyro for rolling missile.

must be perpendicular to a line joining the centers of the interferometer antennas. The gyro with a capacitive pickoff described in Section 5.3 can be used, and only one axis of the pickoff is required. Figure 66 shows the decoupling diagram and provides the equations.

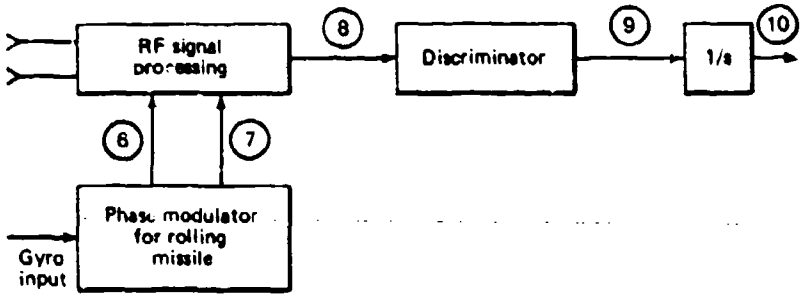

$$6 = \cos\left[\omega_o t + K_G \sin\beta_G \cos(\omega_R t + \theta_G)\right]$$
$$7 = -\sin\left[\omega_o t + K_G \sin\beta_G \cos(\omega_R t + \theta_G)\right]$$
$$8 = -\sin\left[\omega_o t + (2\pi d/\lambda)\sin\beta\cos(\omega_R t + \theta_T) - K_G \sin\beta_G \cos(\omega_R t + \theta_G)\right]$$
set $K_G = 2\pi d/\lambda$
then
$$9 = -\sin\left\{\omega_o t + (2\pi d/\lambda)\left[\sin\beta\cos(\omega_R t + \theta_T) - \sin\beta_G \cos\omega_R t + \theta_G)\right]\right\}$$
$$10 = (2\pi d/\lambda)\sin\epsilon\cos(\omega_R t + \theta_T - \theta_G)$$
where $\epsilon = \beta - \beta_G$

Fig. 66 Rolling interferometer with gyro subtraction.

The signals at points 6 and 7 are the same as those at points 6 and 7 of Fig. 28 with the phase modulation from body motion added to the phase of the oscillator, ω_o.

The modulator used to produce phase shifts greater than 360° is shown in Fig. 67. A reference oscillator triggers a ramp generator that produces a linear voltage ramp at point 2.

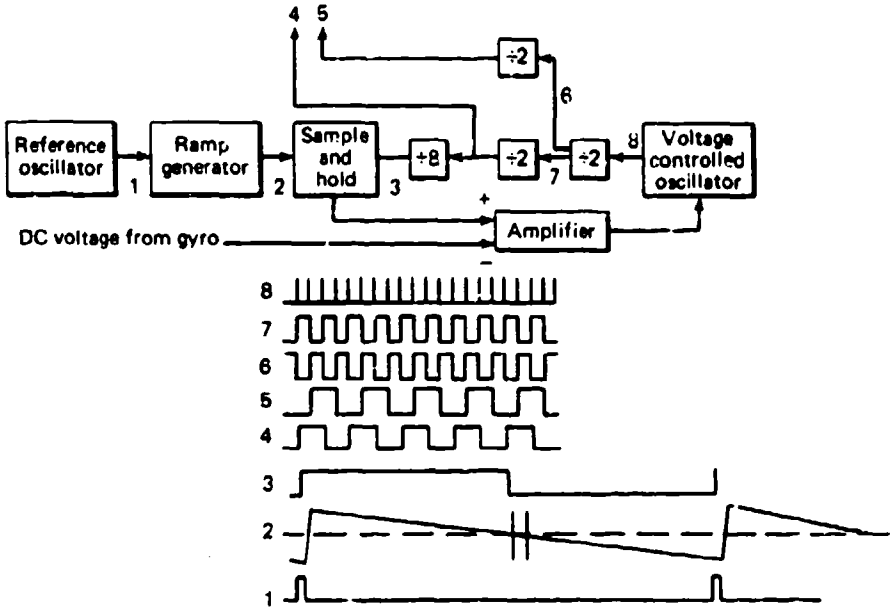

Fig. 67 Phase modulator.

The negative voltage step at point 3 samples the ramp voltage and holds the sampled value until the next sample is provided. This provides a linear voltage as a function of the phase between points 3 and 2. Assume, for the moment, that the gyro input voltage is zero. The amplifier output will change the phase (by momentarily shifting the frequency) of the voltage-controlled oscillator until the output at point 3 samples the ramp at zero volts. The signals at points 4 and 5 are precisely 90° out of phase because of the digital division techniques and are eight times the frequency of the signal at point 3. When a voltage is applied from the gyro pickoff, the high gain loop will shift the phase at point 3 by an amount required to equal the gyro input voltage. The phase change of the signals at points 4 and 5 will be eight times the phase change at point 3 and can easily be greater than 360° if necessary. The gain between the gyro input voltage and the desired phase change at points 4 and 5 can be as great as required for proper decoupling.

This form of body decoupling requires precise knowledge of the incoming frequency in order that the proper gyro gain can be used in the phase modulator. The rolling missile decoupling can also be accomplished by use of the variable line described in Section 5.6. A detailed description of the technique is provided in Refs. 16 and 48.

6.0 INTERFEROMETER GUIDANCE FOR CURRENT AND FUTURE MISSILES

6.1 ATTRACTIVE FEATURES OF INTERFEROMETER GUIDANCE FOR FUTURE MISSILES

6.1.1 Compatibility with Other Guidance Modes

More than fifteen years ago it was recognized that combining a typical RF homing system with a second high-resolution mode of guidance was desirable in order to operate in some countermeasures environments. Numerous attempts were made to combine RF and IR seekers in a common aperture, with little operational success. Many tests were made to determine the feasibility of operating an RF seeker that was partially blocked by an IR seeker forward of the RF seeker, but the errors created by the blockage were greater than could be tolerated. Dual-band RF seekers were also designed to operate with a single aperture. These were more successful, but there were rather tight restrictions on the ratio of the frequencies. The interferometer guidance concept removes many of the multimode restrictions since the interferometer antennas are on the outside diameter of the airframe.

6.1.1.1 RAM Development. A dual-mode missile (in joint development by the U.S. Navy, the Federal Republic of Germany, and the Government of Denmark) called the RAM (Rolling Airframe Missile) is a combined RF and IR seeker. The rolling airframe RF interferometer uniquely determines the target location and points the gyro toward the target. The spinning gyro is also the telescope for the IR seeker and is pointed toward the target with a narrow field-of-view seeker. When sufficient signal is received, the missile control is changed to the IR seeker. Figure 68 shows the front of the RAM with the RF and IR seekers.

6.1.1.2 BT Trimode. A multimode version of the Terrier BT missile was proposed and studied. The original Terrier BT missile used beam-rider guidance. The proposal and studies considered adding an RF interferometer and IR seeker for certain specific environments. Details of this are provided in Ref. 49.

Another program examined various candidates for a wide area missile including various combinations of interferometers and gimballed seekers. Data were measured at a number of microwave frequencies and several configurations. Figures 69 and 70 show the configurations tested, and Fig. 71 shows a sample of the results. Reference 50 provides the detailed test results.

6.1.2 Low-Frequency Capability

The use of widely spaced, physically small antennas of an interferometer permits guidance in an antiradiation mode against signals sometimes considered immune to ARM attack. It has been demonstrated in flight tests that antennas separated by two wavelengths

49. "Terrier BT Trimode Feasibility Study," Surface Missile Systems Dept., JHU/APL MP2-117 (Nov 1967).

50. C. H. Ronnenburg, "Interferometer Antenna Boresight Errors Measured on a Candidate Configuration for the Wide Area Guidance Missile," JHU/APL FIB78U-104 (3 Aug 1978).

can provide excellent guidance against stationary targets. Independent developments at MIT Lincoln Laboratories have also been used to demonstrate the capability to guide against communications signals in the VHF and UHF frequency range (Ref. 2).

Azimuth-only guidance can be accomplished with wing tip antennas on various forms of airframes. Many of these airframes will allow 10 ft or more of separation. If azimuth-only guidance is combined with a radar altimeter for a sea-skimmer missile at 20 ft altitude, good performance can be expected at frequencies near 100 MHz.

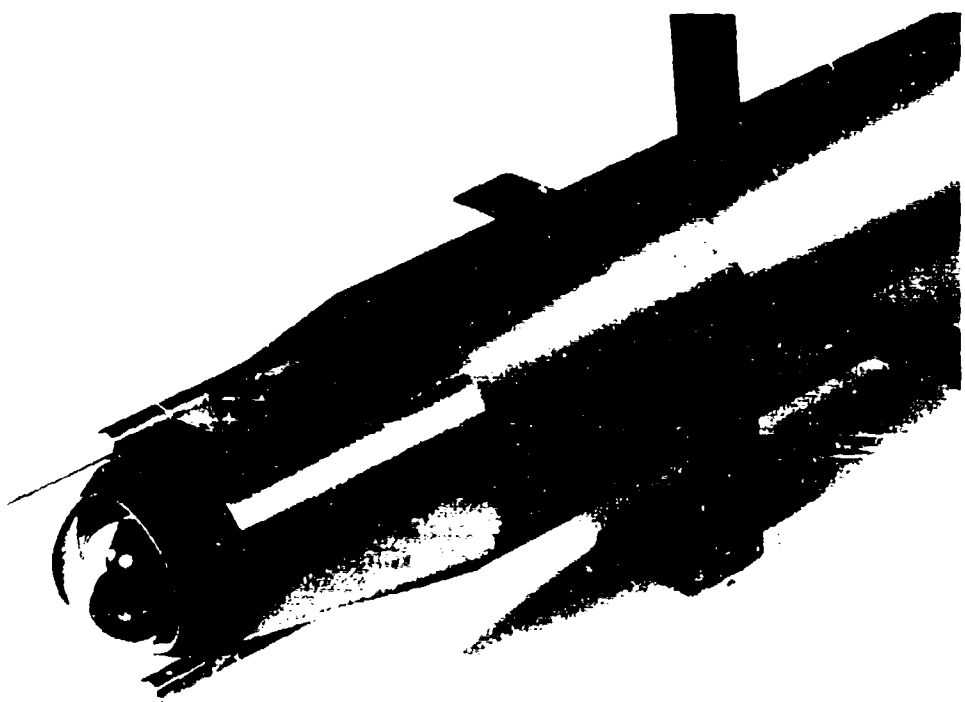

Fig. 68 Rolling-airframe missile mockup.

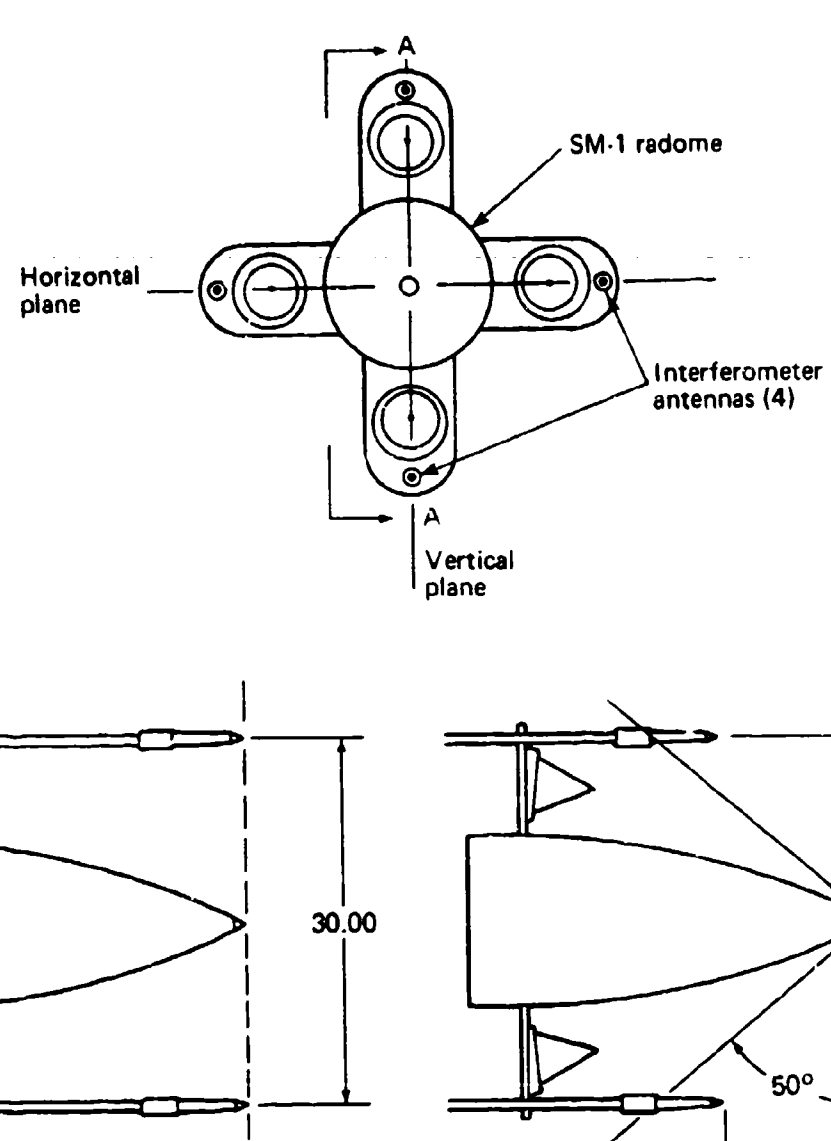

Fig. 69 Configuration for interferometer-plus-radome measurements.

6.1.3 Broadband Coverage

Previous sections have discussed methods for operating over wide frequency ranges for both the angle-measurement and body-decoupling portions of the missile. In practice it was possible to provide a modification kit that could be installed aboard ship to greatly increase

the missile frequency coverage. This was possible because of the simplicity of the interferometer antennas. The modification kit included replacement antenna elements, a broadband microwave mixer, a broadband solid-state local oscillator, and some circuitry needed to adjust the decoupling gain in the gyro path.

6.1.4 Suitability for Guided Projectiles

The development by the Naval Surface Weapons Center (Dahlgren, Virginia) of gyro caging mechanisms that permit gun launching allows the possibility of an RF-guided projectile. The interferometer is uniquely suited to this application because it does not require a gimballed seeker and can therefore be expected to survive the gun launch acceleration without difficulty. In many cases the gun is associated with a target-tracking radar, and therefore, a semiactive seeker appears to be a good choice.

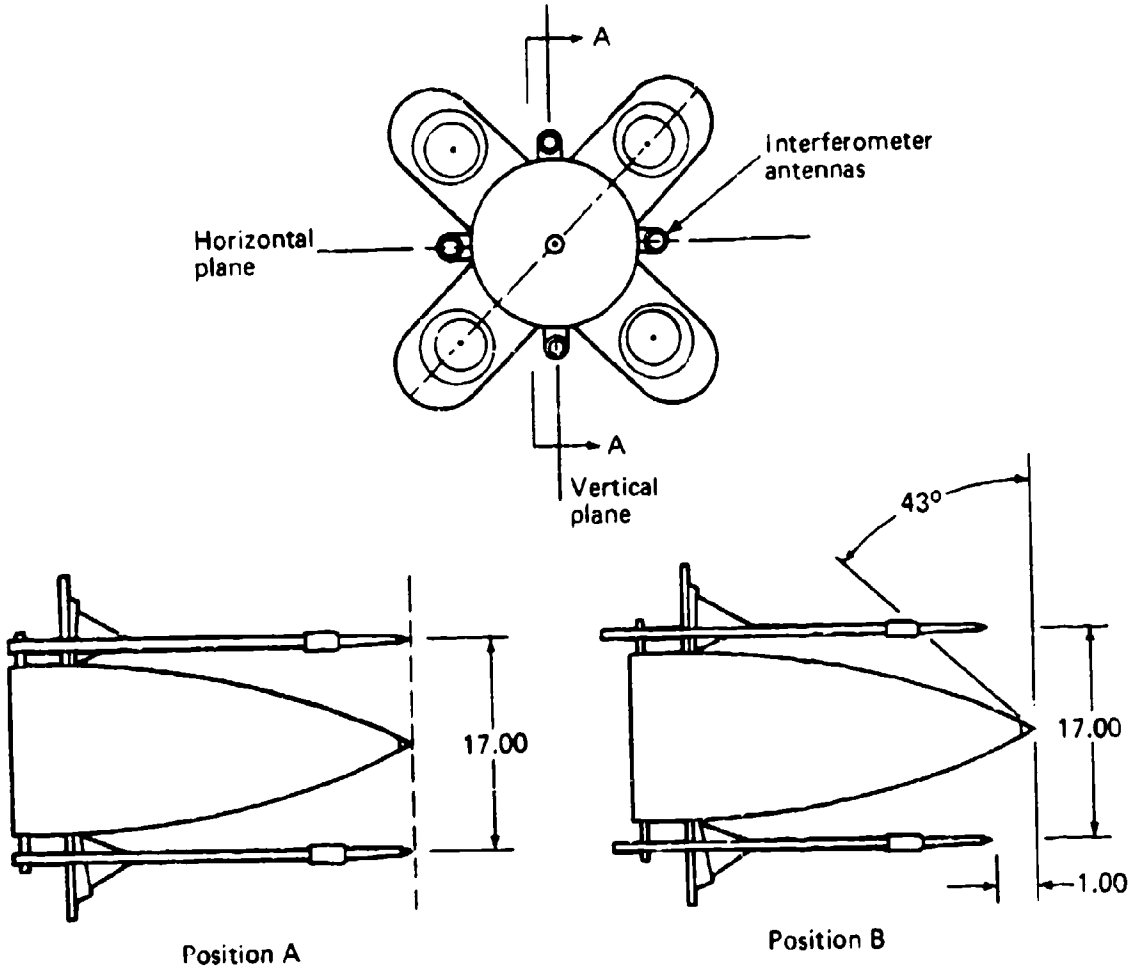

Fig. 70 Configuration for interferometer-plus-radome measurements.

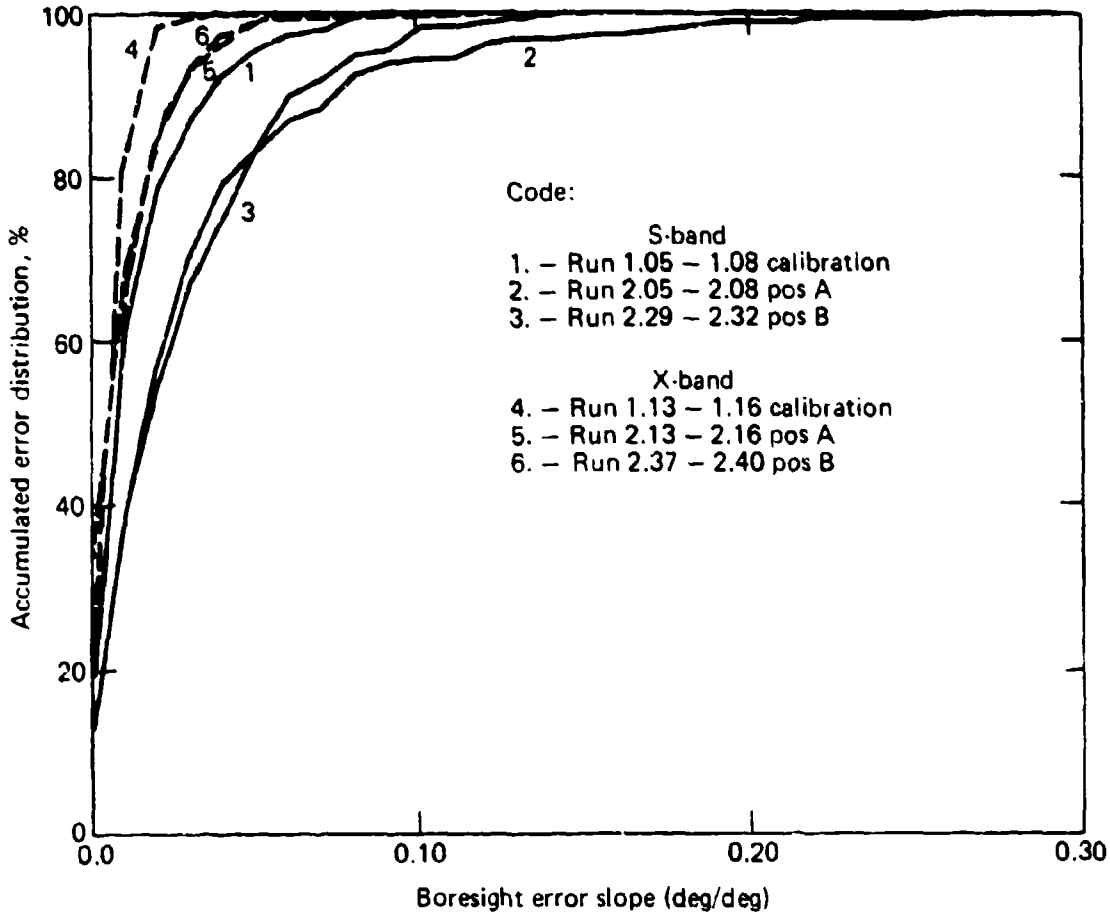

Fig. 71 Accumulated boresight error slope distribution; 30 in. cross-plane interferometer (linearly polarized elements).

6.1.5 Low Cost

Interferometer processing uses techniques that are particularly well-suited to digital technology. The VHSIC (Very High Speed Integrated Circuit) programs now in development will allow a major breakthrough in the types of digital processing that can be considered for missile use. The accuracy available with digital processing will allow some of the heavy and expensive mechanical components to be replaced by digital technology. Processes such as precisely multiplying the body-decoupling gyro signal by the proper gain factor can easily be accomplished by digital technology.

6.2 AERODYNAMIC DRAG CONSIDERATIONS

During the BT tri-mode study the zero lift-drag coefficients were compared for the beam-rider BT missile, BT plus interferometer, and the homing version with appropriate radome. The addition of the interferometer antennas increased the drag of the BT by 11% but was 5% below the homing version.

6.3 MODERN IMPLEMENTATION OF INTERFEROMETER GUIDANCE

6.3.1 Digital Processing

Figure 72 shows a possible ARM seeker using VHSIC technology for the angle processing and discrimination circuits. The seeker shown has a portion dedicated to acquisition and

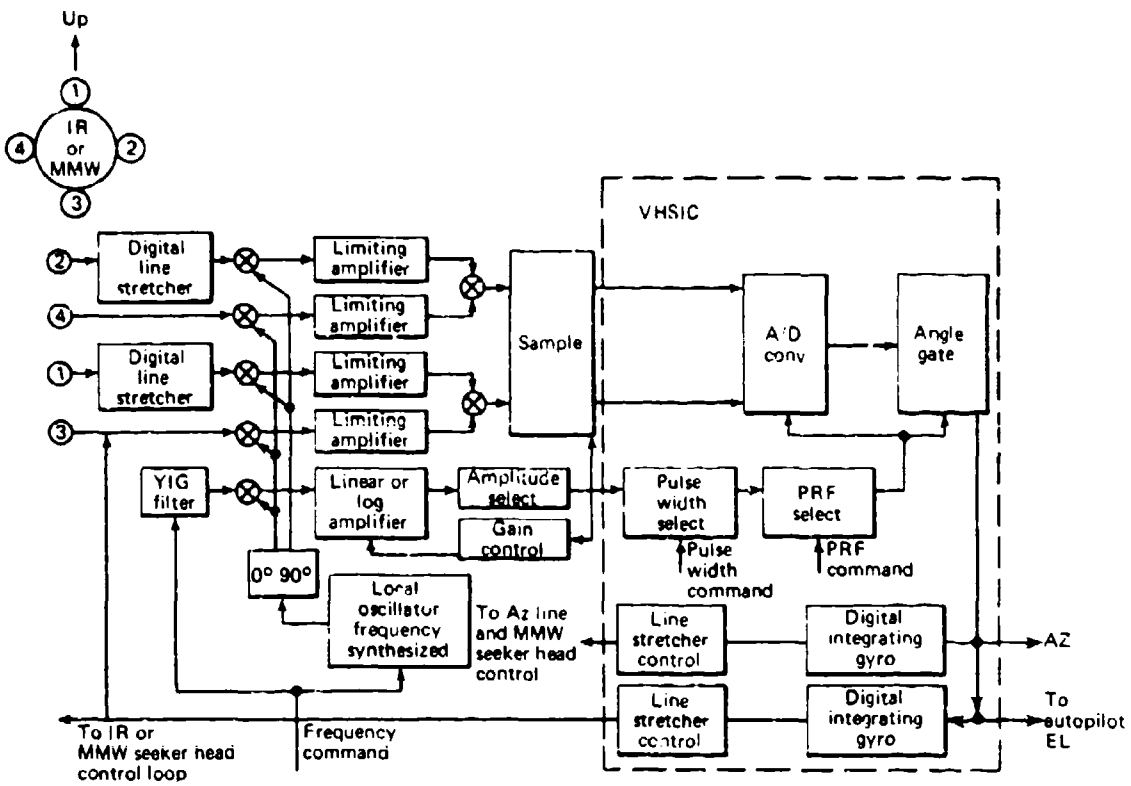

Fig. 72 Interferometer ARM seeker.

detection of a signal and a portion dedicated to angle measurement. Each of these portions is further divided into analog and digital sections. The acquisition portion uses a sample of the signal from one antenna to provide frequency select, amplitude select, pulse-width select, and pulse-rate or pulse-interval select. Frequency discrimination is obtained in the analog section of the circuitry in a superheterodyne receiver with tuning provided on both the local oscillator and a microwave filter. The tunable filter eliminates many problems associated with response to spurious frequencies. The amplitude select circuitry and associated amplifier are also a part of the analog circuitry. The choice of log vs. linear amplifier is controlled somewhat by the mission and the type of amplitude discrimination desired. Linear amplifiers with gain control will allow a large signal to suppress the smaller signals and give a decided advantage to the large signal. This would be desirable for a

nonfluctuating signal. A log response amplifier is usually preferred to detect a fluctuating signal from a rotating antenna. The signal from the amplitude select is normalized in amplitude at the input to the digital portion of the acquisition circuitry. Shaping is also available to provide a squared pulse to the pulse-width select. A standard pulse occurs at the output of the width-select circuit at some specified delay after the leading edge of the input, if the input pulse width is within the limits set by the command. The output pulse of the pulse-rate select is used to accept the angle signal processed in that portion of the seeker.

The angle measurement portion of the seeker uses phase comparison of interferometer pairs. The output of an electrical phase comparator is proportional to the sine of the phase difference at the input rather than proportional to the phase and angle rate as it changes by more than 360°. This is accomplished by a closed loop from the output to an adjustable phase shifter at the input. The angle can be measured directly by the change in phase required to maintain a null at the output. This phase shifter is in the form of an adjustable microwave line length to eliminate the sensitivity to microwave frequency. The body decoupling of missile motion from target motion is accomplished by controlling the adjustable line with the body-mounted gyros. The LOS rate needed for proportional navigation is derived from the torque signal applied to the gyro to maintain a system null.

The output of the pair of phase comparators is in the form of a bipolar video pulse having a duration equal to the input radar pulse. This pulse is sampled and stored for a period to allow acceptance on the basis of pulse width and pulse interval. If these criteria are met, it is then converted to a digital word and examined for angle of arrival, based on the error signal. In the digital angle processor, the error signals are stored to permit an angle gating function. If each signal E_a and E_b are 10-bit words and the minimum and maximum pulse rates are 1 kHz and 100 kHz, respectively, then a register 20 bits wide by 100 bits long should provide the desired storage. An additional bit associated with each word will verify that an angle measurement was received on the particular clock pulse. The purpose of this storage is to allow an examination of a number of angle measurements and determine whether they are from a single target or multiple targets. For example, if two sequential angle measurements indicate a large difference in error signal, it is more appropriate to select one and use it for guidance as opposed to averaging the multiple signals. Examination of the most significant bits of each measurement allows this type of angle sorting. As an example, assume the angles are sorted into five elevation and five azimuth bins giving a total of 25 possible combinations. The sequence of operation could be as follows. On each clock pulse (100 kHz rate) the A/D converter output is read. The first bit of the 21 bits provides an indication that the remaining 20 bits are an angle error measurement of a signal that met the criteria of pulse width and pulse rate. If there is a "1," then the most significant bits of each error signal are examined to determine which of the 25 possible error boxes the signal was in. An accumulator or counter on each error box is an indication of the density of errors at each location, and the accumulator for the particular box is increased by one count.

Various forms of logic are possible for determining initial acquisition. One possible rule is to accept a signal when the count in a particular accumulator exceeds a threshold. Another is to examine the accumulator totals for the largest count after a given number of measurements are made. After initial acquisition, the total storage register is scanned for all signals within the selected "box." These signals are averaged and used to control the digital line in the interferometer lines to step the error to a null. Subsequently errors are obtained only from the box representing the near zero position and multiple targets outside of the zero box will not contaminate the steering signal.

This form of sorting will be extremely valuable in a high-pulse-density environment with signals of unknown pulse-width and pulse-rate characteristics. The angle errors are used in a closed loop to torque the integrating-gyro and line-stretcher control. This torque signal is also a measure of the missile-to-target LOS rate in inertial space, and is, therefore, the appropriate signal to be used for proportional navigation steering commands.

Another form of digital processor was considered in the development of the rolling interferometer. The digital processor was used after an I-and-Q bipolar video phase comparator. A description of the experimental unit is provided in Ref. 51. The phase angle between the two antennas was measured by a series of digital gates. For example, the quadrant is easily determined by the sign of the I and Q video. The octant of the quadrant is determined by the ratio of the absolute magnitudes of the I and Q video. This process can be carried out to any desirable level of resolution.

6.3.2 Strapdown Inertial Instruments

The original concept of interferometer guidance as described in earlier sections of the report used strapped down rate gyros for body-motion decoupling. The problems with instrument accuracy and signal processing errors created the need for platforms such as STAPFUS to provide the required accuracy. The development of small floated integrating gyros and economical digital processing has again changed the picture such that the strapdown instruments now have the required accuracy when they are coupled with digital processing. The size and weight are attractive for small missiles, and the cost could be an order of magnitude below some of the production systems. Figures 73, 74, and 75 show platforms designed for Talos, STANDARD Missile, and Redeye. Figure 76 shows a typical miniature integrating gyro that could be used in conjunction with digital signal processing for body-motion decoupling.

51. H. H. Knapp, "Proposed Digital Output Electronics for ASMD Block I RF Redesign," JHU/APL FIB76U-146 (27 Sep 1976).

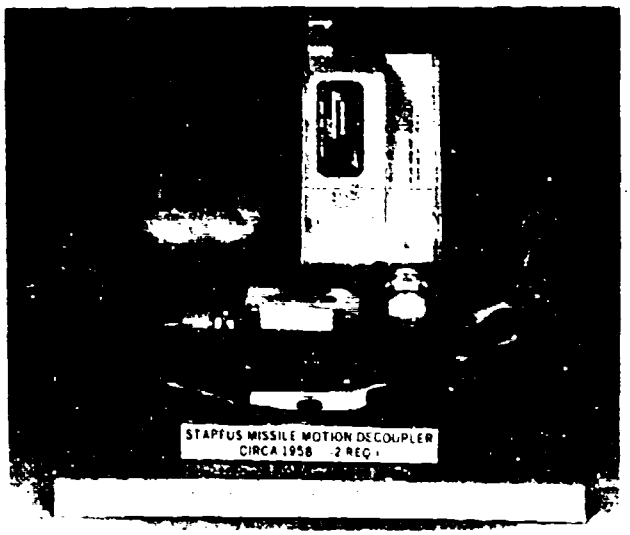

Fig. 73 STAPFUS missile-motion decoupler (circa 1958). (Two were required).

Fig. 74 Missile-motion decoupler (circa 1966). (Two were required).

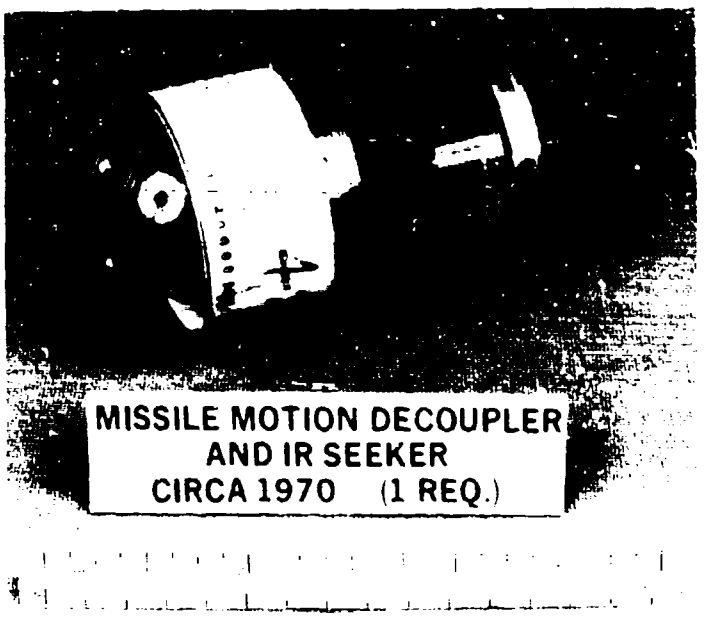

Fig. 75 Missile-motion decoupler and IR seeker (circa 1970). (One was required).

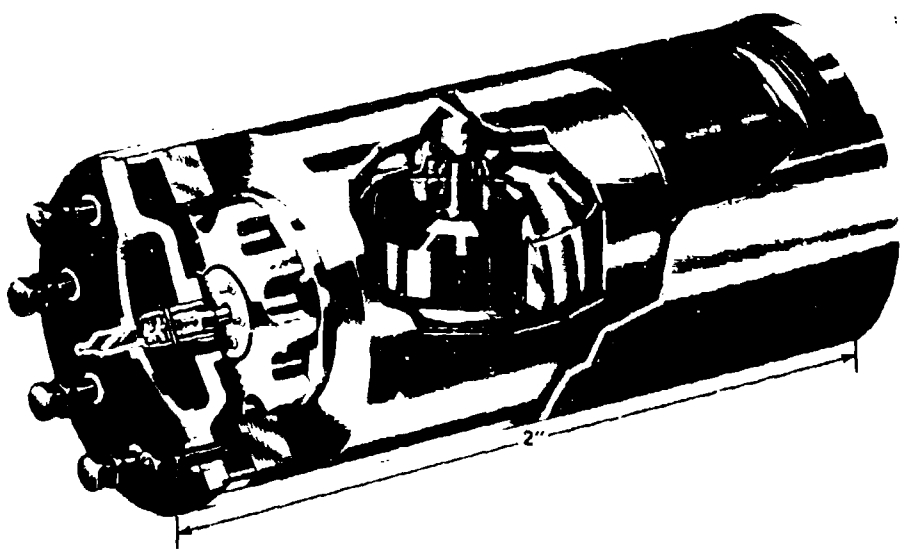

Fig. 76 Typical miniature integrating gyro.

ACKNOWLEDGMENTS

We wish to give our special thanks to A. R. Eaton of JHU/APL whose interest in documenting the background of missile guidance techniques made this report possible and also to R. L. Ely, the JHU/APL problem sponsor; D. A. Cozort of the MIT Library Institute Archives and Special Collections; Z. Carpenter and B. Baker of the JHU/APL Document Library; D. Avery of the JHU/APL internal reports section; and many others from JHU/APL who assisted in locating the many references used in this report.

We also wish to thank O. J. Baltzer and J. R. Wright, both formerly of the University of Texas/Defense Research Laboratory, for some of the historical information.

We especially wish to express our appreciation to L. M. Billard of Technology Service Corporation, who not only provided the editing but was able to decipher the authors' handwriting.

Draft versions of this document were reviewed by an *ad hoc* committee of APL staff members consisting of J. H. Braun, B. D. Dobbins, R. L. Ely, J. E. Hanson, W. C. Hyatt, R. C. Mallalieu, A. J. Pue, and D. J. Yost. Several Members of this review team have extensive experience in interferometer guidance, while others are experts in related areas of missile guidance. Their comments and suggestions have substantially enhanced the quality of this survey.

This list of acknowledgments would not be complete without noting that the successful development of the guidance system described herein and its application to the Talos missile were accomplished through the dedication and talent of many individuals in academia, industry, and government, acting under the inspired leadership of Dr. W. H. Goss, the JHU/APL Talos Program Supervisor.

REFERENCES

1. J. F. Gulick, E. C. Jarrell, and R. C. Mallalieu, "Fundamental Limitations of ARM Seekers at Low Radar Frequencies," JHU/APL FS-77-006 (Jan 1977).
2. I. Stiglitz, *Journal of Defense Research* (Summer 1979) MIT Lincoln Laboratories, Lexington, MA.
3. "Technical Report RAM Missile Round Advanced Development," DTIC/AC-CO20879 (Feb 1980).
4. C. W. Horton, "The Scheme for Missile Navigation Suggested by Dr. L. J. Chu," DRL/UT Internal Memo No. 38 (15 May 1946).
5. C. G. Matland and C. C. Loomis (MIT), "A Preliminary Study of the Radar Homing Head for an AA Guided Missile," METEOR Report M2 (15 Aug 1946).
6. B. Loesch, R. Long, M. Moore, and J. C. Nowell, "Design and Test of Simplified Pulse Interferometer Seeker," DTIC/DLA AD No. 107338 (30 Sep 1955).
7. T. D. Jacot, "Notes on Interferometer Phase Measuring Systems," JHU/APL MED-SR/200 (1 Oct 1969).
8. O. J. Baltzer (DRL/UT), "A Radar Interferometer for Homing Purposes," JHU/APL CM-260 (15 May 1946).
9. C. R. Rutherford (DRL/UT), "Double Modulation Radar Interferometer," JHU/APL CF-505 (3 Dec 1946).
10. "Final Engineering Report: Improved Interferometer Antenna System," prepared for JHU/APL Subcontract 7733 by Chu Associates, Littleton, MA, JHU/APL Accession No. 142788 (30 Oct 1959).
11. A. G. Rawling, "On the Undesirability of the CHU I Type Interferometer Antenna in Homing," JHU/APL BBD-458 (Jul 1958).
12. G. C. Munro, "Mathematical Discussion of a Device Suggested by J. W. Follin, Jr., for Improving the Performance of the Talos Interferometer Homing System," JHU/APL CF-2654 (1 Jul 1957).
13. "Survey of Systems to Provide an Unambiguous Measure of the Angle of the Target Line of Sight," prepared for JHU/APL by Dunn Engineering Associates, Cambridge, MA (20 Sep 1957).
14. J. E. Hanson, "On Resolving Angle Ambiguities of n-Channel Interferometer Systems for Arbitrary Antenna Arrangements in a Plane, JHU/APL TG-1224 (Oct 1973).
15. J. F. Gulick, Jr. and J. E. Hanson, "Interferometric Rolling Missile Body Decoupling Guidance System," United States Patent No. 3,897,918 (5 Aug 1975).
16. J. F. Gulick, J. S. Miller, and A. J. Pue, "Broadband Interferometer and Direction Finding Missile Guidance System," United States Patent No. 4,204,655 (27 May 1980).
17. D. K. Larson, "Performance of the Microwave Associates MPM-258 Line Stretcher," JHU/APL FIB79U-137 (26 Nov 1979).
18. D. R. Marlow, "Interferometer Phase Errors Caused by Receiver Antenna Polarization Mismatches — For Plane Waves of All Polarization Types," JHU/APL MED-SF/220 (10 Sep 1968).
19. R. C. Mallalieu, "The Effect of Incident Polarization on an Interferometer Antenna Behind a Radome," JHU/APL MED-SR/160 (20 May 1969).
20. J. F. Gulick, T. D. Jacot, H. H. Knapp, and H. H. Nall, "An Electromechanical Comparator for Use with the Scanning Interferometer Homing System," JHU/APL CF-2303 (3 Nov 1954).

21. D. Young and E. A. Ripperger (DRL/UT), "Effect of Time Lags and Aerodynamic parameters on the Stability of the DRL Homing System," JHU/APL CM-495 (12 Aug 1948).
22. C. E. Akerman, "Analysis of the Undesired Beta Signals (Squiggles) in the CWI Homing System," JHU/APL CF-2661 (22 Jul 1957).
23. W. P. Bishop, L. B. Childress, J. S. Florio, J. E. Hanson, and H. H. Nall, "Agreement Between Theory and Recent Multiple Jammer Tracking Experiments with the CWI System," JHU/APL BBD-794 (15 Apr 1960).
24. J. E. Hanson, "On the Impossibility of Passive Angular Discrimination of Two Closely Spaced Gaussian Noise Barrage Jammers," JHU/APL BBD-764 (3 Feb 1960).
25. J. E. Hanson "A Note on the Non-Simultaneous Gating of Front End Pulses in the Typhon LR Interferometer System," JHU/APL BBD-1036 (Aug 1961).
26. A. Kossiakoff, "Advanced Missile Guidance," JHU/APL AK-009-70 (13 Jan 1970).
27. R. E. Gingas and J. F. Hartranft, "Investigation of Triple Sensor Missile Guidance," JHU/APL MCM-SR/638 (8 Jul 1970).
28. R. L. McDonald "Two Target Tracking Error Expressions for a Combined Dish Interferometer Receiver," JHU/APL MPA-1-233 (12 Aug 1970).
29. R. E. Christenberry, "An 1103 Evaluation of the Effects of STAPFUS Parameters on the Talos 6B1 (STAPFUS) Missile in the Homing Phase," JHU/APL BBD-675 (17 Aug 1959).
30. G. C. Munro, "Narrow Beam Interferometer Homing in the Presence of Multiple Blinking Jammers," JHU/APL BBD-1395 (15 Dec 1964). (Also, BBD-1395-1 "Supplement to 1395.")
31. R. Ostrander, "Evaluation of the Antiship Capability of the Talos Missile," Final Report, JHU/APL TG-749 (Dec 1965).
32. "Final Report: Surface Target Tracking and Radar Characteristics Test, D/S 491 Event 2," JHU/APL SMS-FS-346 (May 1970).
33. J. R. Wright and R. M. Adams (DRL/UT), "DRL Noise Measurements Report No. 1," JHU/APL CF-1701 (7 Dec 1951).
34. J. R. Wright (DRL/UT), "Performance of Interferometer Tracker Against Large Target Aircraft," JHU/APL CF-1808 (11 Dec 1952).
35. J. R. Wright (DRL/UT), "Measurement with Scanning Interferometer of Angle Noise for Head-On Aspect of Six Aircraft," JHU/APL CF-1809 (6 Jan 1953).
36. O. J. Baltzer (DRL/UT), "Command Homing Guidance with the Scanning Interferometer," JHU/APL CM-592 (31 May 1950).
37. O. J. Baltzer, "Missile Guidance System," U. S. Patent No. 3,001,186 (19 Sep 1961).
38. G. C. Munro, "Effects of Missile Angular Velocity on the Janus Interferometer Systems," JHU/APL CF-1680 (11 Sep 1951).
39. N. A. Brigham, "Recommended TALOS Fixes for Slow Bending Discriminator Weaknesses, and the Differentiating Network," JHU/APL CF-1945 (17 Dec 1952).
40. G. C. Munro, "The STAPFUS Stabilization Loop," JHU/APL CF-2380 (13 May 1955).
41. J. W. Follin, Jr. and G. C. Munro, "Direction Cosine Linkage," U.S. Patent No. 3,215,368 (2 Nov 1965).
42. D. T. Collins, R. P. Borrelli, and A. J. Bassnett, "Direction Cosine Linkage (DIRCOL) Homing System Tests," JHU/APL CF-2811 (1 Jun 1959).
43. G. C. Munro, "REAC Study of a Modified Interferometer Homing System," JHU/APL CF-2663 (6 Aug 1957).
44. G. C. Munro and J. W. Follin, Jr., "The Direction Cosine Linkage," JHU/APL CF-2669 (Sep 1957).

45. C. D. Sayles, "Test Results for the Capacitive Two Axis Pickoff," JHU/APL FIB79U-018 (9 Feb 1979).
46. J. F. Gulick, "A Beta POT Alternative for ASMD," JHU/APL FIB77U-055 (22 Mar 1977).
47. J. F. Gulick, "A Capacitive Two Axis Pickoff for Redeye or Stinger Gyro," JHU/APL JFG-78U-014 (5 Jul 1978).
48. J. S. Miller, "Analysis of Missile Body-Motion Decoupling," Technology Service Corp., W47-190 (26 Mar 1981).
49. "Terrier BT Trimode Feasibility Study," Surface Missile Systems Dept., JHU/APL MP2-117 (Nov 1967).
50. C. H. Ronnenburg, "Interferometer Antenna Boresight Errors Measured on a Candidate Configuration for the Wide Area Guidance Missile," JHU/APL FIB78U-104 (3 Aug 1978).
51. H. H. Knapp, "Proposed Digital Output Electronics for ASMD Block I RF Redesign," JHU/APL FIB76U-146 (27 Sep 1976).

BIBLIOGRAPHY OF INTERFEROMETER GUIDANCE

Publications of The Johns Hopkins University/Applied Physics Laboratory (JHU/APL)

G. C. Munro, "Effects of Missile Angular Velocity on the Janus Interferometer Systems," JHU/APL CF-1680, 11 Sep 1951.

N. A. Brigham, "Recommended TALOS Fixes for Slow Bending Discriminator Weaknesses, and the Differentiating Network," JHU/APL CF-1945, 17 Dec 1952.

J. F. Gulick, T. D. Jacot, H. H. Knapp, and H. H. Nall, "An Electromechanical Comparator for Use With the Scanning Interferometer Homing System," JHU/APL CF-2303, 3 Nov 1954.

G. C. Munro, "The STAPFUS Stabilization Loop," JHU/APL CF-2380, 13 May 1955.

G. C. Munro, "Mathematical Discussion of a Device Suggested by J. W. Follin, Jr. for Improving the Performance of the TALOS Interferometer Homing System," JHU/APL CF-2654, 1 Jul 1957.

C. E. Akerman, "Analysis of the Undesired Beta Signals (Squiggles) in the CWI Homing System," JHU/APL CF-2661, 22 Jul 1957.

G. C. Munro, "REAC Study of a Modified Interferometer Homing System," JHU/APL CF-2663, 6 Aug 1957.

G. C. Munro and J. W. Follin, Jr., "The Direction Cosine Linkage," JHU/APL CF-2669, Sep 1957.

"Survey of Systems to Provide an Unambiguous Measure of the Angle of the Target Line of Sight," prepared for JHU/APL by Dunn Engineering Associates, Cambridge, MA, Sep 1957.

G. C. Munro, "Homing with the CHU Antenna," JHU/APL BBD-419, May 1958.

A. G. Rawling, "On the Undesirability of the CHU I Type Interferometer Antenna in Homing," JHU/APL BBD-458, Jul 1958.

G. C. Munro, "Janus Homing," APL/JHU BBD-555, 12 Jan 1959.

G. C. Munro, "The Ideal Steering Signals for Janus Homing," JHU/APL BBD-557, 13 Jan 1959.

D. T. Collins, R. P. Borrelli, and A. J. Bassnett, "Direction Cosine Linkage (DIRCOL) Homing System Tests," JHU/APL CF-2811, 1 Jun 1959.

R. E. Christenberry, "An 1103 Evaluation of the Effects of STAPFUS Parameters on the Talos 6B1 (STAPFUS) Missile in the Homing Phase," JHU/APL BBD-675, 17 Aug 1959.

"Final Engineering Report: Improved Interferometer Antenna System," prepared for JHU/APL Subcontract 77743 by Chu Associates, Littleton, MA, JHU/APL Accession No. 142788, 30 Oct 1959.

J. E. Hanson, "On the Impossibility of Passive Angular Discrimination of Two Closely Spaced Gaussian Noise Barrage Jammers," JHU/APL BBD-764, 3 Feb 1960.

W. P. Bishop, L. B. Childress, J. S. Florio, J. E. Hanson, and H. H. Nall, "Agreement Betweeen Theory and Recent Multiple Jammer Tracking Experiments with the CWI System," JHU/APL BBD-794, 15 Apr 1960.

J. E. Hanson, "A Note on the Non-Simultaneous Gating of Front End Pulses in the Typhon LR Interferometer System," JHU/APL BBD-1036, Aug 1961.

J. E. Hanson and A. J. Gilberger, "Angle Tracking the Stronger of Two Closely Spaced Gaussian Noise Jammers in Two Angular Dimensions Using Four Interferometer Horns," JHU/APL BBD-1294, 24 Sep 1963.

G. C. Munro, "Narrow Beam Interferometer Homing in the Presence of Multiple Blinking Jammers," JHU/APL BBD-1395, 15 Dec 1964. BBD-1395-1 "Supplement to 1395."

R. Ostrander. "Evaluation of the Antiship Capability of the Talos Missile," Final Report, JHU/APL TG-749, Dec 1965.

"Seeker Head Stabilization Using Integrating Gyros," prepared for JHU/APL Subcontract 230553-T1-36 by Harry Belock Associates, 14 Oct 1966.

"Terrier BT Trimode Feasibility Study," JHU/APL MP2-117, Surface Missile Systems Department, Nov 1967.

D. R Marlow, "Interferometer Phase Errors Caused by Receiver Antenna Polarization Mismatches — For Plane Waves of All Polarization Types," JHU/APL MED-SF/220, 10 Sep 1968.

R. C. Mallalieu, "The Effect of Incident Polarization on an Interferometer Antenna Behind a Radome," JHU/APL MED-SR/160, 20 May 1969.

T. D. Jacot, "Notes on Interferometer Phase Measuring Systems, JHU/APL MED-SR/200, 1 Oct 1969.

A. Kossiakoff, "Advanced Missile Guidance," JHU/APL AK-009-70, 13 Jan 1970.

"Final Report: Surface Target Tracking and Radar Characteristics Test, D/S 491 Event 2," JHU/APL SMS-FS-346, May 1970.

R. E. Gingas and J. F. Hartranft, "Investigation of Triple Sensor Missile Guidance," JHU/APL MCM-SR/638, 8 Jul 1970.

R. L. McDonald, "Two Target Tracking Error Expressions for a Combined Dish Interferometer Receiver," JHU/APL MPA-1-233, 12 Aug 1970.

D. R. Marlow, "Second Generation Decoupling and Output Electronics for a Rolling ARM Guidance System," JHU/APL MPA-1-262, 2 Jun 1971.

J. F. Gulick, "Interferometer Techniques Presentation to the TTCP Specialists Group on Low Cost Guidance," JHU/APL MS-3/3, 2 May 1972.

J. E. Hanson, "On Resolving Angle Ambiguities of n-Channel Interferometer Systems for Arbitrary Antenna Arrangements in Plane," JHU/APL TG-1224, Oct 1973.

N. Dimenco and M. Soukup, "Alternate Guidance RF Receiver Breadboard Engineering Design," JHU/APL TG 1270, Apr 1975.

A. J. Pue, "Modeling of a Two Degree of Freedom Gyroscope in a Rolling Missile," JHU/APL FIC-76-U-008, 25 Feb 1976.

D. J. Yost and A. Arrow, "On Interfacing an IR Seeker with an RF Interferometer System," JHU/APL FIC(1)-76-U-008, 27 Feb 1976.

H. H. Knapp, "Proposed Digital Output Electronics for ASMD Block I RF Redesign," JHU/APL FIB76U-146, 27 Sep 1976.

J. F. Gulick, E. C. Jarrell, and R. C. Mallalieu, "Fundamental Limitations of ARM Seekers at Low Radar Frequencies," JHU/APL FS-77-006, Jan 1977.

J. F. Gulick, "A Beta POT Alternative for ASMD," JHU/APL FIB77U-055, 22 Mar 1977.

C. H. Ronnenburg, "Evaluation of Interferometer Antenna Systems Using an Automatic Data Acquisition System, JHU/APL FIB78U-042, 18 Apr 1978.

J. F. Gulick, "A Capacitive Two Axis Pickoff for Redeye or Stinger Gyro," JHU/APL JFG-78U-014, 5 Jul 1978.

C. H. Ronnenburg, "Interferometer Antenna Boresight Errors Measured on a Candidate Configuration for the Wide Area Guidance Missile," JHU/APL FIB78U-104, 3 Aug 1978.

C. H. Ronnenburg, "Radome Induced Line-of-Sight Errors Measured on a Candidate Configuration for the Wide Area Guidance Missile," JHU/APL FIB78U-80, 11 Oct 1978.

C. D. Sayles, "Test Results for the Capacitive Two Axis Pickoff," JHU/APL FIB79U-018, 9 Feb 1979.

D. K. Larson, Internal Memorandum "Performance of the Microwave Associates MPM-258 Line Stretcher," JHU/APL FIB79U-137, 26 Nov 1979.

Publications of Defense Technical Information Center/Defense Logistics Agency (DTIC/DLA)

B. Loesch, R. Long, M. Moore, and J. C. Nowell, "Design and Test of Simplified Pulse Interferometer Seeker," AD No. 107338, 30 Sep 1955.

R. D. Wetherington and J. L. Birchfield (Georgia Institute of Technology), "Techniques for Generating Guidance Signals from Body-Fixed Sensors," AD No. 707419, 10 Mar 1970.

"Strapdown Seeker Guidance for Air-to-Surface Tactical Weapons," Rockwell International Missile Systems Division, Columbus, OH, AD No. B030995, May 1978.

"Technical Report RAM Missile Round Advanced Development," AC-CO20879, Feb 1980.

Publications of the Defense Research Laboratory/University of Texas (DRL/UT)

O. J. Baltzer (DRL/UT), "A Radar Interferometer for Homing Purposes," JHU/APL CM-260, 15 May 1946.

C. W. Horton (DRL/UT), "The Scheme for Missile Navigation Suggested by Dr. L. J. Chu," DRL/UT Internal Memo No. 38, 15 May 1946.

C. W. Horton (DRL/UT), "On the Radar Interferometer," JHU/APL CF-406, 14 Oct 1946.

C. W. Horton (DRL/UT), "On the Introduction of the Correction for the Change of Bearing of the Missile in the Radar Interferometer," JHU/APL CF-438, 16 Oct 1946.

C. R. Rutherford (DRL/UT), "Double Modulation Radar Interferometer," JHU/APL CF-505, 3 Dec 1946.

D. Young (DRL/UT), "Preliminary Studies of the Dynamic Behavior of a Homing Missile with the DRL Interferometer," JHU/APL CF-694, 21 May 1947.

C. W. Horton and D. Young (DRL/UT), "On the Effect of Missile Roll on Homing Systems," JHU/APL CM-395, 20 Jun 1947.

D. Young (DRL/UT), "Further Studies of the Dynamic Behavior of a Homing Missile with the DRL Interferometer," JHU/APL CF-754, 12 Aug 1947.

D. Young and E. A. Ripperger (DRL/UT), "Effect of Time Lags and Aerodynamic Parameters on the Stability of the DRL Homing System," JHU/APL CM-495, 12 Aug 1948.

R. N. Lane, "A Simplified Scanning Interferometer and a Rate Servo for Gyro Correction," JHU/APL CF-1079, 24 Aug 1948.

O. J. Baltzer (DRL/UT), "A Method for Introducing Roll Compensation Signals into the Homing Interferometer," JHU/APL CF-1181, 24 Feb 1949.

O. J. Baltzer (DRL/UT), "Command Homing Guidance with the Scanning Interferometer," JHU/APL CM-592, 31 May 1950.

J. R. Wright and R. M. Adams (DRL/UT), "DRL Noise Measurements Report No. 1," JHU/APL CF-1701, 7 Dec 1951.

J. R. Wright (DRL/UT), "Performance of Interferometer Tracker Against Large Target Aircraft," JHU/APL CF-1808, 11 Dec 1952.

J. R. Wright (DRL/UT), "Measurement with Scanning Interferometer of Angle Noise for Head-On Aspect of Six Aircraft," JHU/APL CF-1809, 6 Jan 1953.

Publications of the Massachusetts Institute of Technology (MIT)

"METEOR Introductory Report," MIT Guided Missile Program, METEOR Report M1, 15 Jul 1946.

C. G. Matland and C. C. Loomis, "A Preliminary Study of the Radar Homing Head for an AA Guided Missile," METEOR Report M2, 15 Aug 1946.

L. J. Chu, "The Seeker Problem of Guided Missiles," METEOR Report M3, 15 Sep 1946.

United States Patents

O. J. Baltzer, "Missile Guidance System," U. S. Patent 3,001,186 (19 Sep 1961).

J. F. Gulick, T. D. Jacot, H. H. Knapp, and H. H. Nall, "Interferometer Homing System," U.S. Patent 3,181,813 (4 May 1965).

J. W. Follin Jr. and G. C. Munro, "Direction Cosine Linkage," U.S. Patent 3,215,368 (2 Nov 1965).

J. F. Gulick, Jr. and J. E. Hanson, "Interferometric Rolling Missile Body Decoupling Guidance System," U.S. Patent 3,897,918 (5 Aug 1975).

J. F. Gulick, J. S. Miller, and A. J. Pue, "Broadband Interferometer and Direction Finding Missile Guidance System," U.S. Patent 4,204,655 (27 May 1980).

Publications from Miscellaneous Sources

I. Stiglitz, in *Journal of Defense Research* (Summer 1979), MIT Lincoln Laboratories, Lexington, MA.

R. D. Ehrich and W. E. Longenbaker, "Adaptive Control Applied to the Terminal Guidance of Tactical Weapons with Strapdown Seekers," Rockwell International Missile Systems Division, Columbus, OH. Published in *Proc. of AIAA Strategic/Tactical Space Science Meeting*, San Diego, 8-10 Sep 1980.

J. S. Miller, "Analysis of Missile Body Motion Decoupling," Technology Service Corp. W47-190, 26 Mar 1981.

INITIAL DISTRIBUTION EXTERNAL TO THE APPLIED PHYSICS LABORATORY*

The work reported in TG 1331 was done under Navy Contract N00024-81-C-5301, and is related to Task 83, which is supported by Naval Sea Systems Command.

ORGANIZATION	LOCATION	ATTENTION	No. of Copies
DEPARTMENT OF DEFENSE			
Tactical Technology Info. Analysis Ctr.	Columbus, Oh	Technical Library	1
DARPA	Rosslyn, VA	Director, Technology Office	1
DTIC	Alexandria, VA		12
Department of the Navy			
Department Offices			
NAVSEASYSCOM	Washington, DC	A. W. Doherty, PMS-400P	1
		Toshio Tasaka, SEA 880	1
		J. R. Whalen, SEA 6223	1
		SEA 06A	1
		SEA 62	1
		SEA 6221	1
		Library, SEA 9961	2
NAVAIRSYSCOM	Washington, DC	AIR 03	1
		E. B. Beggs, AIR 612	1
		Library, AIR 950D	2
NAVPRO	Laurel, MD		1
CNM	Washington, DC	NMAT 03	1
		NMAT 08	1
ONR	Washington, DC	Chief of Naval Research	1
		Technical Director	1
NRL	Washington, DC	Technical Director	1
		Technical Library	1
Centers			
NWC	China Lake, CA	Technical Director	1
		Mr. Bob Corsine	1
		Librarian	1
NSWC	Dahlgren, VA	Technical Director	1
		Mr. Conrad Brandt	1
		Librarian	1
PMTC	Point Mugu, CA	Technical Director	1
		Mr. Bob Hamilton	1
		Librarian	1
NOSC	San Diego, CA	Technical Director	1
		Technical Library	1
FAC	Corona, CA	Commanding Officer	1
		Technical Library	1
NADC	Warminster, PA	Technical Director	1
		Technical Library	1
NISC	Washington, DC	Technical Director	1
		Technical Library	1
CNA	Arlington, VA	Information and Documentation Center	1
Facilities			
NSWS Engineering Station	Port Hueneme, CA	Technical Library	1
Schools			
U.S. Naval Academy	Annapolis, MD	Weapons Dept.	1
Naval Postgraduate School	Monterey, CA	Lib: Tech. Rpts. Sec.	1

Requests for copies of this report from DoD activities and contractors should be directed to DTIC, Cameron Station, Alexandria, Virginia 22314 using DTIC Form 1 and, if necessary, DTIC Form 55.

*Initial distribution of this document within the Applied Physics Laboratory has been made in accordance with a list on file in the APL Technical Publications Group.

INITIAL DISTRIBUTION EXTERNAL TO THE APPLIED PHYSICS LABORATORY*

ORGANIZATION	LOCATION	ATTENTION	No. of Copies
Department of the Army			
BMDATC	Redstone Arsenal, Huntsville, AL 35807	Technical Library	1
Commands			
DARCOM	Alexandria, VA	Technical Library	1
	Redstone Arsenal, Huntsville, AL 35807	PATRIOT PM	1
MICOM	Redstone Arsenal, Huntsville, AL 35807	Commanding Officer	1
		W. C. McCorkle	1
		E. B. Dobbins	1
		HAWK PM	1
Laboratories			
Harry Diamond Laboratoires	Adelphi, MD 20783	Ross Parkhurst	1
		Technical Library	1
Schools			
United States Military Academy	West Point, NY	Library	1
Department of the Air Force			
AFAL	Eglin AFB, FL 32542	J. R. Mayersak	1
		Technical Library	1
Wright Aeronautical Laboratories	Wright Patterson AFB, Dayton, OH	Technical Library	1
Centers			
RADC	Rome, NY	Chief Scientist	1
		Technical Library	1
Schools			
Air Force Academy	Colorado Springs, CO	Library	1
U.S. GOVERNMENT AGENCIES			
Library of Congress	Washington, DC	Librarian	1
UNIVERSITIES			
Georgia Institute of Technology	Atlanta, GA	Library	1
The Johns Hopkins University	Baltimore, MD	Library	1
Massachusetts Institute of Technology	Cambridge, MA	Institute Archives & Special Collections	1
MIT Lincoln Laboratories	Lexington, MA 02173	Dr. Irvin Stiglitz	1
University of Texas, Defense Research Laboratory	Austin, TX	Tech. Library	1
CONTRACTORS			
Battelle Memorial Institute	Columbus, OH	Technical Library	1
Bendix Missile Division	Mishawaka, IN	Tech. Library	1
CACIAC, ITT Research Inst.	Chicago, IL 60616	C. W. Smoote	3
General Dynamics Pomona Division	Pomona, CA 91766	J. J. May, Mail Zone 4-45	1
Hughes Aircraft Corp., Missile Systems Division	Canoga Park, CA	Mr. V. Bloom	1
MacDonnell-Douglas Aircraft Co.	St. Louis, MO	Technical Library	1
	Huntington Beach, CA	Technical Library	1
Martin-Mariette Corp.	Orlando, FL	Technical Library	1
Raytheon Corporation, Missile Division	Bedford, MA	Mr. Mike Fossier	1
		Mr. John Long	1
RCA	Moorestown, NJ	Technical Library	1
Rockwell Int'l/Missile Syst. Div.	Columbus, OH 43216	R. D. Ehrich	1
Technology Service Corp.	Silver Spring, MD 20910	J. Gulick	10

*Initial distribution of this document within the Applied Physics Laboratory has been made in accordance with a list on file in the APL Technical Publications Group.

INITIAL DISTRIBUTION EXTERNAL TO THE APPLIED PHYSICS LABORATORY*

ORGANIZATION	LOCATION	ATTENTION	No. of Copies
Texas Instruments Corp.	Dallas, TX 75222	Hillary Hall, Mail Station 372	1
The MITRE Corp.	McLean, VA 22101	Technical Library	1
Mr. O. F. Baltzer	Austin, TX 78759		1
Mr. Julian Wright	Austin, TX 78759		1

*Initial distribution of this document within the Applied Physics Laboratory has been made in accordance with a list on file in the APL Technical Publications Group.